Hydrogeochemistry of Groundwaters at and Below the Base of the Permafrost at Lupin: Report of Phase III

NWMO TR-2009-10 June 2009

R.L. Stotler[1]
S.K. Frape[1]
T. Ruskeeniemi[2]
L. Ahonen[2]
M. Paananen[2]
M.Y. Hobbs[3]
K.E. Lambie[1]
M. Zhang[1]

[1] University of Waterloo
[2] Geological Survey of Finland
[3] Nuclear Waste Management Organization

nwmo
NUCLEAR WASTE MANAGEMENT ORGANIZATION
SOCIÉTÉ DE GESTION DES DÉCHETS NUCLÉAIRES

Nuclear Waste Management Organization
22 St. Clair Avenue East, 6th Floor
Toronto, Ontario
M4T 2S3
Canada

Tel: 416-934-9814
Web: www.nwmo.ca

Hydrogeochemistry of Groundwaters at and Below the Base of the Permafrost at Lupin: Report of Phase III

NWMO TR-2009-10

June 2009

R.L. Stotler[1]
S.K. Frape[1]
T. Ruskeeniemi[2]
L. Ahonen[2]
M. Paananen[2]
M.Y. Hobbs[3]
K.E. Lambie[1]
M. Zhang[1]

[1] University of Waterloo
[2] Geological Survey of Finland
[3] Nuclear Waste Management Organization

ABSTRACT

Title: Hydrogeochemistry of groundwaters at and below the base of the permafrost at Lupin: Report of Phase III

Report No.: **NWMO TR-2009-10**

Author(s): R.L. Stotler[1], S.K. Frape[1], T. Ruskeeniemi[2], L. Ahonen[2], M. Paananen[2] M.Y.Hobbs[3], K. Lambie[1], and M. Zhang[1]

Company: [1]University of Waterloo, [2]Geological Survey of Finland, [3]Nuclear Waste Management Organization

Date: June 2009

Abstract

Over the long time frames for which a Safety Case for a deep geologic repository for used nuclear fuel must assess repository performance, glacial and peri-glacial conditions may influence the thermal, hydraulic and mechanical boundary conditions at repository depth. To improve scientific understanding of the influence of climatic evolution on groundwater flow system dynamics in crystalline terrain, the international PERMAFROST project was initiated in 2001. Field research is conducted at the Lupin Mine in Nunavut Canada, situated in an area of continuous permafrost that extends to a depth of 500 m. Phase III of the project is described in this report, and was focused on the collection of representative geochemical and hydraulic information to further describe the groundwater flow system and permafrost geometry.

The results of the initial hydraulic investigations show that the hydraulic conductivity within the first 350 m of bedrock east from the mine is controlled by an interconnected network of fractures, rather than by pervasive planar fault-type structures (fracture-dominated flow). The hydraulic field is heterogeneous; closely spaced research boreholes have hydraulic head differences of up to 160 m, suggesting that either the boreholes are not connected or are only poorly connected. Pressure monitoring at deeper levels within the mine (890 m and 1130 m level) indicated that the water table is located approximately 620 m below surface, suggesting the presence of approximately 100 m of unsaturated zone below the permafrost.

Groundwaters from within the permafrost are typically Na-Cl or Na-Cl-SO_4 type, with highly variable SO_4 concentrations and high NO_3 concentrations (400-2600 mg/L). Geochemical data indicates that much of the dissolved load in the permafrost waters has come from the use of salt for the creation of brine for work in the permafrost areas during mine operation. This interpretation of permafrost waters impacted by mining operations is further supported by tritium and stable isotopic data ($\delta^{18}O$, $\delta^{2}H$, $\delta^{15}N$).

Deep groundwaters are Na-Ca-Cl or Ca-Na-Cl types with a wide range of TDS values, from 2 to 36 g/L. Gases associated with the deep groundwaters are predominantly methane, with ethane and propane as minor constituents. Comparison to other gases from shield environments suggests that the gases associated with the deep groundwater systems have a thermogenic origin, although there may also be a small biogenic component. The thermogenic component of the gases was most likely derived during amphibolite facies metamorphism (low pressure, high temperature) of the original sediments, suggesting that the gases, and by association the matrix fluids and most of the saline groundwaters, are hundreds of millions to billions of years old. This is further supported by ^{36}Cl analysis, which suggests the Cl^- in the subpermafrost system is older than the limit of the ^{36}Cl dating technique (0.5 to 1 million years). A preliminary conceptual model for the Lupin site is presented here.

CONTENTS

LIST OF TABLES

Page

LIST OF FIGURES

Page

1. INTRODUCTION

In the Deep Geologic Repository (DGR) concept for long-term isolation of nuclear fuel wastes considered in the Adaptive Phased Management (APM) approach, it is envisioned that used fuel will be sealed in corrosion resistant canisters and emplaced within an engineered geological repository excavated at a depth of approximately 500 m in a suitable crystalline or sedimentary rock formation (NWMO, 2005). Over the long time frames for which a Safety Case must assess repository performance, glacial and peri-glacial conditions may influence the thermal, hydraulic and mechanical boundary conditions at repository depth. To further advance the scientific understanding of permafrost and its role in influencing flow system evolution and fluid movement, the international PERMAFROST project was initiated by Posiva, Nirex, SKB, the Geological Survey of Finland and Ontario Power Generation in May of 2001 in Helsinki, Finland.

The PERMAFROST project field site is the Lupin Mine in Nunavut Canada, situated approximately 1300 km north of Edmonton in the plutonic crystalline rock of the Canadian Shield in an area of continuous permafrost that extends to a depth of 500 m. Phase I of the project involved a reconnaissance level investigation which relied upon existing mine site information, preliminary surface-based geophysical surveys and geochemical sampling of existing boreholes to develop an understanding of the occurrence, and the geologic and hydrogeologic setting, of permafrost at the site. The results of Phase I are reported in Ruskeeniemi et al. (2002). Phase I field studies were complemented by laboratory studies in which the impact of freezing on the chemical and isotopic composition of Canadian and Fennoscandinavian Shield groundwaters was investigated (Zhang and Frape, 2002).

In Phase II of the PERMAFROST project, which began in the fall 2002, researchers from the University of Waterloo focused on the collection of representative geochemical and hydrogeologic information to further describe the groundwater flow system and permafrost geometry. Also in Phase II, electromagnetic geophysical surveys were conducted by the Geological Survey of Finland to define the lateral variation of permafrost and saline groundwater depths, and noble gas sampling was performed by researchers from the University of Ottawa. Other research activities included targeted drilling to transmissive geologic structures for hydrogeochemical sampling and hydraulic testing, detailed core logging, surface water sampling, fracture infill mineralogy research and hydraulic pressure measurements.

The overall targets of the research at Lupin were outlined in the early stages of the Permafrost project. In Phase II, aspects of geochemistry, isotopes, groundwater dating and development of a conceptual model were the main focus of the hydrogeochemistry group. Specifically, the permafrost events potentially affecting the long-term stability of a deep-seated repository include:

- Long-term stability of the hydrogeological and hydrogeochemical conditions
- Role of non-frozen areas (taliks) as pathways for groundwater flow

The understanding of the hydrogeological and hydrogeochemical conditions at Lupin has improved greatly during Phase I and II, which provided site characterisation data and information on permafrost-related phenomena and processes. Interpretation of data collected in Phases I and II resulted in a new question arising regarding the origin of the observed

unsaturated zone at the base of the permafrost. When an improved understanding of this, and the long-term hydrogeochemical stability of the site in general are obtained, the conceptual model presented here may be further refined.

The work plan for Phase III was focused on research at the Lupin Site. Research at other sites was also considered as there was some uncertainty regarding access to the Lupin mine and also to allow for the comparison of observations made at Lupin against the data from other sites. Priority was given to the research at Lupin due to time limitations on research there, however, negotiations were also conducted with some additional mining companies to evaluate the possibilities for conducting research at their premises.

Objectives at the Lupin site for Phase III included:

- Physical Measurements
    - Ground Penetrating Radar (GPR) measurements of taliks
    - Continued hydraulic head measurements
- Further define chemistry of permafrost and subpermafrost waters
- Determining residence times of waters with ^{3}H, ^{14}C, ^{36}Cl analyses
- Fracture mineral studies
- Conceptual model development

All the work has been carried out in a close co-operation with the team from Ontario Power Generation/Nuclear Waste Management Organization/University of Waterloo (OPG/NWMO/UW). The University of Ottawa sampled noble gases using a diffusion sampler, and from the beginning of 2004, teams from the NASA Astrobiology Institute have conducted research on biochemistry aiming to identify the microbial communities possibly adapted to the permafrost conditions.

Through the PERMAFROST project, it has been possible to identify certain aspects related to the permafrost at Lupin which demand more work to confirm the observations and/or to improve the understanding of the mechanism behind the phenomenon. This is particularly important in order to be able to transform the obtained information to other sites in Canada and Europe. The major outstanding issues are the origin of the observed unsaturated zone at the base of the permafrost and the role of non-frozen areas (taliks) as pathways for groundwater flow. Both of these issues have important consequences for the hydrogeochemical stability in bedrock under permafrost conditions.

2. SITE DESCRIPTION

The Lupin Gold Mine is located in the Nunavut Territory about 1300 km north of Edmonton, Alberta, 80 km south of the Arctic Circle, and 1.3 km from Lake Contwoyto (Figure 1). Lake Contwoyto is 100 km long and between 2 and 5 km wide in the area of the mine. The Lupin Mine is owned by Kinross Gold Corp. (formerly Echo Bay Mines Ltd). Mining activities commenced in 1982 and were suspended in January 1998. The mine was re-opened from April 2000 until August 2003. Following a brief closure between September and December of 2003, mining activities resumed in January, 2004.

All mining activities are located underground, with workings extending to 1450 m below ground surface. Three zones are mined, creating an N-shaped pattern and having a total strike length

of 900 m. Many exploration boreholes have been drilled throughout the mine workings. In this study, horizontal and sub-horizontal boreholes that had been drilled to the east of the mine and below the permafrost (most with a minimum length of 450 m) were selected. These boreholes were selected to allow measurements of the hydrogeological system where changes caused by the presence of the mine would be minimized.

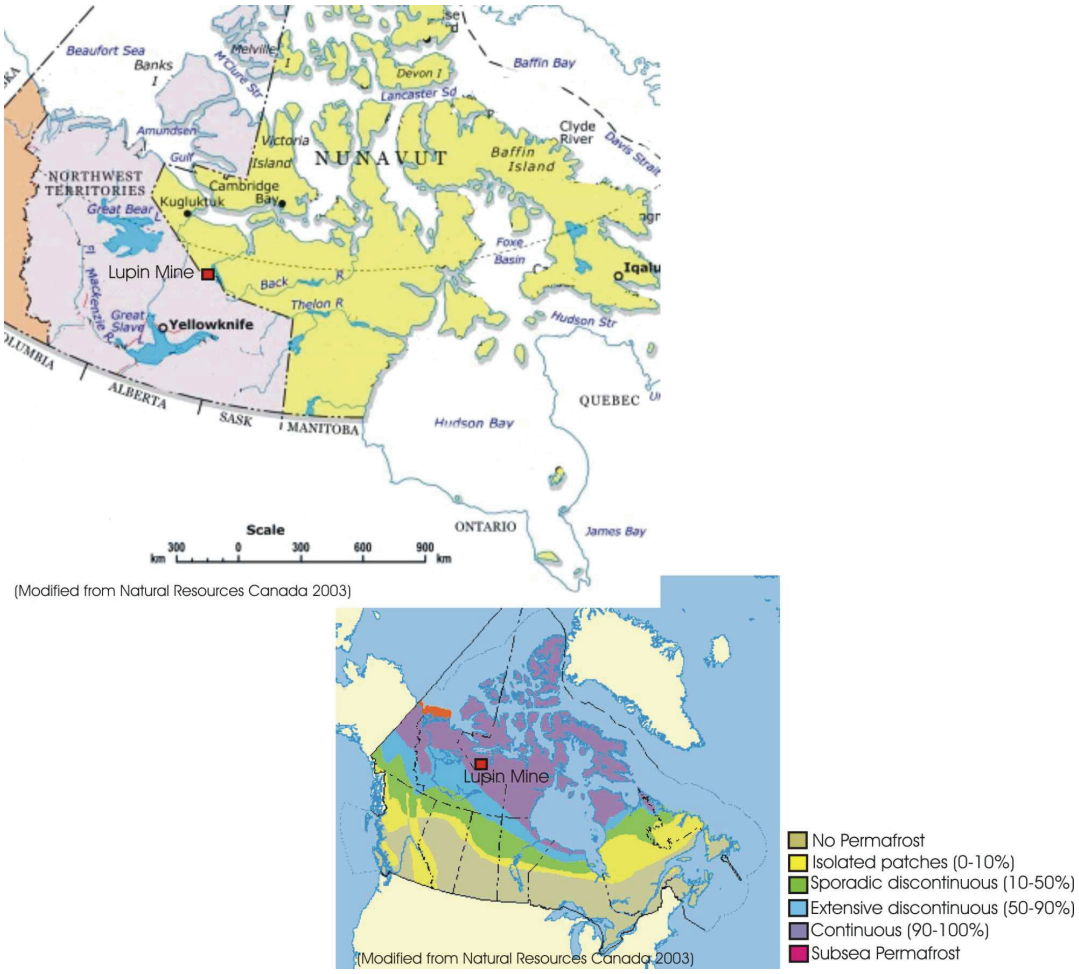

Figure 1: Location of the Lupin Mine and the extent of permafrost in Canada.

2.1 LUPIN MINE GEOLOGY

The gold deposit is located in an Archean metaturbidite sequence that has been subjected to regional and contact metamorphism. Amphibolite facies metamorphism (low pressure, high temperature) has partly destroyed the primary sedimentary structures and produced crystalline rock types, phyllite and quartz-feldspar gneiss, which are the major lithological units at the site.

The sedimentary counterparts (mudstone and graywacke/quartzite) are locally preserved. The lithological units are generally steeply dipping (80-85°).

Three major deformation phases have been identified. The interaction of these deformation events has created a complex fold structure, which is characterised by interference patterns. Large isoclinal folds are bent by younger folding, resulting in distorted semi-closed features. The gold ore is hosted by an amphibolitic iron formation, in which sulphide-poor and sulphide-rich varieties can be distinguished. Mining is focused on a zone of mineralisation which trends roughly N-S.

Three vertical or subvertical structures referred to as V1, V2 and V3 were identified during Phase I of the PERMAFROST project (Ruskeeniemi et al., 2002). Structure V1 is intersected by exploration boreholes at the 250, 890 and 1130 m levels. On the ground surface, the structure is outlined by seismic P-wave minima. It trends roughly N-S, and is hypothesized to be an undulating or discontinuous fracture zone. The trend of fracture zone V2 is also N-S. This zone is generally 1-2 m in width where it intersects the ramp fault (a N-S trending, 1-2 m wide fault zone bisected by the main mine access ramp), and shows evidence of cross-fracturing. The third major structure (V3) is a sub-vertical fault observed at the 890 level, with a thickness less than 0.5 m. This structure is characterized by slickenslides on fractures with calcite and graphite.

In general, fracture infillings are scarce. Most fracture surfaces are polished and may contain some chlorite and/or graphite. Thin calcite fillings are observed in a few fractures. In some shear zones, complex calcite-sulphide assemblages have been observed. The euhedral nature of the calcite and pyrite in these assemblages suggests the crystals formed from hydrothermal solutions. Textural features within these fractures indicate several reactivation episodes. Many of the most prominent infillings occur in sub-horizontal fractures.

2.2 PERMAFROST CONDITIONS AT LUPIN

The site is well within the continuous permafrost zone (Figure 1). Today, the depth of permafrost in the Lupin Mine area extends to between 400 - 600 mbgs. Temperature measurements within the shaft of the mine indicate that permafrost persists to 541 mbgs. The depth of permafrost likely varies due to differences in porosity and heat conductivity of the main rock types (the heat conductivity of amphibolitic rocks is typically higher than for felsic rocks). With the exception of major water bodies, most surface features only affect the thickness of the active layer (the base of which is 1 to 2 m below ground surface) and will not have a significant impact on permafrost conditions at depths of 400 mbgs.

The age of the permafrost at Lupin has not yet been determined, however, the area was glaciated during the last glacial maximum. Peltier (2002) has described the surface hydrogeological response expected due to glaciation. During the advance of an ice sheet, conditions evolve from periglacial to subglacial with the site finally overlain by ice that is several kilometres thick, at the bed of which thermal conditions would be near or above melting much of the time. Permafrost at the Lupin site likely started to form following the rapid retreat of the ice sheet during the last periglacial period, which began approximately 8,000 years ago.

3. PARALLEL AND SUPPORTING STUDIES

Several studies were conducted in parallel with the hydrogeochemical field study by researchers from the University of Waterloo, the Geological Survey of Finland and the NASA Astrobiology Institute. The geophysical GPR survey of taliks around the Lupin site conducted by the Geological Survey of Finland is summarized, and the major findings on lake ice depth and talik existence under various sized lakes are integrated into the discussion. Additional work conducted by the Geological Survey of Finland to determine the mine's water budget is presented as well.

3.1.1 GPR measurement of taliks

Taliks are unfrozen channels in permafrost regions, which may provide routes for discharging or recharging groundwaters through thick, otherwise continuous permafrost. They can be formed in many ways, but typically they are found below large watercourses where the mean annual temperature at the bottom of a lake remains above the freezing point at locations where the lake does not freeze down to the bottom. Near the shallow shore, the ice extends to the bottom when the ice thickness is at its maximum. However, after a certain depth, unfrozen water will occur at the lake bottom. According to Mackay (1992) and Burn (2002), water depth greater than 2/3 of the maximum ice thickness would indicate conditions favourable for the existence of a talik.

The target of the Ground Penetrating Radar (GPR) survey was to gather additional information on the probable talik structures below some of the nearby lakes. Especially interesting is the location of the interface between frozen and unfrozen ground located somewhere near the lakeshore of Lake Contwoyto, since the talik is assumed to be located rather close to the mine. An indirect approach was applied to determine the ice cover thickness and water depth, which can be used to interpret the location of the boundary. More direct observations were also obtained when the properties of the lake bottom sediments were surveyed. The direct and indirect GPR surveys require the use of two different frequencies, and they have different depth penetrations. Using a 400 MHz frequency, high resolution can be obtained, while a lower frequency (40 MHz) provides lower resolution but greater depth penetration (down to about 30 m depth).

3.1.2 The GPR method

GPR is a high-resolution electromagnetic method, based on reflection and refraction of electromagnetic waves at electrical boundaries. The survey system consists of a transmitter, generating high-frequency electromagnetic pulses, and receiver, detecting the reflected waves. The amplitude and travel time of back-reflected waves depends on electrical properties (electric conductivity, dielectric permittivity) of the medium. In highly resistive conditions, GPR can provide information from the depth of up to some tens of meters. In Figure 2, the principle of GPR is presented.

The depths of the reflecting boundaries can be calculated from the Equation (1). This requires an assumption of dielectric permittivity of the medium:

$$e_r = (c/v)^2 \qquad (1)$$

where e_r = relative dielectric permittivity
c = velocity of light (velocity of electromagnetic radiation in vacuum)
v = velocity of electromagnetic radiation in the media.

By solving for v and substituting it into Equation (2), the depth can be calculated:

$$d = vt/2 \quad (2)$$

where d = depth
v = velocity of electromagnetic radiation in the media
t = two-way travel time.

In the depth calculations, the following values of relative dielectric permittivity have been used:

- Snow: e_r = 2
- Ice: e_r = 3
- Water: e_r = 80.

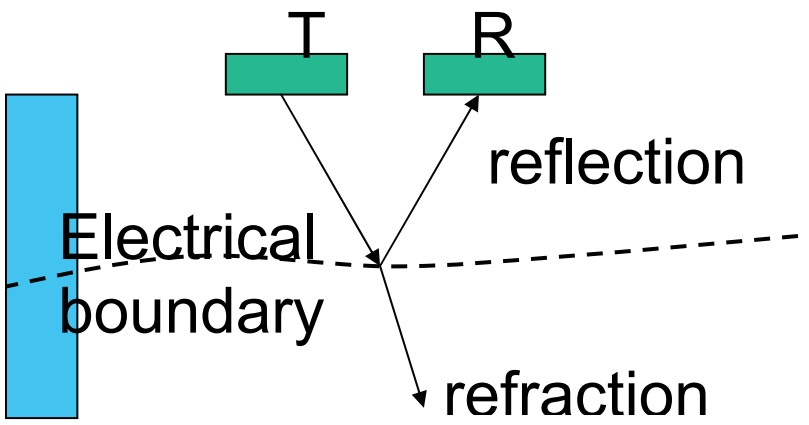

Figure 2: The principle of GPR. T = transmitter, R = receiver.

At the Lupin site, a SIR-2000 pulse radar (by GSSI) with 40 MHz and 400 MHz antennas was used. The measuring time with the 40 MHz frequency was 600 ns (nanoseconds) and with the 400 MHz frequency the measuring time was 40 ns.

3.1.3 GPR at Lupin

Direct observations of the talik boundary beneath Lake Contwoyto were obtained by conducting a ground penetrating radar (GPR) survey. The GPR survey was carried out on ice between the 20th and the 26th of May in 2004 (Figure 3). At this time of the year the ice cover on the lakes has achieved its maximum thickness and the possible disturbing effects of the bottom currents or runoff from the mainland are minimal. The mean diurnal temperatures are still well below zero in May. Although the temperature regime at the lake bottoms is not likely to vary much

during the short summer, the goal of the study was to monitor the extreme permafrost conditions, and therefore the study was conducted in early spring.

Total length of all survey lines used is 28.9 km. A typical survey line was 100 – 200 m long, starting from the mainland and extending far enough out over the lake that the ice cover reached its maximum thickness and free water was observed below the ice. A few long lines exceeded a length of 2 kilometers. Most of the survey lines were traced across the shoreline of Lake Contwoyto. Some test lines were run over small lakes of different diameters to find out the threshold value for talik formation potential. Figure 4 shows the locations of the survey lines at the central study area. Several other smaller lakes in the area were also included in the survey.

Figure 3: It was possible to conduct the survey under the arctic conditions using a vehicle provided by Kinross Ltd. The main unit of the radar and the batteries were in the warm cabin while the antenna was positioned in the sled. The coordinates and the orientation for the survey lines were obtained from GPS.

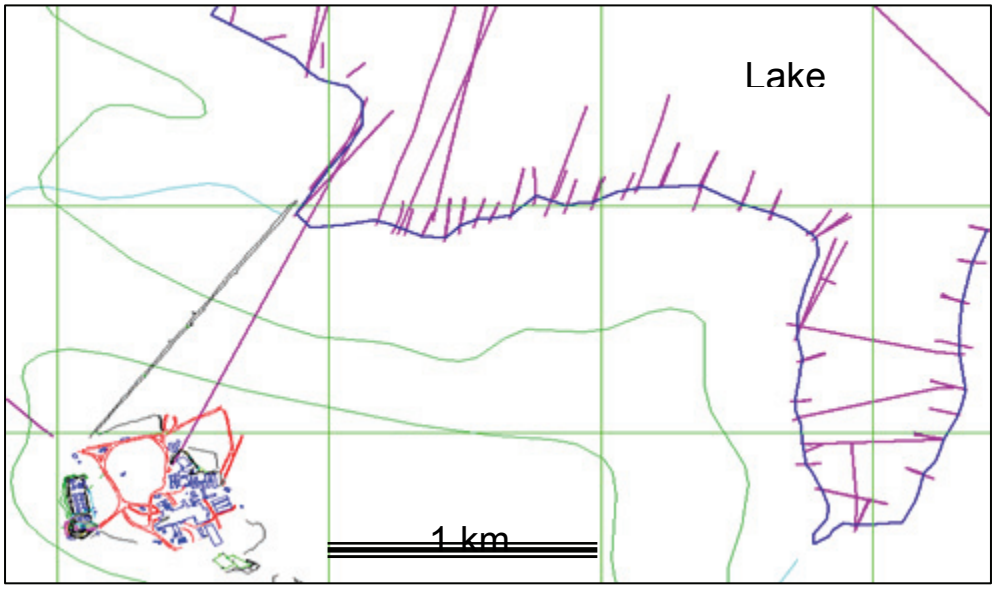

Figure 4: Locations of the GPR survey lines at the central study area. Blue = lakeshore, violet = survey lines. The mine is shown in the lower left corner.

3.1.4 Interpretation of the survey of ground penetrating radar

The primary GPR results are presented as digital images of reflection profiles, showing the amplitudes of reflected pulses on a black-white colour scale, corresponding to their two-way travel time and lateral location. From the profiles, reflecting boundaries were interpreted visually by Mr. Juha Majaniemi, Geological Survey of Finland. In Figure 5, the reflection profiles of three survey lines and their interpretation are presented as an example. The applied frequency is 400 MHz, and the survey direction is from the mainland to the lake. First (on the left side of Figure 5) there is only a snow cover on frozen ground. The upper red line presents the snow/ice boundary, and its starting point indicates the location of the shoreline. The lower red line depicts the ice/water boundary. It can be clearly seen that the ice (the light area between the red lines) thickens as a function of distance until it reaches its maximum thickness and free water begins to occur below the ice. According to the GPR interpretations, snow cover thickness is typically 0.5 m and ice thickness is typically 1.5 m. The snow thickness varies close to the shore due to drifting in lee slopes.

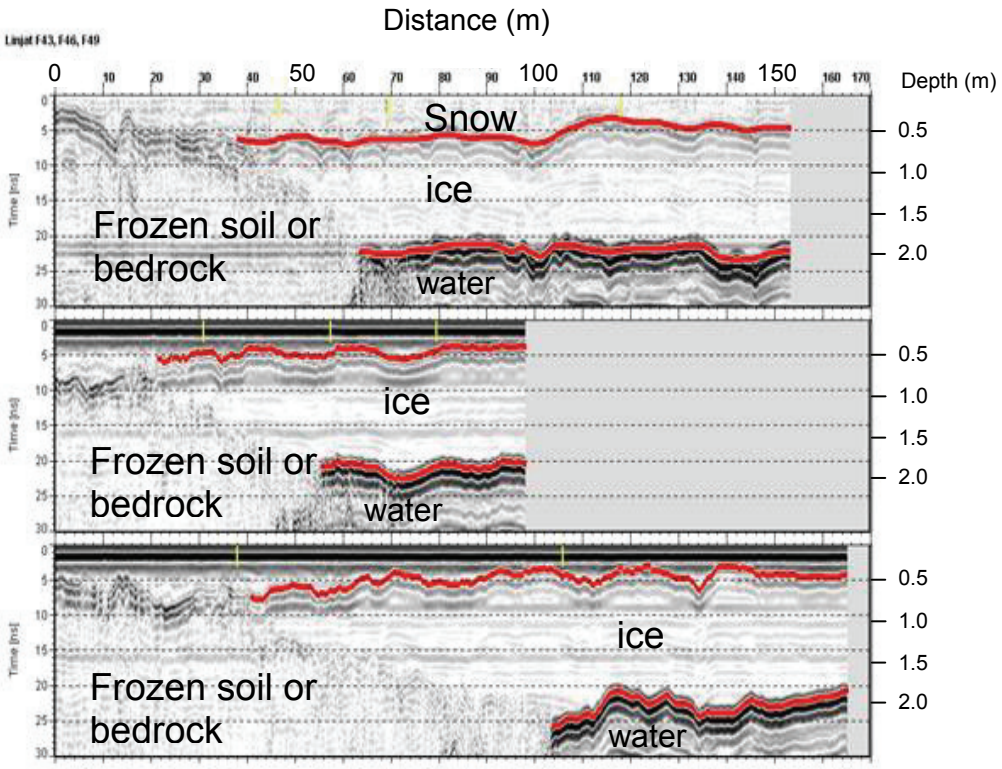

Figure 5: Reflection profiles of three GPR survey lines (F43, F46 and F49) and their interpretation (400 MHz frequency). Upper red line: snow/ice boundary; lower red line: ice/water boundary. The depth scale is calculated based on the following layer model: 0.5 m snow (e_r = 2) and ice (e_r = 3) below the snow.

Figures 6 and 7 represent the results from two survey lines with a 40 MHz antenna. Compared to the 400 MHz frequency, resolution is poorer but depth penetration is better. The snow/ice and ice/water boundaries can not be distinguished, but the properties of the lake bottom sediments can be studied down to 30–35 m depth. The interface between frozen and unfrozen ground can be clearly observed as no reflections are seen from the frozen soil or bedrock, while the unfrozen material is characterized by numerous reflections. The survey line in Figure 6 starts from the mainland, and the shoreline is located at c. 50 – 60 m with the interface between frozen and unfrozen ground below. Maximum water depth is 6.7 m from the snow surface.

The survey line in Figure 7 runs from the mainland to the lakeshore at c. 50 m distance. The water layer is rather shallow here, but unfrozen sediments/bedrock can be observed as intense reflections. Between 150 and 230 m, frozen ground is encountered again, probably indicating a pitfall. From 230 m onward, the ground is unfrozen, and the lake starts to deepen.

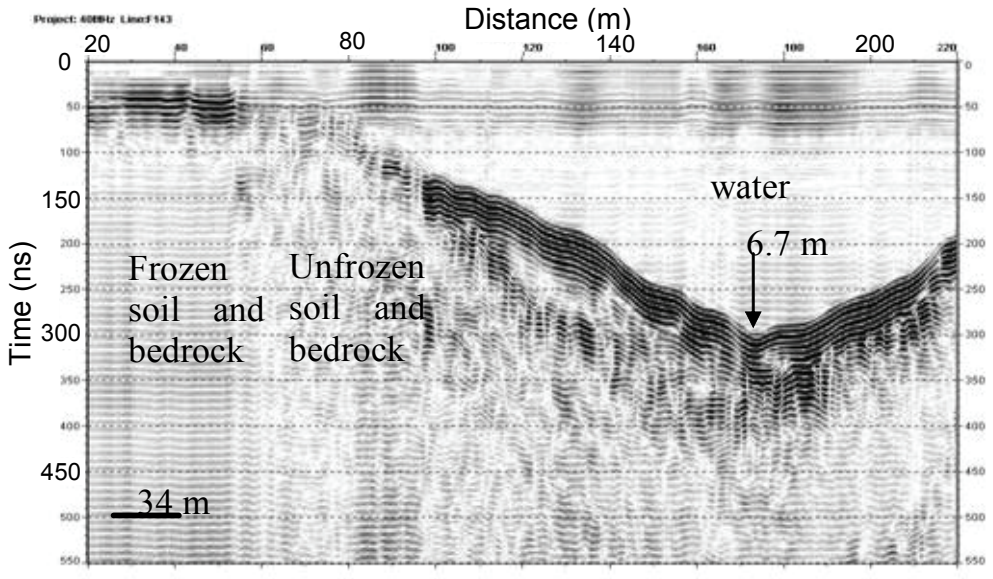

Figure 6: Reflection profile of survey line F143, 40 MHz. Water depth at c. 170 m mark is calculated according to the following layer model: 0.5 m snow (e_r = 2), 1.5 m ice (e_r = 3) and water (e_r = 80) below it. The survey depth at c. 30 – 40 m mark is calculated for frozen soil/bedrock (e_r = 5).

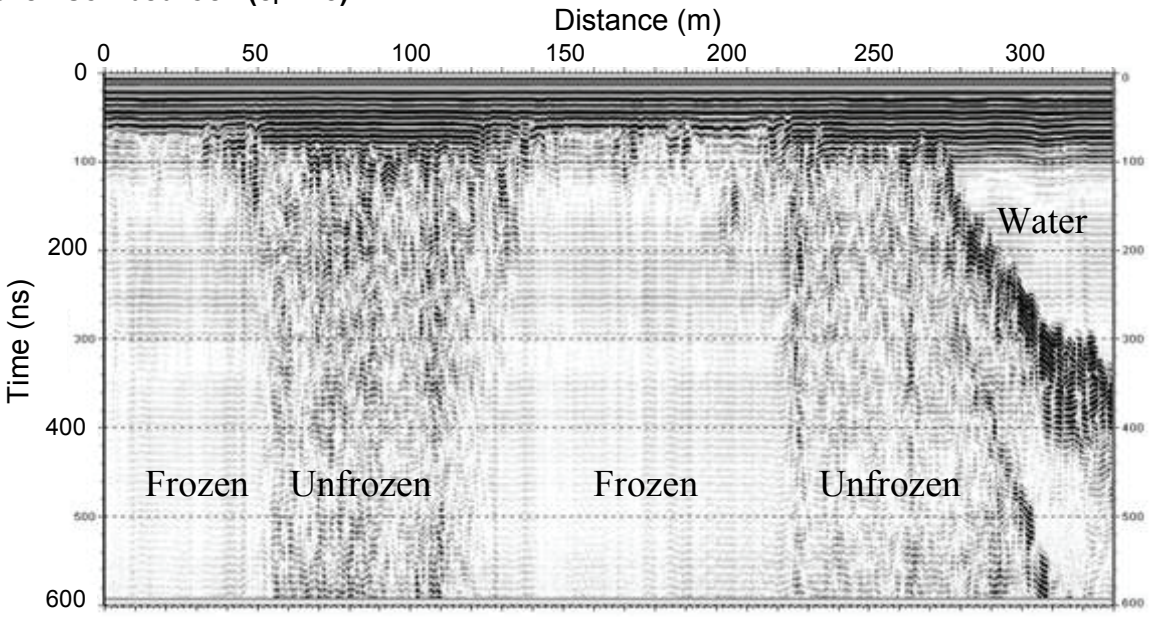

Figure 7: Reflection profile of survey line F116, 40 MHz. The line runs from the mainland to the lake. In the middle of the line, a shoal is encountered. The areas of frozen and unfrozen ground are clearly visible.

The lake bottom sediment seems to be rather homogenous gravel or sand with some scattered boulders. No clays or comparable layers were observed.

The interpretations of the survey lines along the shoreline of Lake Contwoyto are collated in Figure 8. Cyan colour in the profiles indicates thoroughly frozen areas, starting from the lakeshore. Red colour depicts free water below the ice layer, starting typically 30 – 60 m from the lakeshore. This interface is marked by a violet line and it shows the maximum extent of the frozen ground below the lake. Although the maximum depth penetration of the survey is only 30-40 m, the results from geothermal modeling exercises and other research sites (Burn 2002) indicate that the interface between the frozen and unfrozen ground is vertical, therefore no significant displacement with depth is expected.

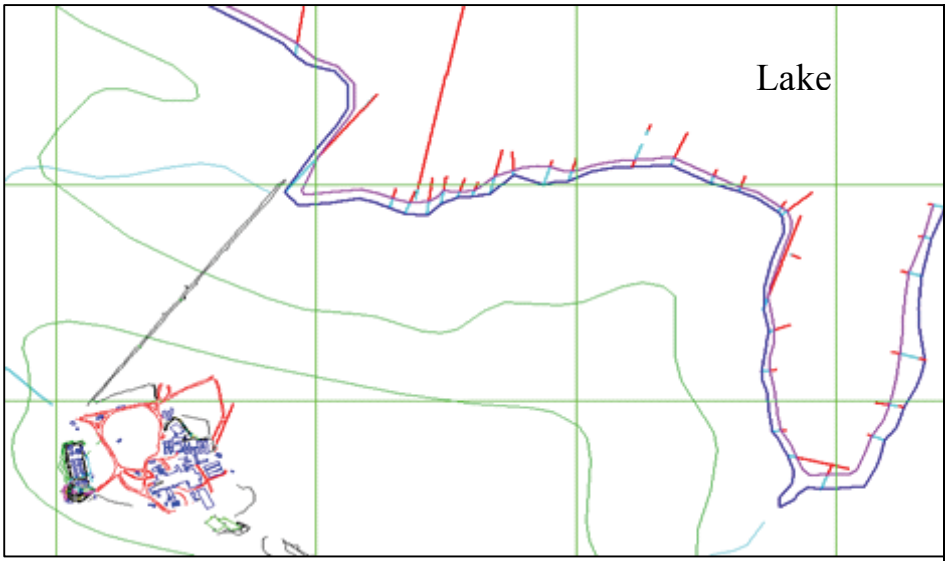

Figure 8: Interpretation of the GPR survey lines at the central study area. Cyan: thoroughly frozen area, red: free water below the ice layer, blue: lakeshore, violet: interface between thoroughly frozen area and free water (based on GPR survey lines). The coordinate grid is 1 x 1 km^2.

Figure 9 shows the interpretations of some GPR lines measured on the smaller lakes SW, W and NW of the mine. Although the diameter of the lakes does not necessarily correlate with the depth of water, certain observations were made regarding lake diameter and talik potential. The lake smaller than 300 m in diameter (Lake 3) froze throughout, while lakes wider than 400– 500 m in diameter retained free water, at least in the deeper basins. It is reasonable to assume that these larger lakes are able to support an open talik beneath (open to the ground surface but enclosed to permafrost below and at its sides) and the lakes wider than 500 m may have potential for a through talik (open to the ground surface and to the unfrozen ground beneath it. Permafrost encases it along the sides).

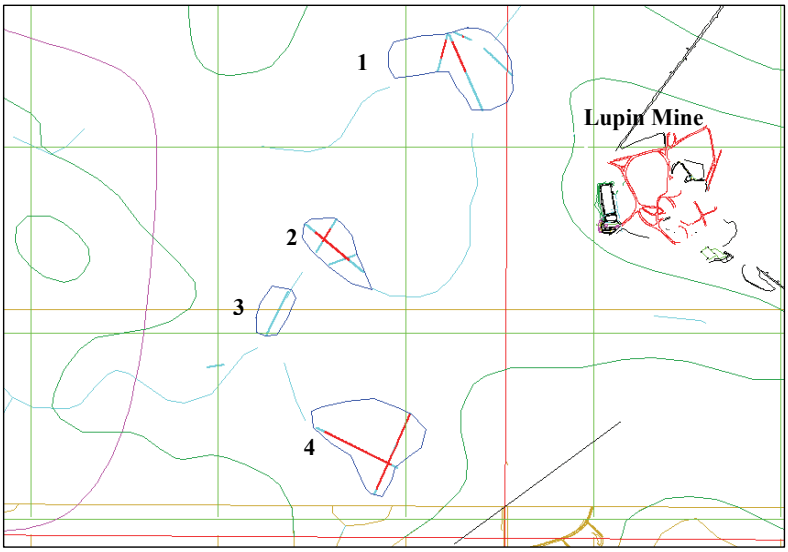

Figure 9: GPR survey lines measured at the smaller lakes and their interpretation. Cyan: thoroughly frozen area, red: free water below the ice layer, blue: lakeshore. The green coordinate grid is 1 x 1 km^2.

3.1.5 The potential role of taliks

The aim of the ground penetrating radar (GPR) survey was to map the interface between permafrost and potential talik structures located below lakes in the Lupin area. The rationale of the GPR survey was that thermal conditions define the distribution of permafrost. If the mean annual ground temperature (at the lake bottom) is below 0°C, conditions are favourable for development or preservation of the permafrost. Positive mean annual temperatures would indicate the potential for disintegration or absence of permafrost (i.e. a talik). There are also empirical guidelines for predicting the occurrence of taliks. According to Mackay (1992) and Burn (2002), water depth greater than 2/3 of the maximum ice thickness indicates potential for talik formation.

The GPR survey was carried out in May 2004 when the ice thickness was at its maximum, c. 1.5 m thick. The interpretation of the survey with a 400 MHz antenna indicated a thoroughly frozen area, extending some tens of meters from the shoreline. Beyond this, water was observed to occur beneath the ice. Free water below the ice layer, particularly during this study when the ice thickness is at its maximum, indicates positive mean annual temperatures at the lake bottom. Accordingly, a talik could be located 30 – 60 m from the shoreline. Based on the model by Mackay (1992) and Burn (2002), a talik could be located 50 – 100 m from the shoreline, supposing that the geometry of the lake bottom is constant. Interpreting GPR data collected using the lower 40 MHz frequency, areas of frozen and unfrozen ground (talik) were distinguished. The results also indicate that the interface between permafrost and the talik is almost vertical beneath the lake, at least to the depth of the upper tens of meters.

The results from the GPR surveys of the smaller lakes also indicate unfrozen water below the ice cover after a certain threshold size of the basin. Extrapolating the results from the smaller lakes suggests that, in the Lupin area, a lake with a size of at least 500 m x 250 m and the

depth of at least 1.5 – 2.5 m may have an open talik beneath the lake, and lakes larger than this have potential to support through taliks.

These interpretations have important implications for hydrogeological considerations. It has been postulated that the deep permafrost effectively seals most of the potential flow routes in the crystalline bedrock, however, if taliks exist, they may act as tube-like conduits through the frozen ground. Figure 10 illustrates lakes in the vicinity of the Lupin mine, with lakes smaller than 300 m in diameter likely freezing throughout, somewhat larger lakes with the potential to support open taliks beneath and lakes wider than 500 m with the potential for a through talik. The potential occurrence of taliks shown in Figure 10 illustrates that the deep permafrost may not necessarily provide a continuous barrier to flow, however future research to determine the role of taliks as pathways for groundwater flow is needed.

The type of talik formation described above requires water basins deep enough to prevent thorough freezing. Their occurrence is not likely during extreme dry and cold climatic conditions, but when warming permits short summer seasons, melt water or rainfall will form ponds and lakes in depressions and the permafrost may begin to degrade due to the geothermal heat flow. Whether these unfrozen conduits provide routes for flow and transport depends on their geological setting, *ie*. their relation to the fracturing and faulting of the underlying bedrock and presence of a driving force. For example, a remote mountain chain could provide such a gradient.

The preliminary geothermal modeling with the Lupin data presented in this report (Section 3.1.4), the work of a number of other modeling groups (*e.g*. Burn 2002) and practical experience at numerous mine sites give support for the interpretation of talik formation at Lupin presented above. The formation of a through-talik is a function of three factors: an insulator (water body, ice sheet, peat bog etc.) at surface, geothermal heat, and time. Due to the physical nature of the heat conductivity, the temperature isotherms are vertical close to the surface. This implies that the interface between the frozen and unfrozen ground would be parallel to these isotherms and forms a vertical wall. This also explains why a relatively slim tube-like structure remains unfrozen under deep permafrost conditions.

The brackish waters observed at 1130 m level (Table 9) may represent inflow from a talik existing below Lake Contwoyto. The salinity is in the same order as in the groundwaters encountered at 890 m level and above. The water is not tritiated and the dating suggests long residence times (Table 9), which would be expected for water infiltrating downwards in a low conductivity media. Taliks also provide a potential route for the surficial microbe populations to interact with the subpermafrost populations. Preliminary hydrogeological modelling indicates that the flow from the talik towards the mine is a realistic scenario, especially under conditions where it is forced by the drawdown due to mining activities.

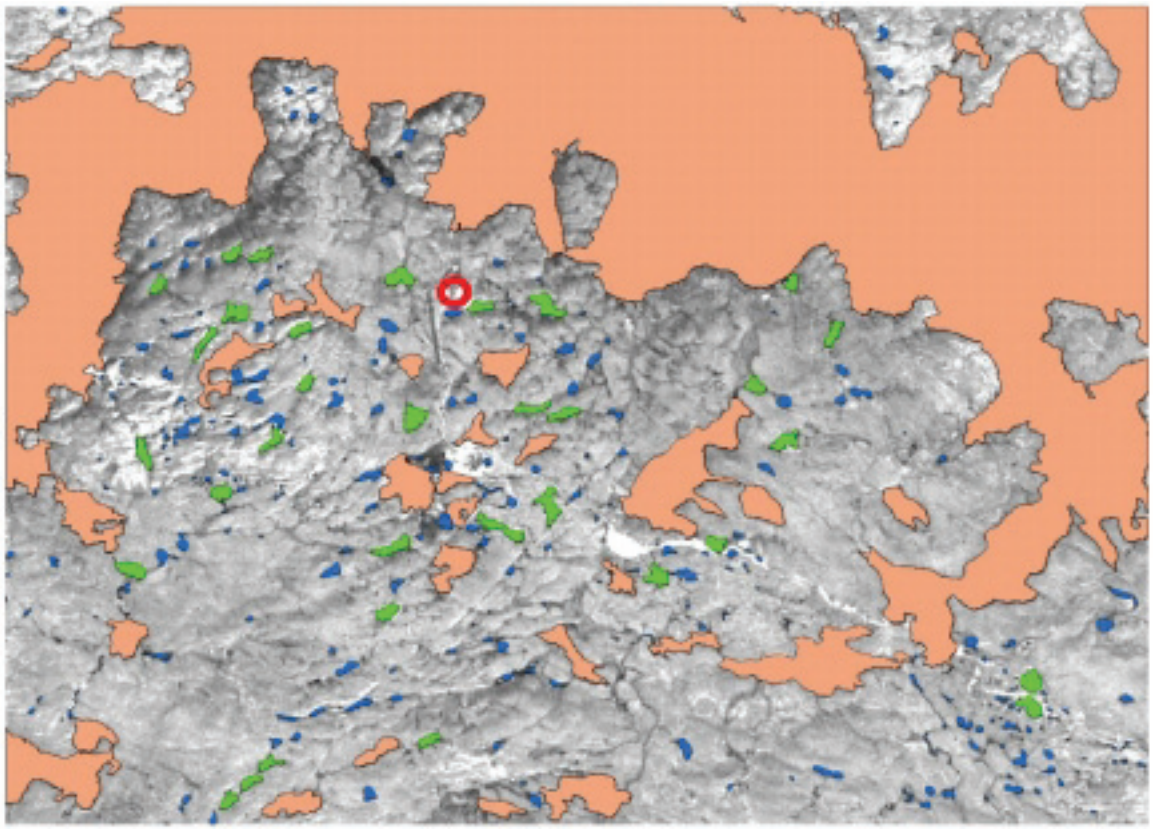

Figure 10: An interpretation of talik potentials based on thermal conditions beneath the lakes in the Lupin area. Potential taliks are classified as open (green) and through taliks (peach). Small lakes and ponds (blue) are frozen down to the bottom most of the year. The satellite image covers an area of 23 x 32 km. The location of the mine facility is indicated by a red ring.

3.2 HYDRAULIC HEAD MEASUREMENTS

Mechanical margot-type plugs with a half-inch lead-in were used to seal a number of research boreholes 3 m from the collar. This depth was assumed to be sufficient to avoid the interference of artificial fissuring generated by the mining activities. A valve and a standard, industrial pressure gauge were installed at the end of the plugs for long-term monitoring. The reading accuracy of the standard gauges ranged from about 20 kPa to 100 kPa (0.2 – 1 bar) and of the more accurate digital pressure gauges from 9 to 17 kPa (0.09 – 0.17 bar), respectively, depending on the scale of the gauge.

Hydraulic pressures were measured in nine boreholes at levels 890 and 1130 in the Lupin mine. The monitoring holes at level 1130 m are subhorizontal, roughly parallel, drilled eastwards and are between 205 and 500 m long. Borehole 1130-273 is the exception, which was drilled northwards and, thus provides information from a previously unexamined area. These holes cover a plane with the area of 500 x 500 m^2. The distance between the collars of the boreholes is about 300 m, and all boreholes produce water and gas. Figure 11 gives the location of the monitoring holes at 1130 m level. Borehole 188 at 890 m level is in a comparable position to 1130-197.

Hydraulic head measurements began with 2 boreholes in late 2002. Since that date, the number of sealed boreholes has increased to 9, either by replacing permanent plugs with margot-type plugs or by sealing newly drilled boreholes, with the latest boreholes sealed in May 2004. The borehole sealing has worked well, with only 2 plugs popping out - one from 1130-192 and one from 1130-197. The sealing/resealing times, the head readings and corresponding depths of the groundwater table, as well as the lengths and the orientations of the boreholes are given in Table 1. Borehole 1130-64, which produces the most dilute water (2 $g \cdot L^{-1}$) at 1130 m level, was sealed for sampling purposes. The up-handed 39-m long hole generates some pressure (7.5 bar), but is likely equivalent to the length of the borehole. Several other boreholes drilled nearby also produced water, but were not sealed for sampling.

A.

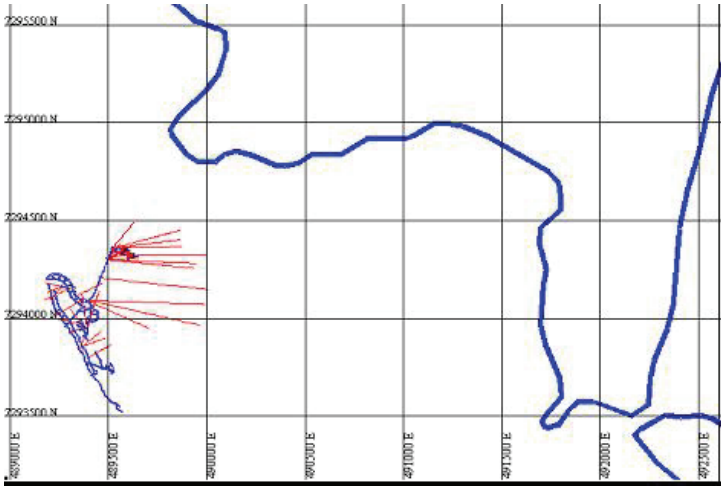

B.

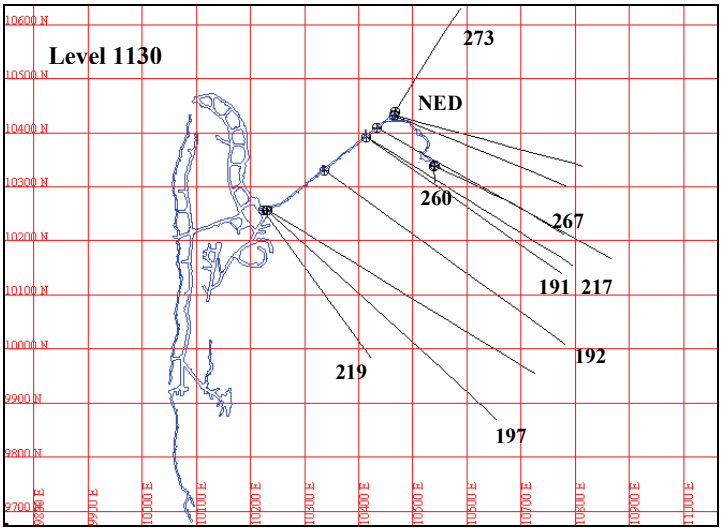

Figure 11: Drilled boreholes at the 1130 m level with respect to the lake (A) and sealed and monitored boreholes (B) (Ruskeeniemi et al. 2002). The coordinate grid is 1000 m (A) and 100m (B). Borehole numbers are located next to each monitored borehole (B). NED is the New Exploration Drift completed in April 2002.

The first hydraulic head observations in 2002 showed that the groundwater table was considerably below the permafrost and that significant differences in hydraulic head existed between the boreholes (Table 1, Figure 12). Over time, a slow increase in heads occurred, and after the multiyear monitoring, with the exception of two boreholes, the groundwater table was 200–300 m deeper than where the base of the permafrost was believed to be. Throughout the monitoring period, borehole 1130-192 showed higher pressures distinct from the nearby holes. This is an interesting observation, since no obvious difference in the fracture pattern was seen in the borehole video survey (Ruskeeniemi *et al*. 2004). Nevertheless, even this borehole indicates a water table depth 40–50 meters below the base of the permafrost.

Borehole 1130-273 has the highest heads observed in the nine boreholes (Table 1). The very first pressure readings in February 2004 showed that the hole is pressurising quickly and the readings from March 2005 indicated that water table is at 537 m depth. It took one year for the water table to recover from 602 m (3.3.2004) to 537 m (3.3.2005) before declining slightly to 552 m (5.10.2005) (Table 1). Prior to sealing, the outflow of the borehole was estimated to be about 3 $L \cdot min^{-1}$ for six months, with considerable gas production observed. This borehole demonstrates that in the close vicinity (within 220 m distance) of the mine, there are isolated hydraulic units which lack natural flow routes towards the mine. Unfortunately, the hole was drilled in the late stages of our project and we were unable carry out a video survey in the hole, thus the distribution of the open fracturing in this part of the system is not known.

Table 1 and Figure 12 give the available pressure readings. Interestingly, the hydraulic heads decreased slightly between March and October 2005, during a time when the deeper levels of the mine were allowed to flood. It can be observed that the boreholes cluster in three groups based on the depth of the calculated groundwater table: high (890-188, 1130-192 and 273), intermediate (1130-191, 197, 217 and 260) and low (1130-219 and 267) (Figure 12). There are some obvious explanations for the common or diverging behaviour, such as the close location and interaction of holes 191 and 217, and the leakage of 197, but in general, the explanation for these groupings is poorly understood. However, the observation is consistent with the outcome from the electromagnetic SAMPO soundings which indicated considerable differences in the depth of the groundwater table at the site (Paananen and Ruskeeniemi 2002).

Table 1: Estimated freshwater heads in nine boreholes. Calculation of freshwater head uses the mine level (*i.e.* 1130 or 890 m) as the Elevation Datum, and assumes 1 kPa = 0.102 m of water.

Sampling Date	890	1130							
	188	192	197	191	217	219	260	267	273
6-9 Dec-02	745	672							
27-Feb-03	710	670	870	930	930				
25-28 Mar-03	698	651	789	864	868				
5-Apr-03		647	785	847	854				
20-25 May-03	686	619	777	806	803	937			
24-Aug-03	662	620	778	785	785	913			
3-Mar-04	679	611	802	784	784	891	780	918	602
14-May-04	659	599	751	760	760	874	815	871	553
25-Nov-04	647	586	742	744	744	981	750	860	549
3-Mar-05	637	592	744	747	744	975	770	992*	537
5-6 Oct-05	640	582	738	751		993	760	*leaking	552
Sealing Date	*05-Dec-02*	*03-Dec-02 22-Feb-03*	*25-Feb-03 29-Feb-04*	*24-Feb-03*	*24-Feb-03*	*24-May-03*	*02-Mar-04*	*02-Mar-04*	*28-Feb-04*

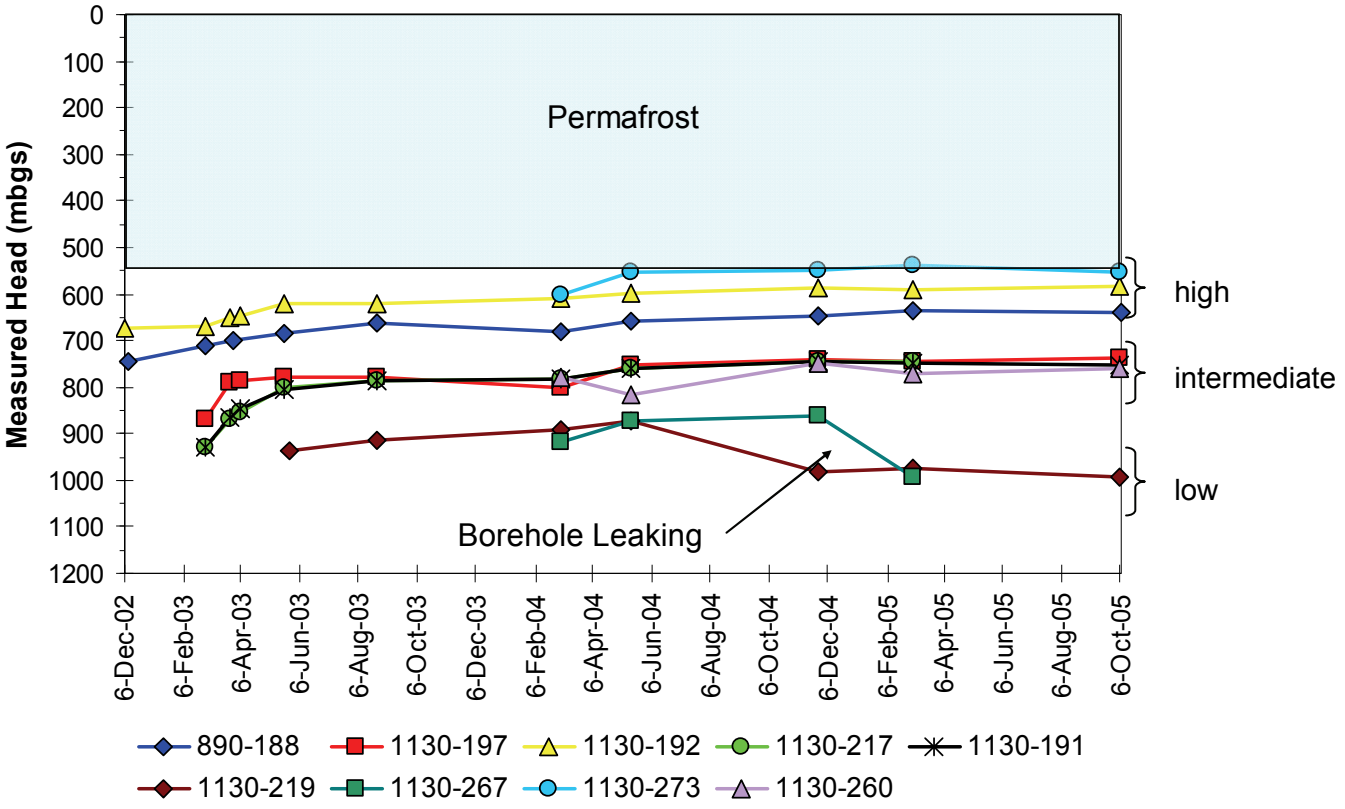

Figure 12: Change in the hydraulic head as a function of time. The depth is based on hydraulic pressure observations in eight boreholes at 1130 m level and in borehole 188 at 890 m level (see Table 1). The base of the permafrost is assumed to be at 540 m depth.

3.3 MINE'S WATER BUDGET

Several natural and anthropogenic sources contribute to the water budget of the mine. The former group includes natural groundwater, although its introduction to a particular mine level involves flow through boreholes. The latter is composed of alien water types, fresh or saline, which are deliberately brought underground (drilling brine, potable water). All water spills are collected in dirty sumps and are re-circulated after clarification. Water ending at the bottom of the mine is pumped up to the surface into the sewage lagoon at a rate of slightly above 50,000 m^3 per year.

Most of the mine's water sources are not well defined due to the lack of long-term consumption or monitoring records. However, certain assumptions can be made based on the field observations and data collection carried out during this project. The following water budget is a reconstruction representative of the mine prior to the year 2003 when the research boreholes were still flowing freely.

3.3.1 Fresh water

The fresh water consumption is related either to the lunch rooms or to the Mechanical Shop at 650 m level. The fresh water is pumped directly from Lake Contwoyto and is distributed to the different underground levels through a 2 inch diameter pipe line. There are six permanent refuge stations which serve as lunch rooms. The taps are flowing continuously at an average flow rate of 3.1 L/min/tap (9800 m^3/year) to avoid over pressurization and breakage of the pipe line. The fresh water consumption at the 650 m level Mechanical Shop is mainly due to one tap flowing continuously with the rate of 12.4 $L \cdot min^{-1}$ totalling 6500 m^3 per year. The water consumption at the related high-pressure washing station is difficult to estimate due to casual use, but is approximately 100 m^3 per year, bringing the mine's total annual fresh water intake to 16 400 m^3.

3.3.2 Brine

Sodium chloride brine has been used historically as process water (eg. as a drilling brine) in the permafrost levels of the mine. Over time, the brine consumption has varied greatly. During the first years of development, all the activity took place in the frozen ground and a large amount of brine was pumped down to the working levels. When the mine was deepened below the base of the permafrost, much of the process water was recirculated brine since the inflow of the groundwater was limited. Dirty brine was collected to clarification sumps from which the clear water was again pumped to the production levels.

The brine was produced by dissolving NaCl salt in fresh Lake Contwoyto water in large tanks. The target concentration was 6.6 wt-% of NaCl. However, in practice the NaCl concentration in the brine has varied a lot. Brine was pumped down to the mine according to need and no records of brine usage were kept. In 2003 the salt consumption was reported to be 71,000 kg which would correspond to 1076 m^3 of brine.

3.3.3 Groundwater

Groundwater flow into the mine was insignificant until the early 1990's when the exploration drift was run and the boreholes were drilled at the 1130 level. The newly excavated drifts seem to drain the exposed fracture networks rather quickly as indicated by the flow rates of the

boreholes in the new exploration drift at 1130 m level. In addition, PERMAFROST Project workers have visited the area several times a year since the tunnel was drifted in 2002 and observed that only minor amounts of water was dripping from the walls and ceiling although the exploration boreholes are flowing generously (Table 2).

Table 2 provides the flow rates from the boreholes known to be flowing in 2003. Due to rough rock surfaces and fracturing at collars, a bypass of 20% is assumed to influence the measurements.

Table 2: Measured flow rates from boreholes known to be open in 2003.

Level	Borehole	Length (m)	Orientation	Flow ($L \cdot min^{-1}$)	Flow/year (m^3)
890	188	523	subhorizontal	7.7	4047
1105	57	482	subhorizontal	2	1051
1130	181	495	subhorizontal	4.3	2260
1130	192	549	subhorizontal	6.4	3364
1130	197	574	subhorizontal	4.5	2365
1130	175	900	subvertical	4	2102
1130	176	900	subvertical	4	2102
				Total measured flow	**17 292**
				Total including estimated 20 % bypass	**20 750**

3.3.4 Additional water sources not included in the calculation

There are number of additional sources which contribute to the mine's water budget. Their quantification and their relative importance are difficult to assess, but their quantities are estimated to be 14, 774 m^3/year (i.e. the difference between the annual pumping rate of 53,000 m^3 and the identified sources (38, 226 m^3)) (Table 3). The major contribution of this added water is assumed to be from approximately 10 sealed, but variably leaking, boreholes. The following additional sources may also be contributing to the mine's water budget: melt water seepage along the ramp especially during spring time, breaks in the fresh water pipe line, fluids from the waste fill pumped into the abandoned drifts, and melting of the base of the permafrost. Data available at this time is not able to quantitatively assess relative inputs from these potential sources.

Table 3: The water budget of the Lupin mine calculated for the year 2003.

Water source	Annual amount (m^3)	% of the total
Fresh water	16 400	31
Brine	1 076	2
Groundwater	20 750	39
total	**38 226**	72
Not defined	14 774	28
Annually pumped	**53 000**	100

4. HYDROGEOCHEMICAL STUDIES

4.1 GROUNDWATERS

4.1.1 Chemistry

Water Samples

Chemistry samples were collected during all four field trips conducted during Phase III of the PERMAFROST Project. Most of the samples were collected from the sealed research boreholes at the 890 m and 1130 m levels in connection with other sampling activities (gases, microbes, groundwater residence times, etc.). The goal was to observe possible changes in groundwater conditions, and to achieve a complete characterisation of the groundwater system for a given sampling opportunity. By March 2005, a total of 145 chemistry samples were collected from the site. The samples have been analyzed for major and trace elements including rare earth elements. For more details on these analyses, see Ruskeeniemi *et al*. 2002 and 2004.

Crush and Leach

In order to further explore pore fluid chemistry, Phase II of the PERMAFROST project included collection of sections of core from exploration boreholes at the site for crush and leach studies (Frape et al., 2004). Preliminary results from the crush and leach analyses were reported in Frape et al., 2004, and final results from the crush and leach analyses from boreholes 570-105, 550-112, 570-106 and 890-188 are presented in this report. This allows for the comparison of pore fluid compositions (as estimated by crush and leach samples in Phase II) with water compositions for samples collected as part of Phase III of the PERMAFROST project (Section 4.1.1).

4.1.1.1 Trends with depth

The tritium with depth diagram (Figure 13) illustrates the division of very young waters (water molecules) from older, probably resident, groundwaters. The surface waters and precipitation have a considerable range of ^3H (7 to 20 TU) in keeping with tritium distributions reported by other studies in the region (Rossi 1999). The tritium concentration in shallow waters and waters associated with the ramp fault within the permafrost reflect the rapid infiltration of tritiated surface waters due to drawdown from mining activities. The drilled holes 570-105 and 550-112

have initial tritium values equivalent to the surface waters used as drill fluids (Figure 13). However, with time the tritium levels dropped, particularly in borehole 105, likely as the drill fluid slowly drained from the borehole and was replaced by older fluids from within the rock mass. Deeper subpermafrost fluids often have small amounts of tritium, possibly due to slight contamination from mine activity. Boreholes closer to the location of the suspected talik had slightly higher tritium levels, which may potentially indicate a connection to young, tritiated surficial waters via the talik structure. Interestingly the tritium levels in several boreholes decreased below detection with time after the boreholes were packered and sealed, suggesting contamination with ^{3}H occurred during drilling of the boreholes.

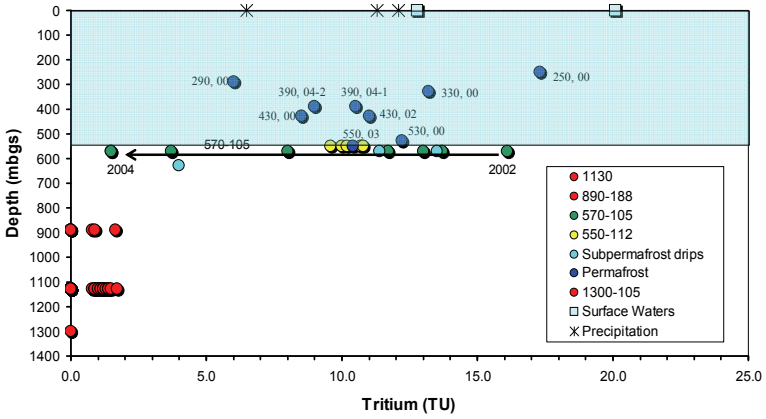

Figure 13: Depth vs. tritium activity for water samples from throughout the Lupin Mine. Blue shading shows the depths affected by permafrost. Permafrost samples are labelled with the depth and the year of sampling.

Figure 14 illustrates the influence of a major spill of salt at the site, and salt (NaCl) used in drilling within the permafrost. Most shallow and permafrost waters are Na-rich, likely due to NaCl salt contamination. With time the drilled boreholes, particularly 570-105, show a trend towards more Ca-rich, rather than Na-rich, waters. A similar change with time is observed in the deeper packered boreholes. This trend may be due to the influence of the resident groundwater at the site, which appears to be Ca-dominated.

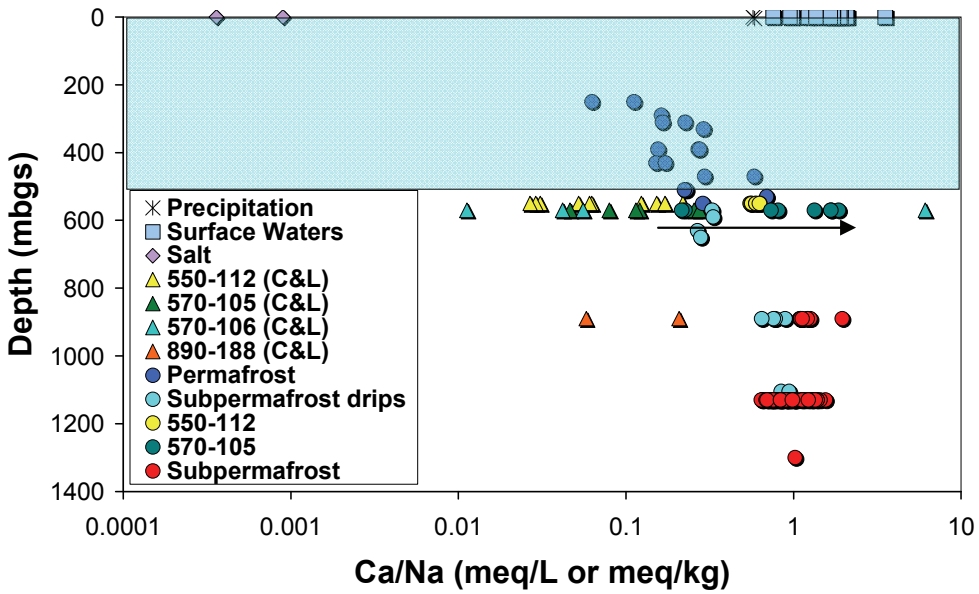

Figure 14: Ca/Na trends with depth in Lupin waters. Black arrow illustrates the trend of more Ca-rich waters with time in 570-105.

Looking at major anions at the site, waters associated with drips and other flows in the permafrost zone appear to fall on a mixing line between an anthropogenic NaCl salt and the deeper Ca-rich fluids (Figure 15). However, the research boreholes, particularly 570-105, show a deviation from the trend. Results from rock leaching studies (C&L) revealed dilute fluids, although similar matrix salinities were found at High Lake (Holden et al., 2009). The lack of matrix salts means that for many parameters, the geochemical signature of saline fluids found in faults cannot be overprinted by rock pore fluids. Using the current data set, it is not possible to determine whether the low salinity is due to site specific or periglacial/glacial processes. As the research boreholes have been shown to generally penetrate more isolated rock zones and have fewer contaminated zones, and assuming fluids extracted during C&L are representative of matrix fluids, the deviations in fluids from these boreholes with time is probably reflecting the influence of the resident rock fluids.

A.

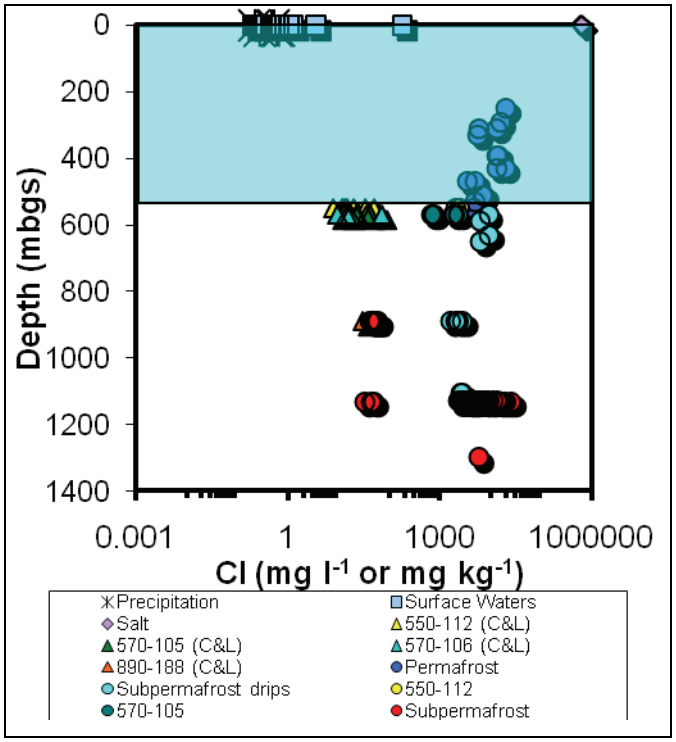

B.

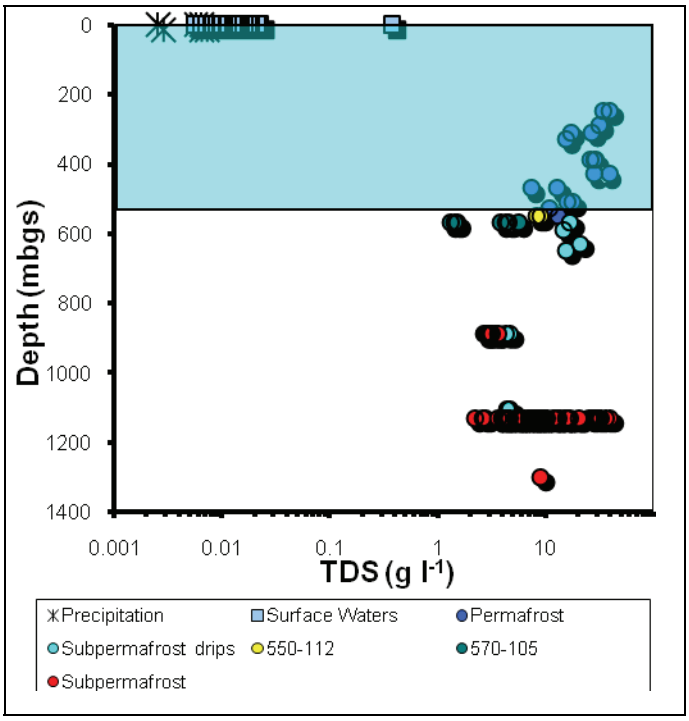

Figure 15: Chloride (A) and dissolved solid (B) trends with depth at the Lupin site.

TDS values tend to follow the same trend as Cl with depth. Interesting to note is the variation of TDS with time in the individually packered boreholes on the 890 and 1130 level (Figure 16; Stotler 2008). The salinity of the water in the boreholes varied over the five years of the study (up to ± 10 $g \cdot l^{-1}$ in a single borehole) and does not correlate with the hydraulic heads (Figure 12, Figure 16). For instance, the highest pressured borehole, 1130-273, has a variable TDS around 8-12 $g \cdot l^{-1}$. The other high-pressure hole (1130-192) has the highest salinity recorded from the site (38 $g \cdot l^{-1}$). Only boreholes 890-188 and 1130-64 showed a constant TDS over the 5 years of study. Boreholes 1130-192 and 1130-175 both show an increasing trend in TDS with time, but the remaining boreholes sampled showed no consistent pattern in TDS. The TDS/head data suggests the boreholes may be intersecting different fracture networks which have different salinities. Possibly due to a connection created by the drilling and sealing of the boreholes, the fracture networks may currently be in a transient state and are seeking a new equilibrium. Like the pressure data (Figure 12), boreholes can be grouped into 3 sets based on salinities; a high salinity water (~38 $g \cdot l^{-1}$), medium salinity water (between 8 and 20 $g \cdot l^{-1}$), and a low salinity water (< 5 $g \cdot l^{-1}$) (Figure 16).

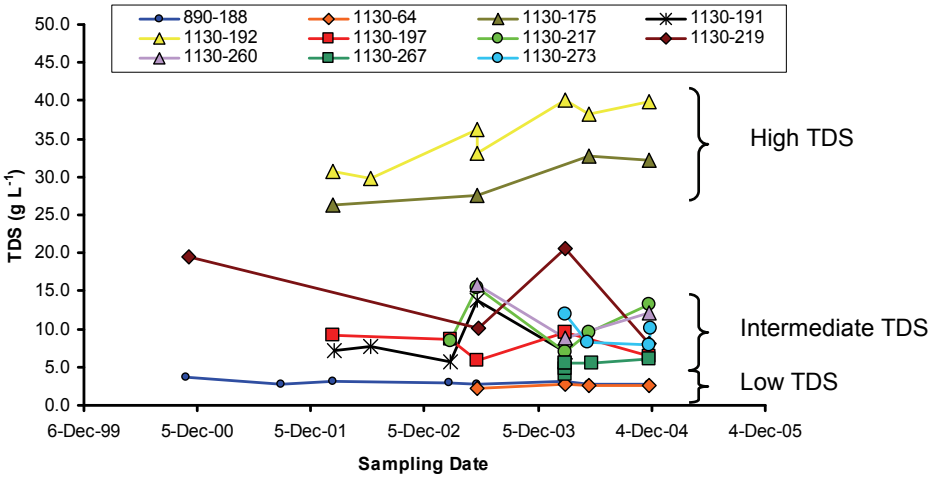

Figure 16: TDS variability in various boreholes in different sampling events at the Lupin site.

Bicarbonate concentrations range from 0 – 281 mg/L within the permafrost/subpermafrost part of the site (Figure 17). As with most other parameters, this is most likely due to variable inputs and potential mixing between waters associated with faults open to surficial areas in and around the mine. These downward penetrating fluids (which are also associated with salt and nitrate 'contamination') are mixing with older 'matrix' fluids that have a similar or lower HCO_3 content. As well, a strong control on the bicarbonate system may be due to the abundant carbonate found as fracture fillings throughout the rock mass from 250 meters to approximately 600 meters in depth. In general, the permafrost waters have the highest concentrations of bicarbonate and often have greater than 10 tritium units (Figure 13; Figure 17), indicating that a considerable component of these waters is very young. The origin of the bicarbonate ions in this young component may have implications on the evaluation of carbon dating of the permafrost waters. It should also be noted that the surficial waters are very low in HCO_3.

Deeper permafrost and subpermafrost fluids have much lower concentrations of HCO_3 (Figure 17). The bicarbonate concentrations in the deeper borehole fluids are variable over the sampling period 2000-2005; but fall within a narrow range of values for each borehole (*e.g.* 192:

5.5 to 9.2 mg l^{-1}) (Stotler 2008). Low values of bicarbonate similar to those found at Lupin occur at many other Canadian Shield sites in fluids at similar depths; however, these fluids have much higher salinity than at Lupin (Frape and Fritz, 1987).

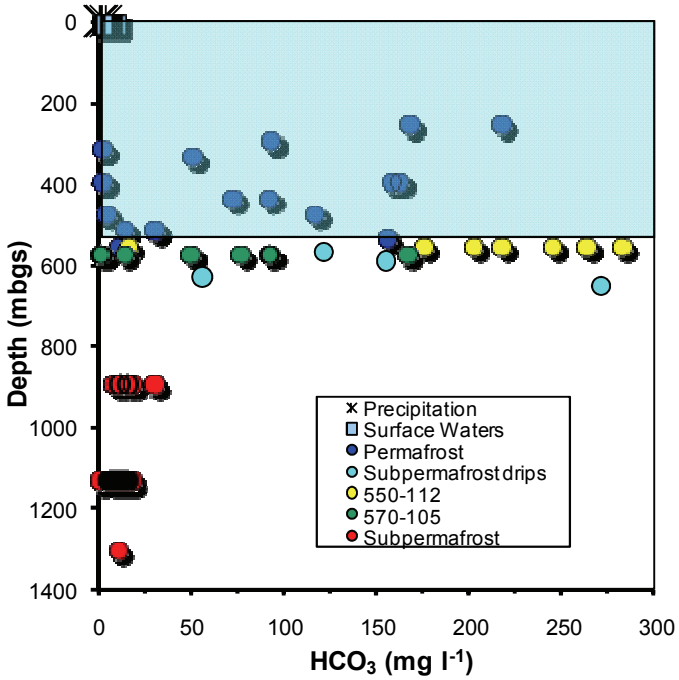

Figure 17: Trends in bicarbonate with depth at the Lupin mine.

Concentrations of SO_4 and NO_3 are elevated within the permafrost zone (Figures 18 A and B), and this is assumed to be due to contamination from salt and blasting powders. Again the drilled research boreholes show decreases in SO_4 and NO_3 concentrations with time as the impact of the contamination is mitigated by mixing with uncontamined in situ ground waters (Stotler 2008). Deeper boreholes in the subpermafrost zone show little or no increase in sulphate and nitrate over time (Stotler 2008). The crush and leach studies on sections of core did not find sulphate in the rock matrix (nitrate was not analyzed).

It has been reported in the literature that pelitic rocks like those at Lupin can contain considerable amounts of NH_4-NH_3 (1000 ppm) (Haendel et al. 1986, Bebout and Fogel 1992, Bebout 1997, Holloway et al. 1998, Mingram and Bräuer 2001). As well, other sites in Yellowknife (Giant and Con mine) and northern Manitoba (Fox mine) have recorded NO_3 at depth in mine waters (30 – 350 mg·l^{-1}) (Frape and Fritz 1981, MacDonald 1986). Initially, it was assumed the elevated values of nitrate found in the permafrost at Lupin (Figure 18B) were attributable to mining activities (nitrogen from the use of ammonium-nitrate/fuel oil explosives). However, of all the Canadian or Fennoscandian Shield sites studied, only samples from the Macassa, Sigma, and Con Mines have recorded nitrate concentrations over 100 mg·l^{-1}, and only Macassa over 1000 mg·l^{-1} (3070 mg·l^{-1}) (Fritz and Frape 1981, MacDonald 1986, Jones 1987). Studies at the URL site in Manitoba showed small increases in NO_3^- concentrations in fractures adjacent to blast sites, however concentrations returned to pre-blast levels within only two hours

of the blast (Gascoyne and Thomas 1997). However, some researchers have described nitrogen quantities of 1000 mg·kg^{-1} in similar metaturbidites (Table 4) (Holloway et al. 1998, Mingram and Brauer 2001) not associated with mines. It has also been shown that the massive amounts of nitrogen in metaturbidite rocks contributes large percentages of nitrate to streams in mountain watersheds in California (Holloway et al. 1998).

A.

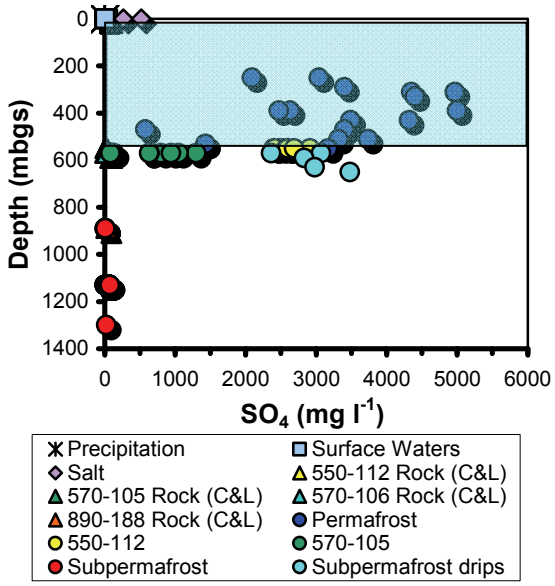

B.

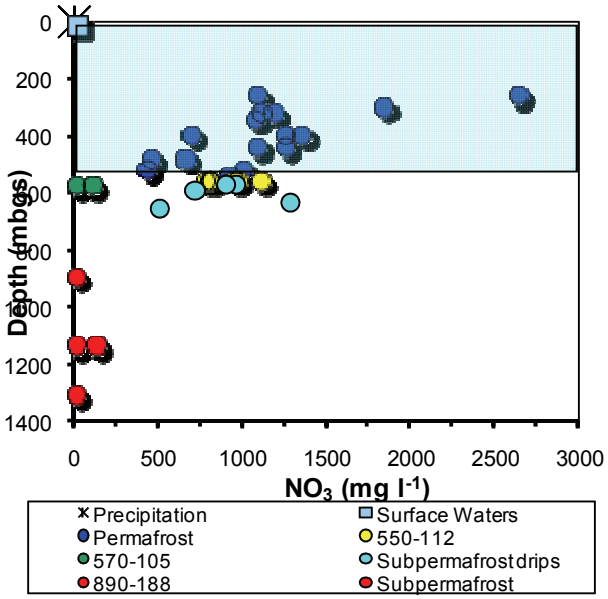

Figure 18: Trends with depth of sulphate (A) and nitrate (B) in waters and crush and leach samples from the Lupin site.

Table 4: Comparison of the nitrogen content of different metamorphic rocks similar to those found at the Lupin site.

Rock Type	Metamorphic conditions	mg-N kg^{-1}	NH_4^+ ppm	$\delta^{15}N$ ‰	Ref.
Phyllite		1034 ± 255			1
Slate		977 ± 377			1
Biotite Schist		717 ± 145			1
Metavolcanic breccia		385 ± 92			1
Greenstone		245 ± 52			1
Low grade unit	<2 kbar, 300°C		620-775	1.2-3.2	2
Phyllite	~2 kbar, 300°C		460-875	1.7-2.6	2
Garnet-Phyllite	~9 kbar, 470°C		376-896	2.3-5.5	2
Mica Schist/Eclogite	>12 kbar, 550°C		150-539	2.5-5.2	2
Gneiss/Eclogite	>12 kbar, 730°C		76-130	5.7-10.5	2
Transition Zone			40-370	1.2-3.8	2
Gneiss Unit	6-8 kbar, 590-650°C		35-120	2.5-3.6	2
KTB pilot hole			35-362	1.2-12.2	2

1. Holloway et al., 1998
2. Mingram and Bräuer, 2001

To differentiate between some of the potential sources of nitrogen at the Lupin site, $\delta^{15}N_{NO_3}$ and $\delta^{18}O_{NO_3}$ were analyzed (Figure 19). The measured range of $\delta^{15}N_{NO_3}$ and $\delta^{18}O_{NO_3}$ values were +2.62 to +11.73 ‰ AIR and -0.78 to +27.62 ‰ SMOW, respectively. Eight of the eleven samples have $\delta^{15}N$ values between 4.5 and 8.0 ‰ AIR, close to NO_3 fertilizer values (fertilizer $\delta^{15}N$ and $\delta^{18}O_{NO3}$ are very similar to expected ammonium-nitrate fuel/oil explosive mixture values), but very few actually plot within the range (Figure 19). The similarity of $\delta^{15}N_{NO_3}$ values at Lupin to NO_3 fertilizer values suggests that a significant portion of the NO_3 in the permafrost may be due to blasting at the mine. In two of three repeat analyses over four years, $\delta^{15}N$ values remained very similar, with $\delta^{18}O_{NO3}$ changing ~20‰, but in opposite directions. In the third repeat analysis, $\delta^{18}O_{NO3}$ remained the same but $\delta^{15}N$ increased by 3‰. This variability in $\delta^{18}O_{NO3}$ and $\delta^{15}N_{NO_3}$ over time may be due to a varying proportion of a natural component to the nitrate, however the nitrogen content in rocks at the Lupin site have not been studied to date. It may be that the nitrate at the Lupin site is a blasting remnant, and that denitrifying bacteria and conditions are absent in the permafrost at the site, resulting in the persistence of remnant nitrate from blasting at the site. Microbial studies in the subpermafrost have isolated several denitrifying bacteria, however they are not obligate denitrifiers, and there is no direct evidence for denitrification in the subpermafrost waters (Bakermans et al., 2008; Stotler 2008).

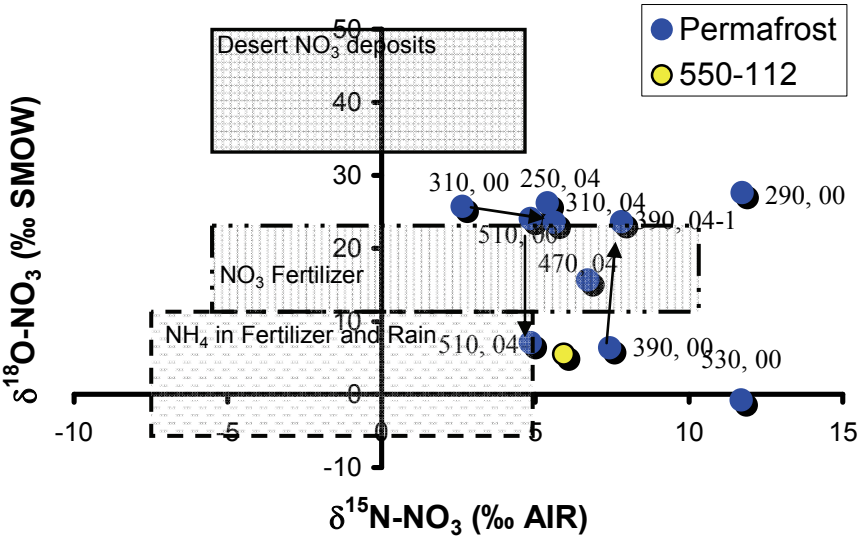

Figure 19: $\delta^{18}O$ vs. $\delta^{15}N$ in nitrate in permafrost samples from the Lupin site. Typical values for NO_3 (desert deposits, fertilizer (amyl-nitrate)) and NH_4 (fertilizer, rain) (from Kendall and Aravena 2000) are shown. Numbers by each data point (i.e. 310, 00) indicate sample depth and year sampled, respectively.

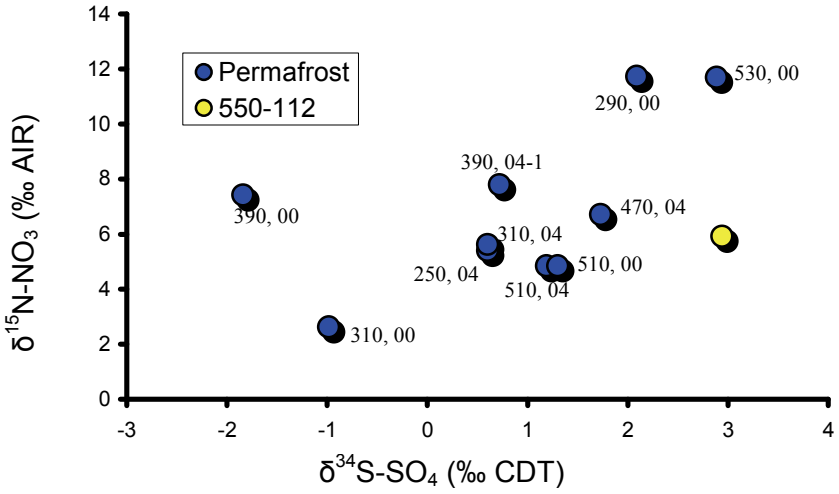

Figure 20: $\delta^{34}S$ in sulphate vs. $\delta^{15}N$ in nitrate in permafrost samples from the Lupin site. Numbers by each data point (i.e. 310, 00) indicate sample depth and year sampled, respectively.

In groundwaters at the Lupin Mine, sulphate concentrations are highest in waters sampled in the permafrost zone, and decrease with depth (Figure 18A). Sulphate concentrations in permafrost waters are up to two and a half orders of magnitude higher than concentrations in deeper waters at the 890 and 1130 levels (0 and 35 mg L^{-1}). Between the 290 and 390 levels waters have some of the highest sulphate concentrations, and are acidic (pH ~ 3.2 to 7.6) (Stotler 2008). Three possibilities for the source of these high sulphate concentrations were investigated and are described in Stotler (2008): importation of sulphate with the drilling brine;

dissolution of sodium sulphate precipitated due to permafrost formation; or oxidation of iron formation sulphide minerals. Based on sulphate concentrations in the drill salt (Figure 18A), and the Na-source at the site (drill brine; Figure 14), oxidation of sulphide in the iron formation (Section 2.1) is likely responsible for the high concentrations of sulphate in the permafrost waters. In a process similar to acid mine drainage, this oxidation of sulphate in the permafrost has resulted in the acidification of permafrost waters, however it is unclear whether the formation of sulphate was coincident with formation of permafrost (i.e., whether or not oxic conditions are a typical permafrost phenomenon) or is an artefact of mining operations at the site.

As waters become more oxic and sulphate concentrations increase, $\delta^{34}S$ values become more depleted (Figure 21). Comparing the isotopes of sulphate ($\delta^{34}S$ and $\delta^{18}O$-SO_4) from Lupin samples with other shield sites, it is evident that the isotopic composition of sulphate in the deeper Lupin groundwaters is similar to other shield brines (Figure 22) (Fritz et al. 1994). However, the evolution of waters from the shallow permafrost to the deeper waters at Lupin is different (based on $\delta^{18}O$, $\delta^{34}S$ of sulphate) than what was observed at the Palmottu site in Finland (Figure 22), which has previously been described as a hydrothermal end-member.

$\delta^{18}O$ values of sulphate were analyzed to determine whether sulphide oxidation was occurring naturally, or is an artefact of mining operations. The two most probable sources of oxygen in sulphate at Lupin are i) oxygen bound to the water molecule or ii) gaseous or dissolved oxygen. The $\delta^{18}O$ value of atmospheric or dissolved oxygen is +23.7‰ SMOW (Kroopnick and Craig, 1972), and an abiogenic fractionation of -10 ‰ SMOW is associated with the incorporation of oxygen from atmospheric or dissolved oxygen into dissolved sulphate, while fractionation associated with oxygen derived from the water molecule is only -3 ‰ (Krouse and Mayer, 2000). Based on the $\delta^{18}O$ values of SO_4 in the permafrost waters (-12 to -16 ‰ VSMOW; Figure 22), the most significant source of oxygen for sulphate is from water, indicating that the oxidation of sulphides to produce sulphate occurred largely in the absence of atmospheric or dissolved oxygen (Figure 23). Figure 23 is a plot of the expected difference between the $\delta^{18}O$ of water and sulphate over a range of temperatures compared with Lupin samples at the sampling temperatures, considering only equilibrium fractionation. As shown in the plot, Lupin samples have a much smaller $\Delta^{18}O$ than is expected for the current temperature regime (i.e. 0° C), indicating (if an equilibrium model were to be used) that either the sulphate formed at much, much higher temperatures (roughly equivalent to ore formation temperatures), or that sulphate production occurred in the absence of atmospheric or dissolved water.

Table 5: $\delta^{34}S$ of sulfide minerals associated with calcite filled fractures from the Lupin mine.

Associated with calcite or quartz vein	Sample	Sample Depth	Mineral	$\delta^{34}S$ (‰CDT)
Calcite	105779	300 m	Pyrite, some chalcopyrite	-2.5
Calcite	105778	440 m	Chalcopyrite	-33.2
Calcite	105780	475 m	Pyrite	12.5
Calcite	105781	490 m	Pyrite, some chalcophyrite	2.1

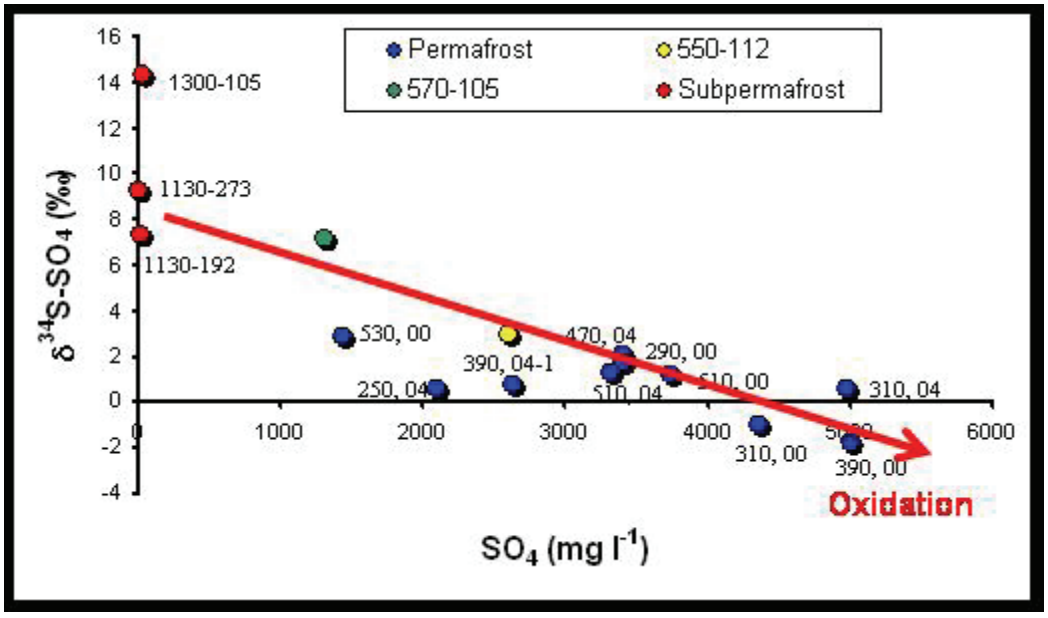

Figure 21: Sulphate concentrations versus $\delta^{34}S$ in dissolved sulphate analyzed in samples from the Lupin Mine. Numbers by each data point (i.e. 310, 00) indicate sample depth and year sampled, respectively.

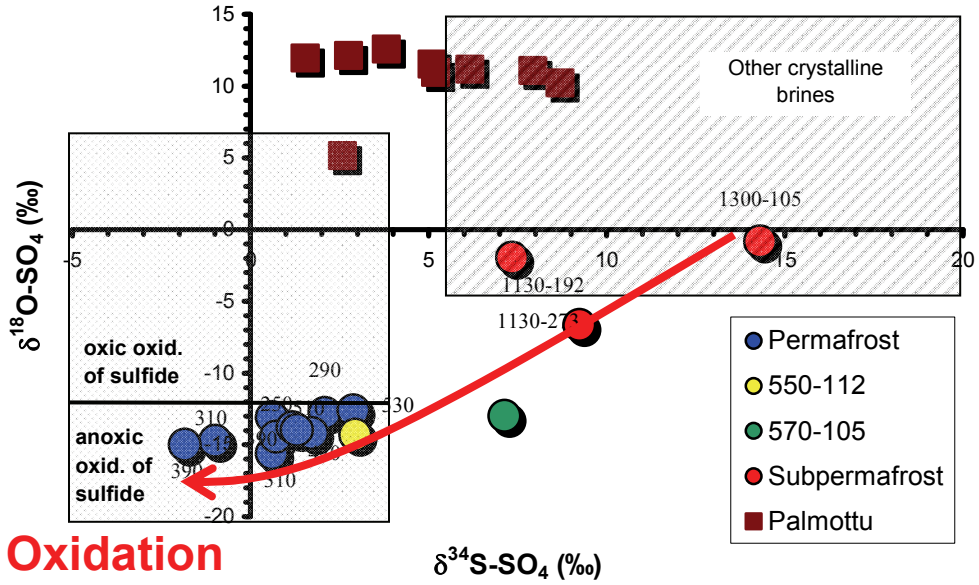

Figure 22: Oxygen ($\delta^{18}O$) and sulphur ($\delta^{34}S$) isotopic composition of sulphate in Lupin groundwaters compared with the Palmottu hydrothermal end-member (Blomqvist et al. 2000). Deep Lupin waters plot in the same area as other crystalline brines (Fritz et al. 1994).

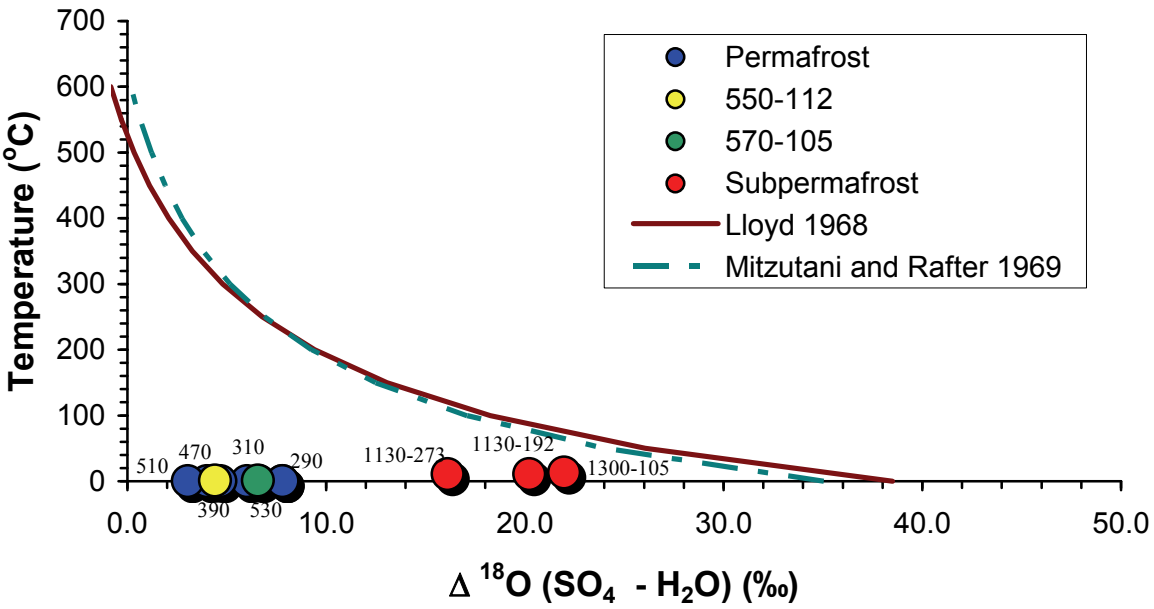

Figure 23: Expected equilibrium fractionation of $\delta^{18}O$ between water and sulphate over a range of temperatures, compared with $\Delta^{18}O$ measured in Lupin samples.

Isotopic ($\delta^{34}S$) values for sulphide minerals are reported in Table 5. With the exception of the sample from 440 m depth (which was mostly chalcopyrite but contained considerable impurities), the samples are typical of sulphides in this type of geologic environment (eg. Rye and Rye, 1974).

4.1.1.2 Multiple fluids and mixtures

4.1.1.3 Ionic evidence

Isotopic data and concentrations of ions which are often key components of deep shield fluids can be useful to defining and distinguishing different water types (Frape et al. 1984). Figure 24 plots the two most common cations, Ca and Na, against each other, and Figure 25 plots the two anions, Cl and Br, against each other, while in Figure 26, the ratios of the cations to anions are plotted. The end members separate in a very similar manner in Figures 24 and 25. The surface waters and atmospheric precipitation have very low concentrations of most ions and therefore tend to fall in one area of the plots. At the other extreme are the subpermafrost, deep fluids at the site. The drilling salt used at the site is an additional possible end member when discussing the fluids found between surface waters and deep saline waters.

The crush and leach values of rock core from research boreholes are plotted on Figures 24, 25 and 26, and may provide an indication of matrix fluid compositions that could potentially mix with allocthonous and deep groundwater at the site. It is interesting to note that in Figure 25, waters from 570-105 plot along with the deep groundwaters while waters from 550-112 plot more closely to the permafrost waters. Waters from research borehole 550-112, and most

permafrost and subpermafrost drip samples deviate from the trend observed for the deep groundwaters (Figure 25). With drilling salt as a potential endmember, the Br versus Cl plot in Figure 25 indicates that contamination by the drilling salt used at the site has probably occurred in the permafrost, subpermafrost drip and in borehole 550-112. The cation versus anion plot (Figure 26) shows the grouping of the permafrost, subpermafrost drips and 550-112 samples near the drill salt sample, again suggesting the samples have been impacted by drill salt contamination. The sections of research borehole 570-105 that are beyond the suspected contamination (~49m) have shown a steady increase in Br and Cl concentration with time, and a trend towards Ca dominated versus Na dominated water (Stotler 2008).

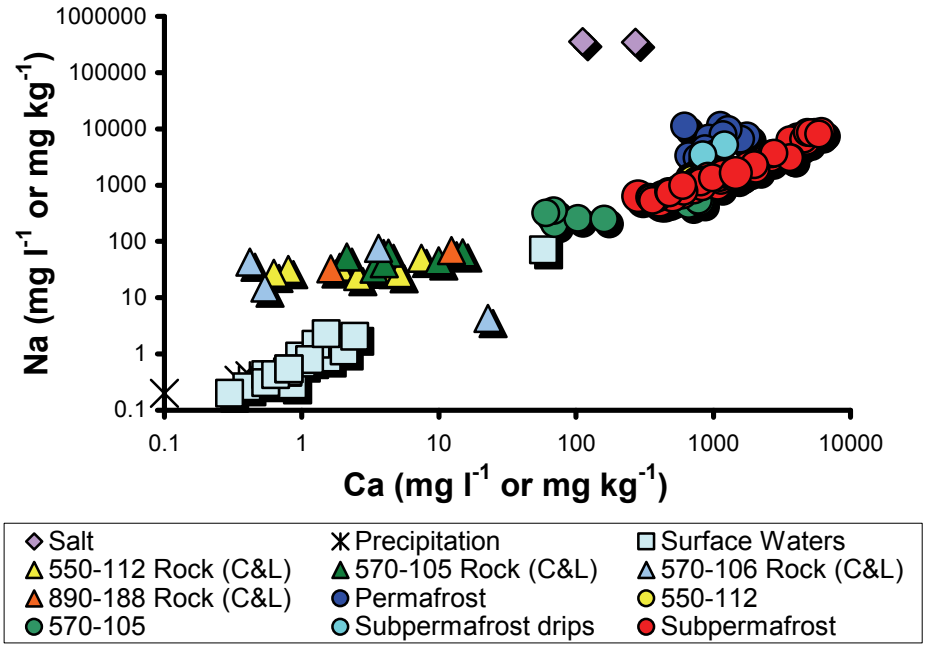

Figure 24: Sodium vs. calcium in Lupin waters, matrix fluids, and imported salt.

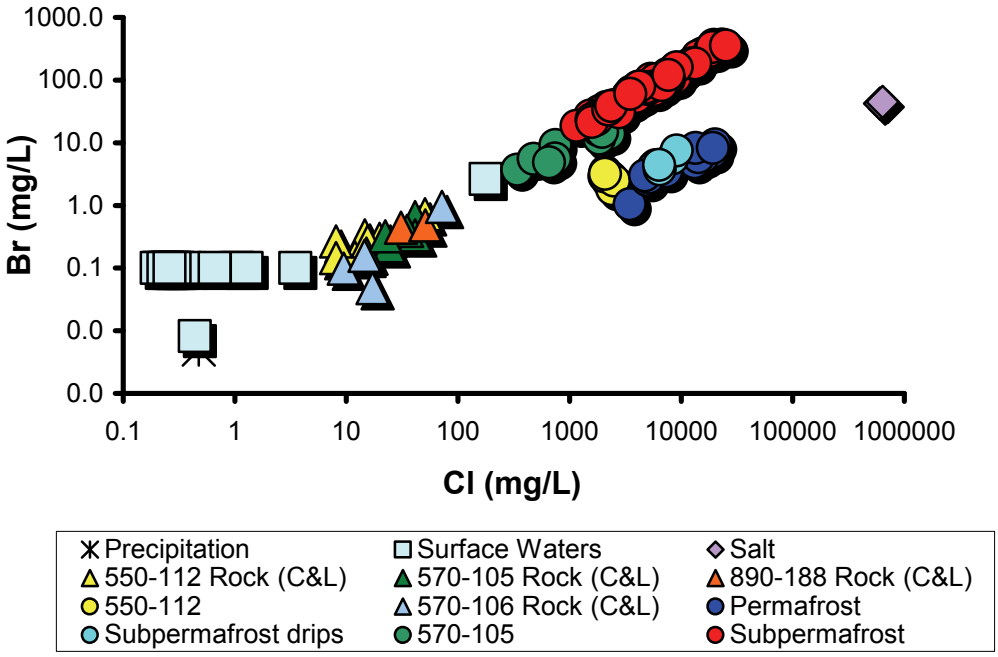

Figure 25: Br vs. Cl plot of waters from Lupin showing two different trends; the permafrost samples demonstrating likely drill salt contamination, and subpermafrost waters representing the natural deep groundwaters. It is noteworthy that the waters from 570-105 group together with the deep groundwaters, while borehole 550-112 has more in common with the permafrost waters.

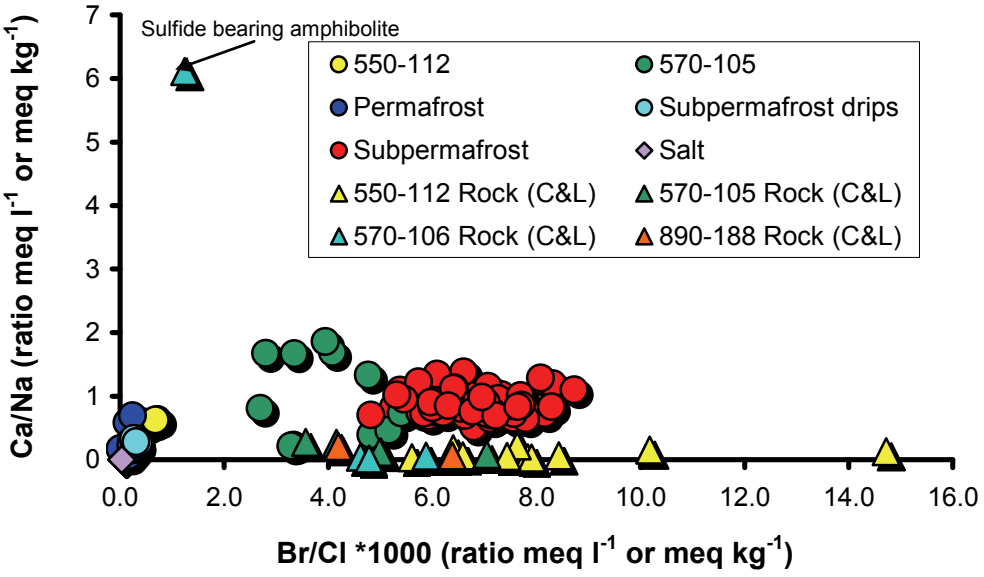

Figure 26: Ratios of cations vs. anions in Lupin waters, matrix fluids, and imported salt.

4.1.1.4 Rare earth elements

Analysis of rare earth elements (REEs) provides additional evidence of multiple fluids in the subsurface at the Lupin site. REEs consist of the elements known as the "Lanthanides" in the periodic table (atomic numbers 57 "Lanthanum" through 71 "Lutetium"). REEs exhibit a gradual decrease in ionic radii from La through Lu, resulting in subtle differences in chemistry which varies predictably with atomic number and leads to strong fractionation as a group and within the group. One of the easiest ways to analyze REEs is to plot concentrations normalized to a standard (typically Condrite for igneous and metamorphic terrains, and Shale for sedimentary terrains) across the REE group by increasing atomic number. When looking at plots of REEs, it is most important to look at the relative fractionation of the light REEs (LREEs, i.e. La, Ce, Pr, Nd, Sm) through the middle REEs (MREE, i.e. Eu, Gd, Tb, Dy) towards the heavier REEs (HREEs, i.e. Ho, Er, Tm, Yb, Lu). In other words, the shape of the line connecting the concentrations of the various REEs can quickly show differences in the source of the fluid and its interactions with different rock units.

REEs have been analyzed in all the types of waters sampled at the Lupin site (surface waters, permafrost water, sub-permafrost water, crush and leach waters) as well as the salt introduced to the mine. A number of samples analyzed had very low concentration of REEs, and often the MREEs and HREEs were non-detectable. As expected, surface waters in the Lupin area have very low REE concentrations, with an average of 89% LREE, 7% MREE, and 4% HREE by concentration, showing an average depletion factor from LREEs to HREEs of 12.72, with a very small negative Eu anomaly, and less REEs relative to condrites (Figure 27). The surface waters plot in a very tight group with similar concentrations, and have a very narrow range of LREE, MREE, and HREE, from 87% to 92% LREE, 6% to 8% MREE, and 2% to 5% HREE. Each surface water sample has a very similar REE pattern when compared with condrites. Matrix waters (as inferred from crush and leach experiments) also show a slight average depletion factor from LREEs to HREEs of 12.11, with negligible Eu anamoly (Figure 28A). The matrix waters REE concentrations varied more than surface waters, and have a slightly larger range of LREE (80% to 100%), MREE(0% to 12%) and HREE (0% to 12%). The salt used in the mine has a very distinct REE signature, showing a slight depletion in MREEs compared to both LREEs and HREEs (Figure 28A). The salt had higher REE concentrations than all but one of the crush and leach samples. The percentage of LREE:MREE:HREE for salt is 80%:10%:10%, with a LREE to HREE enrichment factor of 8.06.

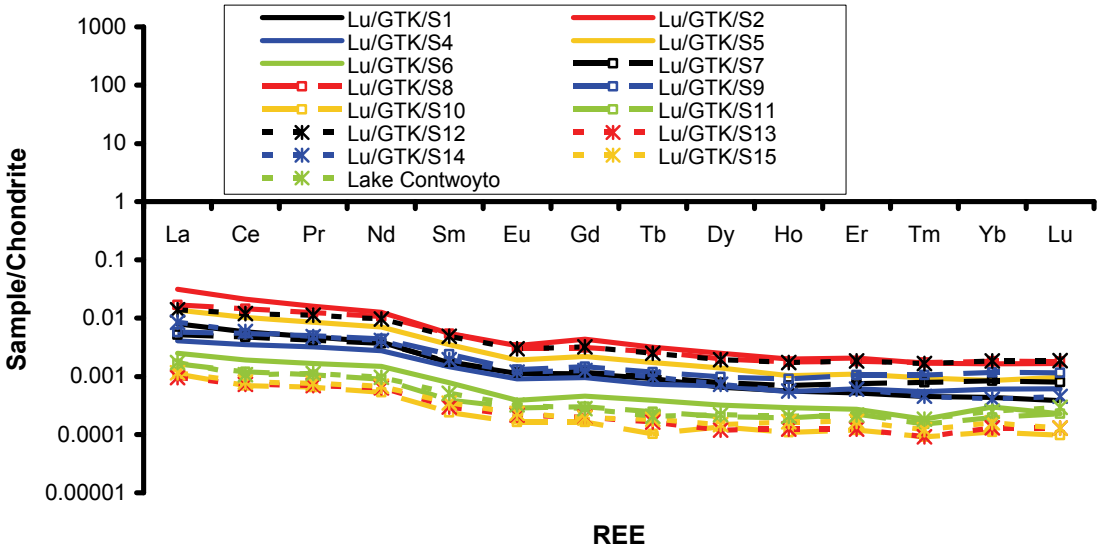

Figure 27: Condrite-normalized REE diagram of surface waters in the Lupin Area.

A.

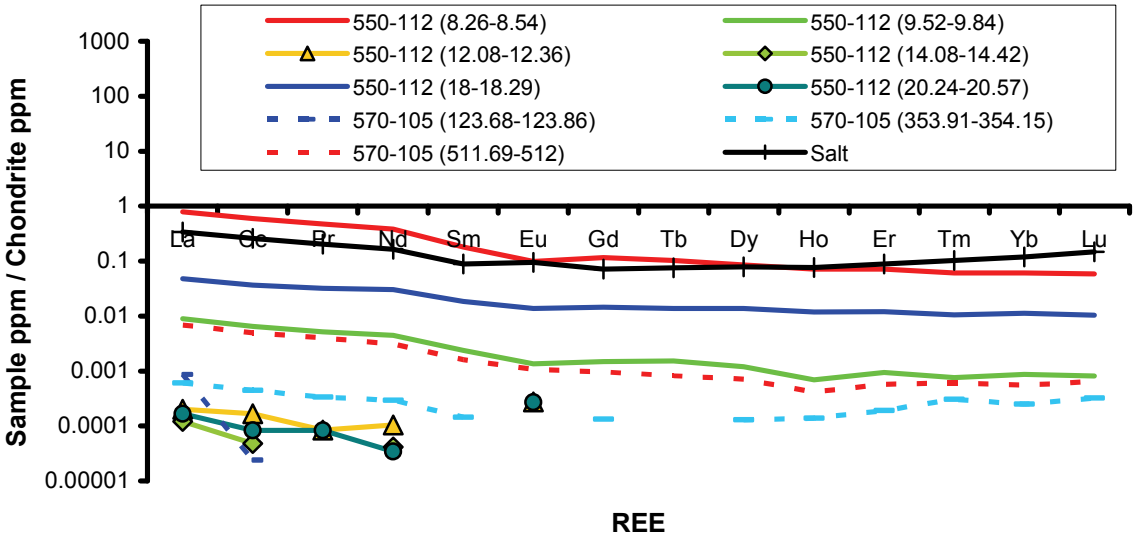

B.

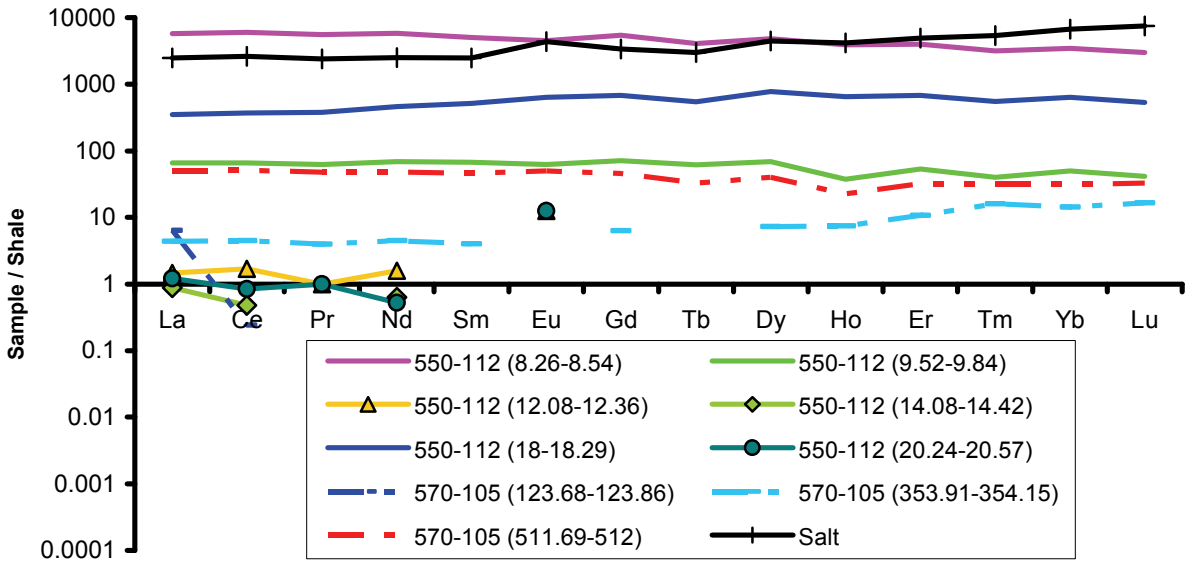

Figure 28: Crush and leach experiments and mine salt REE diagram (A) condrite normalized and (B) shale normalized. Number in brackets after sample name indicates depth in borehole from which the sample was collected.

Permafrost waters have the highest REE concentrations of all the groups sampled (Figure 29), consistent with waters of lower pH (Smedley 1991). The permafrost fluids have a REE pattern

very similar to those observed in sedimentary environments (flat line – Figure 28B; Figure 29B). The salt shows a slight depletion in MREEs compared to both LREEs and HREEs, as seen in Figure 28A, while permafrost water REEs show a trend of depletion from LREEs to HREEs (Figure 29). Comparing the REE patterns of permafrost waters and matrix water as interpreted from crush and leach experiments, (Figure 29D), most permafrost waters have a similar REE pattern and the 550-112 borehole waters tend to plot within the same magnitude as the matrix waters from the crush and leach experiments, unlike in the ion plots (Section 4.1.1.3) where 550-112 borehole waters plotted close to permafrost waters.

A.

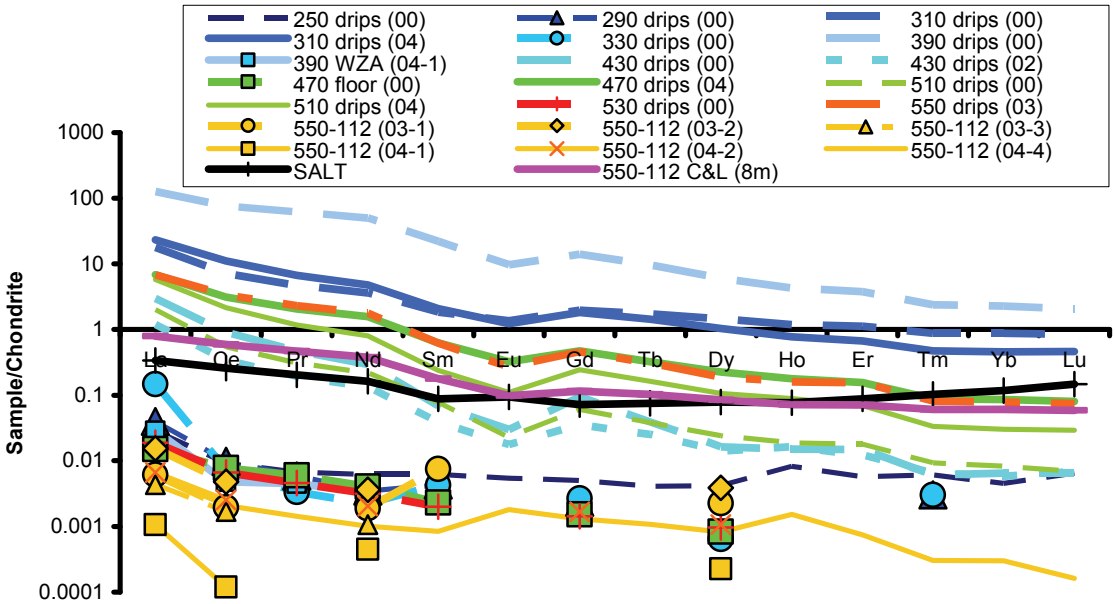

B.

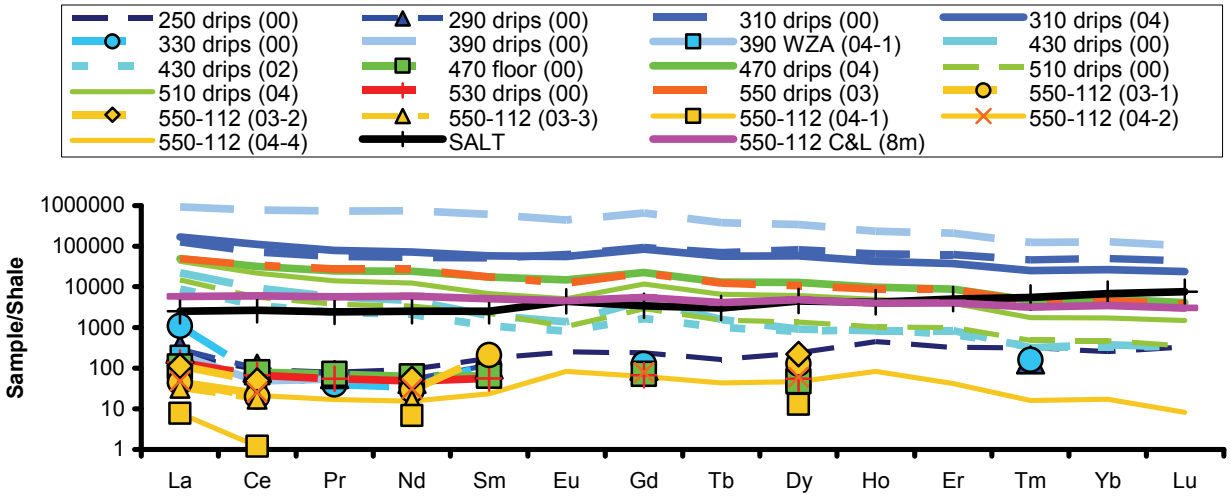

C.

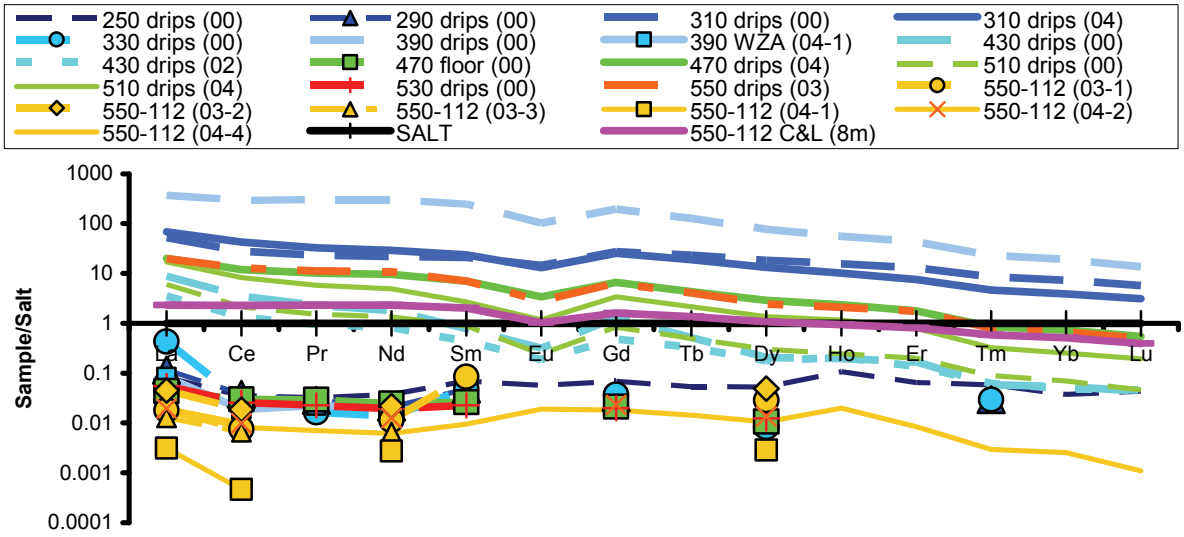

D.

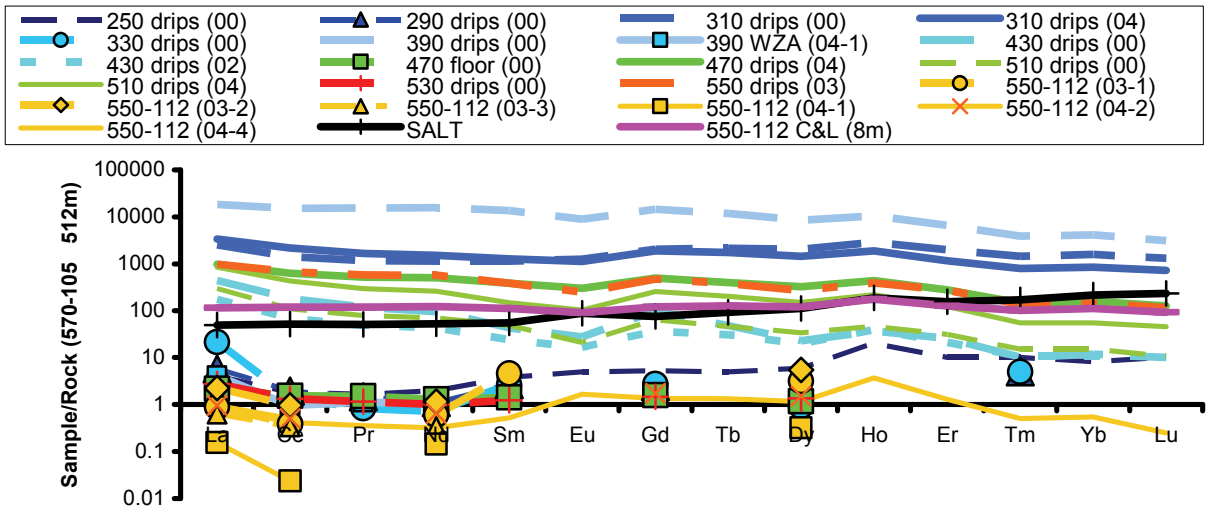

Figure 29: Permafrost water REE diagram (A) condrite normalized (B) shale normalized (C) mine salt normalized (D) normalized to C&L sample 570-105 512m.

In most sub-permafrost water samples, all REEs could not be measured, including the 570-105 waters (Figure 30A). The REE pattern of these waters shows a slight positive Eu anomaly that produces a distinct pattern compared to the permafrost waters. This positive Eu anomaly is often indicative of reducing conditions, where the reduced Eu(II) has a larger ionic radius and chemical properties which are unlike the 3+ REEs (*i.e.* Haskin and Paster 1979, Brookins 1989). At the 890 level however, the water sampled contained a unique REE pattern (Figure 30B). At this site, it was possible to measure every REE in only one unpressurised borehole sample. One of the most intriguing aspects of the 890-188 REE patterns is the negative Ce

anomaly and general lack of any Eu anomaly (Figure 30B). The negative Ce anomaly is consistent with oxidation of Ce(III) to Ce(IV), which has a smaller ionic radius. The deepest waters, at the 1130 and 1300 levels have a unique signature when compared with the matrix, salt and other waters in the mine (Figure 30C). At the deeper levels, there is a highly positive Eu anamoly, regardless of whether or not boreholes were sealed at the time of sampling. This positive Eu anomaly is greater in magnitude than that found in 570-105, likely attributable to the more reducing conditions at depth in the mine.

A.

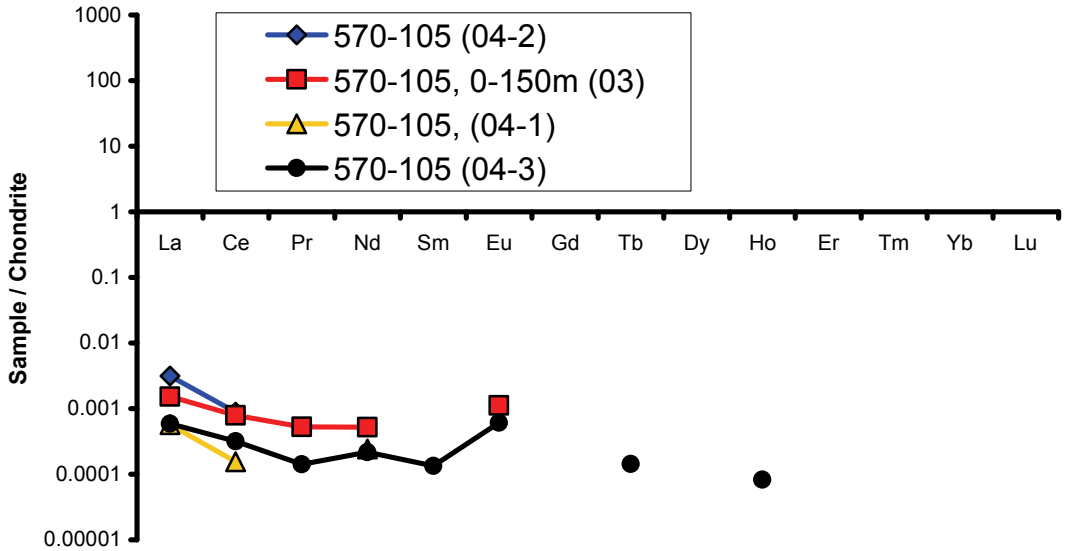

B.

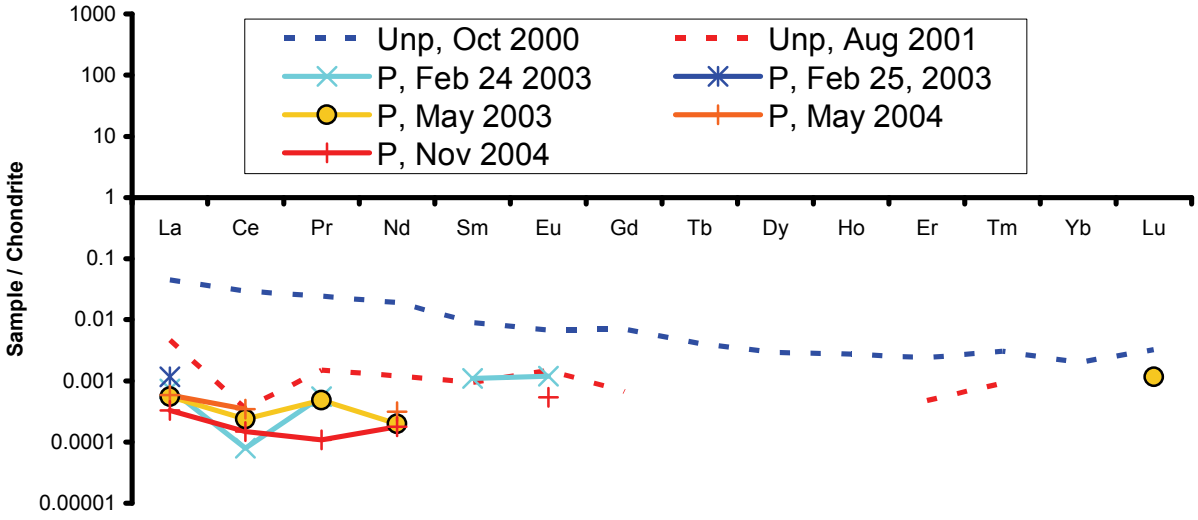
Unp, Oct 2000
Unp, Aug 2001
P, Feb 24 2003
P, Feb 25, 2003
P, May 2003
P, May 2004
P, Nov 2004
Sample / Chondrite
1000
100
10
1
0.1
0.01
0.001
0.0001
0.00001
La
Ce
Pr
Nd
Sm
Eu
Gd
Tb
Dy
Ho
Er
Tm
Yb
Lu

C.

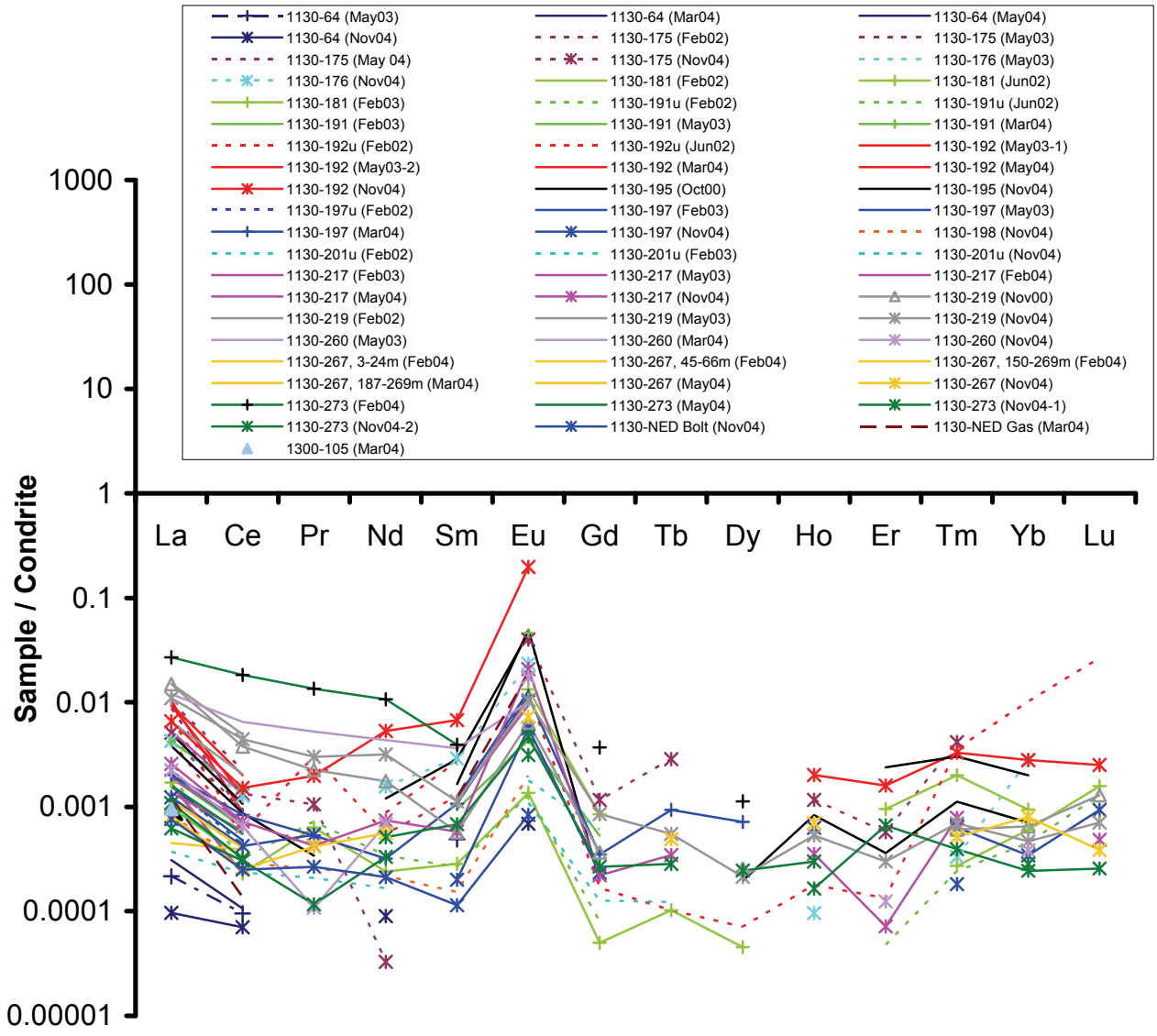

Figure 30: Condrite normalized REE patterns from (A) borehole 570-105 (B) 890-188 and (C) 1130 and 1300 levels.

REE patterns of subpermafrost water compared with the rock matrix water from the 570-105, 512 m crush and leach experiment suggest the REE in subpermafrost water is very similar to that in the rock matrix fluid (Figure 31). Again, the deepest waters show a positive Eu anomaly compared with the matrix fluid likely due to the more reduced conditions at depth in the mine.

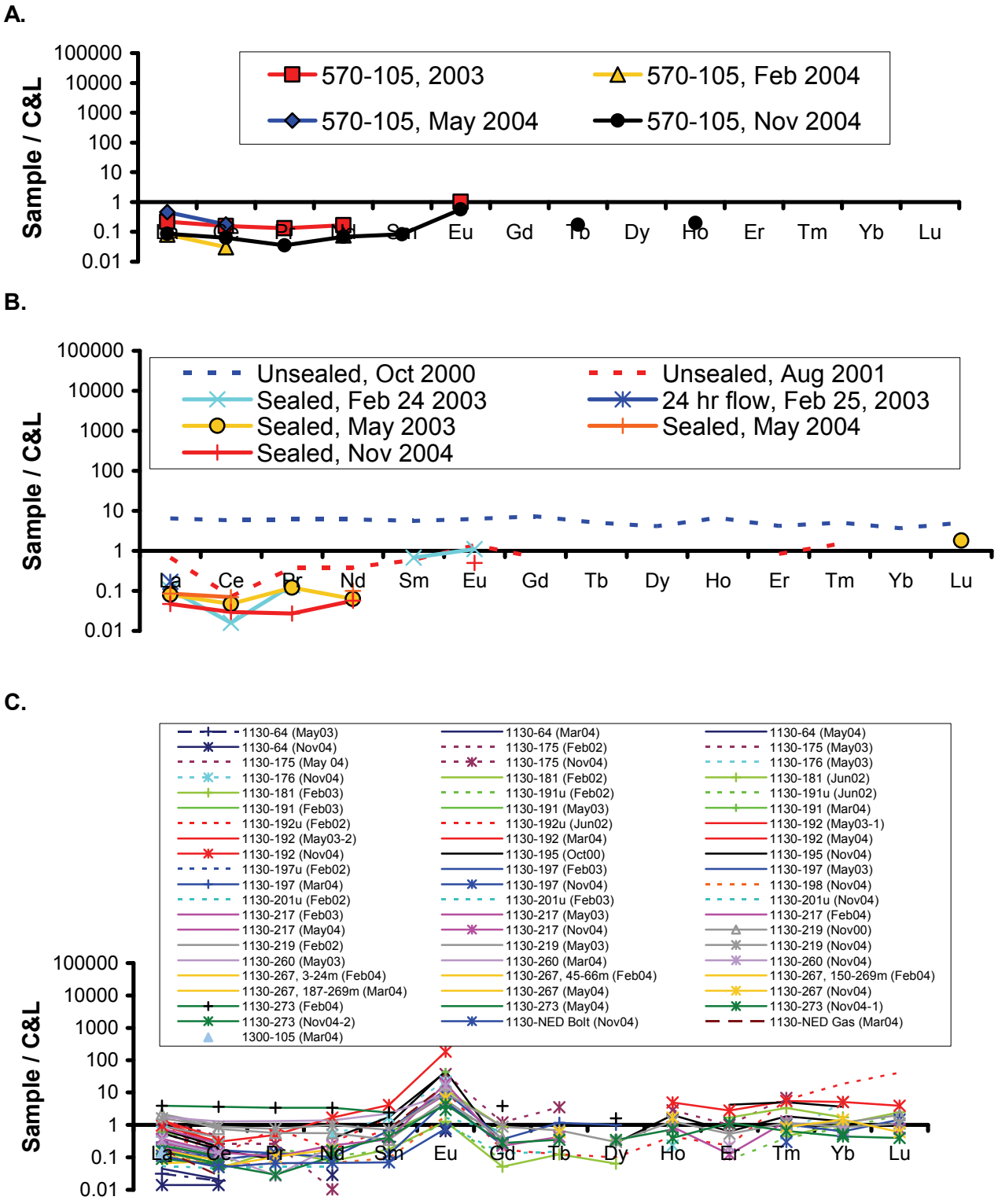

Figure 31: Subpermafrost REE patterns normalized to crush and leach 570-105, 512 m for (A) borehole 570-105 water (B) 890-188 water and (C) 1130 water.

Generally, REE analyses of waters from the Lupin site show distinct patterns for permafrost waters and subpermafrost waters, suggesting they are of different origin/history. While some permafrost waters show similarities to matrix fluids as measured in crush and leach samples, in others the influence of the salt contamination is evident. Waters from boreholes 570-105, 890-188, and 1130 have similarities in their REE plots, indicating a lack of significant drill salt contamination in these samples. Some of the biggest differences in REE patterns are observed in single boreholes over time when comparing pre- and post- packered samples (ex. Figure 30). This is a reflection of the different redox conditions in an open and sealed borehole where, for example, a greater positive EU anomaly is observed under more reducing conditions. REE patterns measured in water from borehole 570-105 are much more similar to uncontaminated subpermafrost waters than the permafrost waters which are likely impacted by drill salt contamination.

4.1.2 Isotopic systems

4.1.2.1 Stable isotopes of water

Stable isotopes of water (δ^2H, $\delta^{18}O$) sampled at the Lupin mine generally fall along the global meteoric water line (Figure 32). The subpermafrost waters all plot in one area, with the deepest sample (1300-105) in the center of the deep samples. Permafrost waters plot along a line, with about a 7‰ SMOW range in $\delta^{18}O$. The range in isotopic values of the permafrost waters, as well as their slight deviation away from the GMWL likely reflects the mixing of surface waters used for drilling with natural permafrost waters. Samples from the 550-112 borehole all plot near the upper limit of the permafrost samples, close to surface water samples, indicating the likely contamination of these samples with drilling waters. Samples from the 570-105 borehole plot between the lower end of the permafrost samples and the subpermafrost boreholes, which further supports the interpretation that the water from the 570-105 borehole is more similar to the the uncontaminated waters sampled deeper in the mine, and has not been significantly impacted by the drill water contamination observed in the permafrost zone.

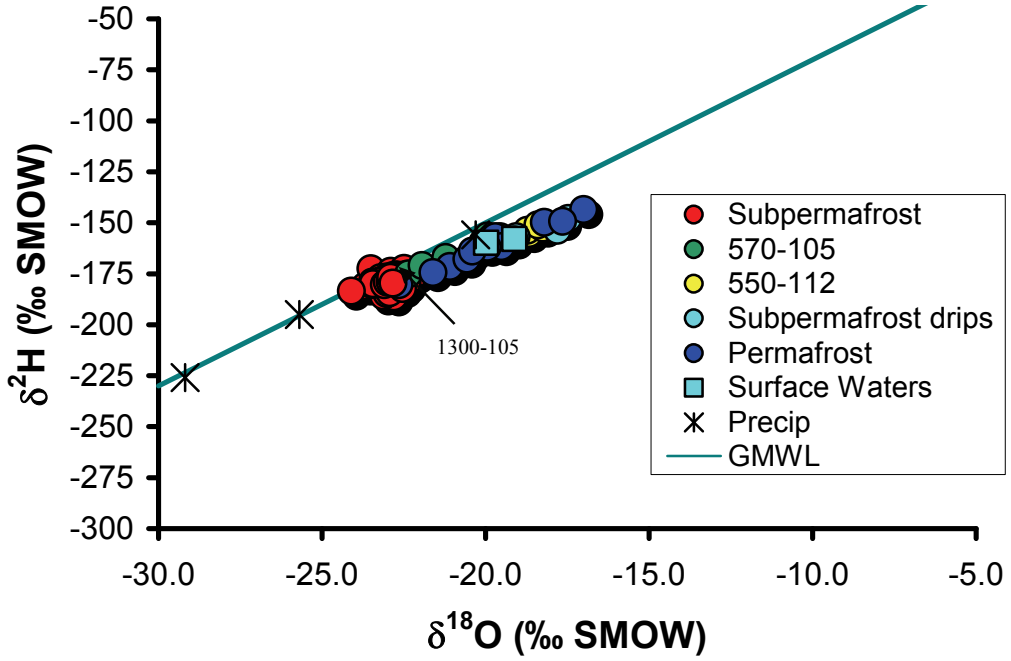

Figure 32: $\delta^{18}O$ vs. $\delta^{2}H$ of waters sampled in the Lupin area, as well as groundwaters sampled in the mine.

In Figure 33, the stable isotopes of water ($\delta^{2}H$, $\delta^{18}O$) are plotted along with tritium content of the samples, however, no correlation between stable isotopes of water and tritium content is observed (Figure 33).

A.

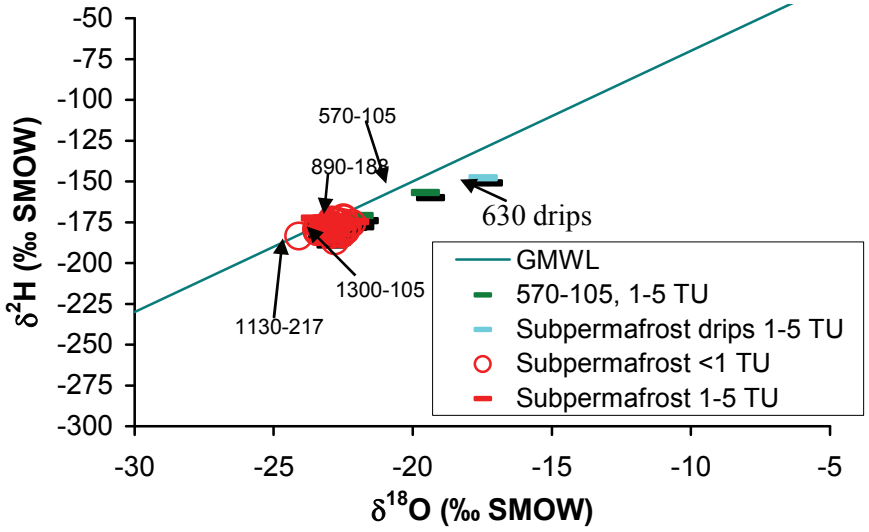

B.

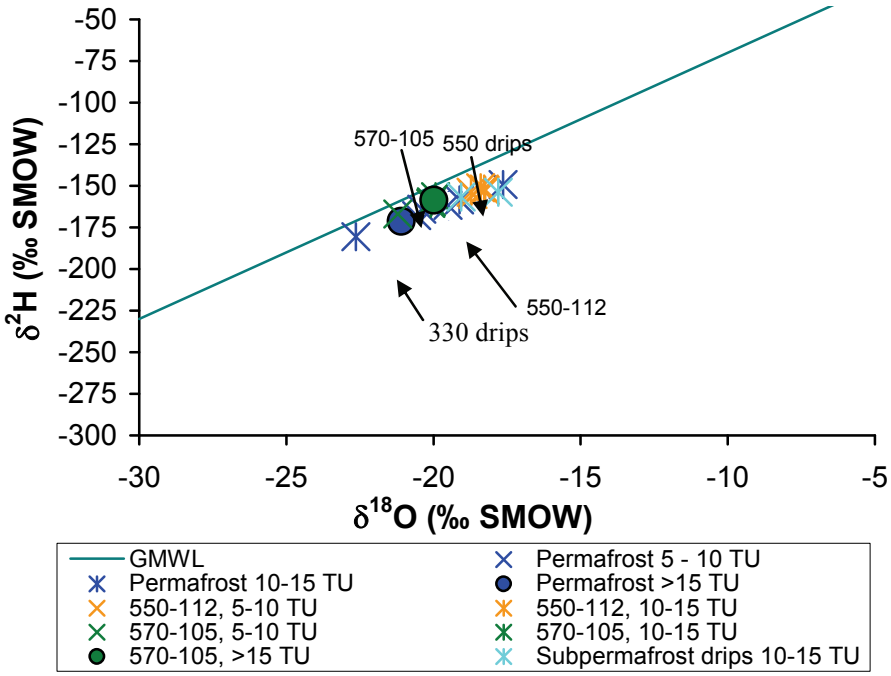

Figure 33: $\delta^{18}O$ vs. $\delta^{2}H$ of groundwaters sampled in the Lupin mine with their tritium content.

4.1.2.2 Chlorine isotopes

Dissolved chloride in water and crush and leach samples from the Lupin site were analyzed for $\delta^{37}Cl$. Salt used to create mine-mixed brine was also analyzed. Assuming the salt used to mix the brine was from the same source throughout the mine's history, the chlorine isotopic signature of most of the mine waters, including permafrost waters, does not closely match that of the mine salt, suggesting the chlorine in the mine waters may not have originated from the salt (Figure 34 A). The chlorine may have originated from the matrix fluid (i.e. the chlorine was leached out of the matrix fluid), however the chlorine content of the mine waters is much higher than the matrix fluid, even though the stable isotope signatures are similar (Figure 34 B). Alternatively, the salt used to mix the brine may have been from different sources (i.e. different $\delta^{37}Cl$ values) over the mine's operation periods, and the isotopic signature of the mine waters may now reflect the mixing of these different salts. It was not possible to ascertain if the same salt source was used for mixing the drill brine over the mine's history.

A.

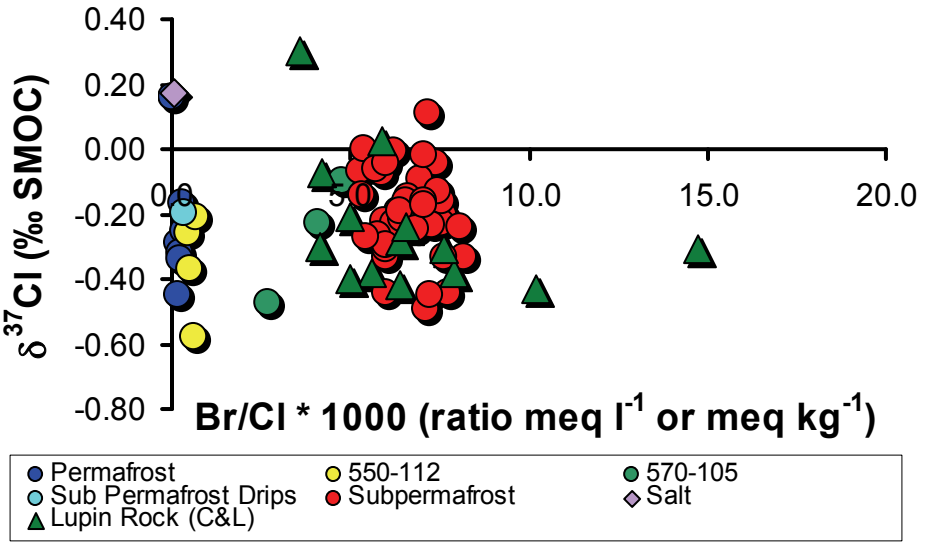

B.

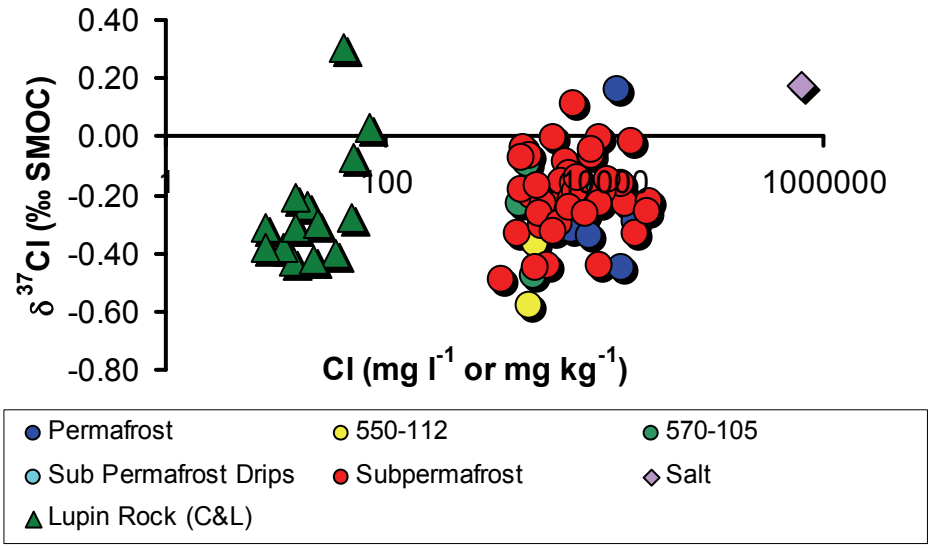

Figure 34: Chlorine isotopic signature of mine waters, matrix fluid, and salt compared with (A) bromine/chlorine ratio and (B) chlorine content.

4.2 CARBON SYSTEM

There are four main components of the carbon system at Lupin; bicarbonate, dissolved in groundwaters in quantity in the permafrost portions of the mine (Figure 17); methane gas at depth (Section 4.2.1); calcite in both subhorizontal and subvertical veins located throughout the mine (eg. Table 5); and graphite in shear zones and slickensides, which are often associated with the ore, but sometimes associated with larger calcite veins as well. To understand the entire system, each component must be studied in detail.

When considering isotopic studies of carbon, it is important to keep in mind (Ohmoto and Goldhaber 1997):

1. The magnitude of equilibrium fractionation between two coexisting species (i.e. CH_4 and $C_{graphite}$) is temperature dependant (less fractionation with increasing temperature);
2. Pressure effects are negligible at less than 10 kbar;
3. When in equilibrium, more oxidized species are more enriched in heavier isotopes (i.e. $\delta^{13}C_{HCO_3} > \delta^{13}C_{C(graphite)} > \delta^{13}C_{CH_4}$);
4. Fractionation factors between carbonate minerals and CO_3^{2-} are small (<1.5‰ at T=25°C and <0.5‰ at *T*>110°C);
5. Equilibrium reaction rates are almost instantaneous between aqueous species of the same valence ($CO_{2(aq)}$-H_2CO_3-HCO_3-CO_3^{2-}), reaction rates are slowest between CO_2 and CH_4. Where CH_4 is produced by the reduction of CO_2 or elemental carbon (i.e. graphite), the species are initially out of equilibrium, but over long residence times, the two species may attain chemical and isotopic equilibrium;

6. The time required for CO_2-CH_4 species to reach equilibrium is ~10^4 years at 400°C and ~10^7 years at 300°C. Thus, the observed difference in $\delta^{13}C$ between the species is expected to be much smaller than equilibrium values;
7. Equilibrium between CO_2 and CH_4 may be independent of both pH and total carbon content;
8. Modern day seawater bicarbonate (HCO_3^-) has a $\delta^{13}C$ value of ~0‰, while seawater and atmospheric CO_2 have $\delta^{13}C$ values of ~ -7‰.

4.2.1 Gas data – Methane and associated gases

In February 2002, five boreholes in the 1130 m exploration drift were sampled for hydrocarbon gases. Sampling conditions were not ideal as horizontal holes (191, 192 and 197) were open, and vertical holes (175 and 176) were situated in shallow standing pools of water. To collect better quality samples, additional sampling rounds were carried out in February and May of 2003, after sealing and pressurising the boreholes. In February 2003, samples were taken both immediately after opening the boreholes and after letting the boreholes flow for one or two days to allow for comparison of the results. For most of the boreholes, the first samples collected in 2003 were taken shortly after the boreholes were sealed, which explains why higher oxygen concentrations were measured during the initial sampling before the boreholes were allowed to flow (i.e. 192) (Table 7). Samples were also collected during the February/March, May, and November 2004 field trips, and additional boreholes were sampled as they were packered and pressurized (267, 273). Samples were collected for analyses of the chemical and isotopic compositions of the hydrocarbon gases, and for noble gases by a team from the University of Ottawa, Canada. Water and gas samples were taken simultaneously in order to allow for a total geochemical characterisation of the groundwater.

The gas volumes released from a unit volume of water were estimated using a simple experimental setup. First, the packer valve was partly opened and adjusted to achieve a steady flow rate. For the gas samples, this technique was successful because a constant flow rate was required for only a relatively short time period. The gas was collected in a water-filled glass bottle submerged in a larger bucket of water. The in-flowing gas forced the water out of the glass bottle, and once all the water in the bottle was replaced by the collected gases, a known volume of gas had been collected. Knowing the gas volume, the flow rate and the collection time, the volume-volume ratio can be calculated, and the results are presented in Table 6. The highest amount of gas, 0.5 L_{gas}/L_{water}, was observed in borehole 1130-192, which also has the highest salinity and the highest hydraulic pressure. The other holes at this level produced between 0.14 to 0.33 L_{gas}/L_{water}, while borehole 188 at level 890 m, produced only 0.09 L_{gas}/L_{water}. The volumes of gas per kilogram of water are very comparable to those reported by Sherwood Lollar et al. (1994) at a number of other crystalline shield sites.

Table 6: Gas volumes measured during the gas sampling at the 890 and 1130 levels in May 2003.

Depth-Borehole No.	Gas Vol. (L)	Flow (L/min)	Collection time (min)	Water Vol. (L)	Gas Vol. (L)/ 1 L water	pH	Pressure during sampling (kPa)
890-188	0.4	0.62	7.3	4.53	0.09	-	-
1130-64	-	-	-	-	-	-	-
1130-191	0.7	0.47	4.5	2.13	0.33	8.18	3240
1130-192	0.4	0.27	3.0	0.80	0.50	8.40	4960
1130-197	0.7	0.54	6.5	3.51	0.20	8.36	3720
1130-217	1	0.91	4.1	3.73	0.27	8.13	3240
1130-219	0.4	0.45	6.1	2.78	0.14	8.28	1930

- = not measured

The volume percentages of component gases measured in gas samples from the 1130 m and 890 m level are given in Table 7. In every borehole, the relative percentage of oxygen in the gas samples decreased with time, while the relative percentage of methane increased. Hydrogen and carbon isotopic signatures of methane (C_1), ethane (C_2) and propane (C_3) were also measured (Table 8), although it was difficult to analyze the isotopic composition of propane in any of the samples due to its low concentration. Allowing the borehole to flow for an extended period of time did not appear to produce an effect on $\delta^{13}C$ values. Over the year and a half the boreholes were sealed, gases became enriched by about 1‰ with respect to $\delta^{13}C$ and around 10-17 ‰ with respect to $\delta^{2}H$.

Table 7: Volume % of selected gases from several boreholes in the Lupin Mine.

Sample	Date	N_2	O_2	CO_2	CH_4	C2	C3	i-C4	n-C4
						Vol %			
890-188	19-Feb-03[1]	28.62	1.34	0.50	68.6	0.51	0.002	ND	ND
890-188	21-Feb-03[2]	27.94	1.22	0.47	69.8	0.51	0.002	ND	0.0002
890-188	24-May-03	28.54	1.12	0.47	74.4	0.55	0.014	ND	0.0002
1130-64	07-Oct-05	36.96	2.06	0.14	64.4	0.11	0.004	0.0003	0.0001
1130-160	01-Oct-05[3]				69.6	2.40	0.169		
1130-175	22-May-03	9.63	0.89	1.67	86.7	1.89	0.094	0.007	0.007
1130-176	22-May-03	11.00	0.93	1.42	84.7	1.60	0.089	0.008	0.007
NED-Ground	26-Feb-03	26.92	2.05	0.98	72.6	1.09	0.002	0.0028	0.003
1130-191	25-Feb-03[4]	23.00	1.41	0.98	73.4	1.04	0.002	0.0025	0.003
1130-191	25-Feb-03[4]	19.76	1.56	1.15	73.4	1.18	0.002	0.002	0.003
1130-191	23-May-03	15.82	1.01	1.38	81.1	1.49	0.080	0.004	0.004
1130-192	21-Feb-03[1]	14.48	1.66	1.64	19.5	0.48	0.002	ND	0.001
1130-192	22-Feb-03[2]	64.97	15.89	0.50	81.0	1.69	0.002	0.0001	0.004
1130-192	22-May-03	11.00	1.13	1.92	86.7	2.05	0.124	0.006	0.006
1130-197	24-Feb-03[1]	19.93	1.53	1.07	75.2	0.97	0.002	0.007	0.001
1130-197	25-Feb-03[2]	20.11	1.65	1.07	72.6	0.92	0.002	ND	0.001
1130-197	23-May-03	22.69	1.01	0.88	77.4	0.93	0.033	0.001	0.001
1130-217	24-Feb-03	17.38	1.42	1.23	76.6	1.29	0.002	0.0003	0.002
1130-217	23-May-03	15.13	1.03	1.43	81.5	1.61	0.083	0.004	0.004
1130-219	25-May-03	16.16	1.01	1.17	82.2	1.27	0.046	0.001	0.001
1130-267	16-May-04	27.5	1.24	0.79	69.5	0.83	0.037	0.0018	0.002
1130-273	15-May-04	13.92	1.13	1.32	81.8	1.42	0.068	0.0042	0.005
1130-273	07-Oct-05	17.66	1.04	1.03	78.9	1.02	0.004	0.0003	0.0001

[1]Sample taken shortly after borehole opened
[2]Sample taken after redox measurements had stabilized; borehole was flowing continuously from prior sample
[3]Sample analyzed at University of Indiana
[4]Two samples taken; initial sample taken immediately after borehole was sealed and was predominately gas, second sample taken after borehole stabilized and was fluid and gas

Table 8: Hydrogen and carbon isotope signatures of methane, ethane, and propane of the Lupin Mine gas samples.

Sample	Date	δ^2H (‰)			$\delta^{13}C$ (‰)			
		Methane	Ethane	Propane	Methane	Ethane	Propane	CO_2
890-188	19 Feb 2003[1]	-336	-249	ND	-56.1	-33.0		
	21 Feb 2003[2]	-336	-290	ND	-56.0	-35.1		
	24-May-03	-359	ND	ND	-54.6	-37.8	ND	
	18-May-04	-335	BLOQ	ND	-55.4	-36.6	BLOQ	
	Oct 05[4]	-340	-253	-189	-56.1	-36.7	-33.5	-21.9
1130-64	07-Oct-05	-339	BLOQ		-51.5			
	Oct 05[4]	-330			-50.3	-27.3	-27.3	-55.3
1130-160	Oct 05[4]	-323	-276	-172	-46.1	-34.9	-33.2	-26.4
1130-175	22-May-03	-347	-249	ND	-44.7	-35.2	-32.11	
	28-Nov-04	-330	-312	ND	-44.6	-35.1	BLOQ	
	Oct 05[4]	-328	-290	-179	-44.3	-34.5	-33.3	-18.6
1130-176	22-May-03	-344	-243	ND	-44.7	-35.7	-32.3	
NED-Ground	26-Feb-03	-329	-312	ND	-47.3	-32.8		
1130-191	25 Feb 2003[3]	-334	-306	ND	-45.6	-33.4		
	25 Feb 2003[3]	-327	-314	ND	-45.5	-31.4		
	23-May-03	-350	-253	ND	-45.7	-35.3	ND	
	01-Mar-04	-332	-312	ND	-46.0	-36.5	BLOQ	
	Oct 05[4]	-319	-305		-47.1	-34.9	-33.1	-21.1
1130-192	21 Feb 2003[1]	-326	-283	ND	-44.7	-33.5		
	22 Feb 2003[2]	-322	-307	ND	-44.7	-33.6		
	22-May-03	-329	-234	ND	-42.4	-35.5	-32.97	
	15-May-04	-328	-306	ND	-44.6	-35.5	BLOQ	
	Oct 05[4]	-324	-295	-196	-42.4	-35	-34.2	-23
1130-197	24 Feb 2003[1]	-329	304	ND	-50.0	-32.3		
	25 Feb 2003[2]	-330	-306	ND	-50.2	-33.9		
	23-May-03	-349	-231	ND	-48.7	-36.1	ND	
	01-Mar-04	-338	-302	ND	-49.0	-36.6	BLOQ	
	Oct 05[4]	-341	-281	-183	-50.6	-35.3	-33.2	-24.3
1130-217	24-Feb-03	-328	-303	ND	-46.8	-33.1		
	23-May-03	-349	-251	ND	-40.5	-35.7	ND	
	15-May-04	-337	-308	ND	-45.2	-36.6	BLOQ	
1130-219	25-May-03	-349	-228	ND	-47.7	-35.5	ND	
	28-Feb-04	-331	-306	ND	-44.5	-35.9	BLOQ	
1130-267	16-May-04	-335	-307	ND	-47.0	-35.3	BLOQ	
	Oct 05[4]	-344	-290	-179	-47.8	-35	-33.6	-21.1
1130-273	15-May-04	-336	BLOQ	ND	-45.6	-34.2	BLOQ	
	07-Oct-05	-333	-319		-48.2	-34.4		
	Oct 05[4]	-344	-289	-178	-46.3	-34.3	-32.9	-15.7

[1] Sample was taken immediately after borehole was opened and allowed to flow
[2] Sample was taken after borehole had been allowed to flow for at least one day for redox and pH measurements
[3] Borehole was extremely gassy with little to no water at time of sample 1, but water had been flowing for about 10 minutes at the time of the second sample
[4] Samples analyzed at University of Indiana
ND = Non-Detect
BLOQ = below limit of quantification

The $\delta^{13}C$ results for hydrocarbon gases associated with the deep groundwaters at Lupin are compared to other gas data of both thermogenic and abiogenic origin from Sherwood Lollar et al. (2002) in Figure 35. A trend towards more positive values (more enriched in ^{13}C) with increasing carbon number is observed in the Lupin samples. Comparing this trend to trends observed for gases in other Shield environments suggests that gases at the 1130 level may have a thermogenic origin (Figure 35). As in most Shield sites, there may also be a very old bacterial component.

In Figure 36, the isotopic compositions of methanes from Lupin are compared to other Shield sites in Canada and Finland. On this figure, the well-established fields for bacterial and thermogenic methanes are shown. Many of the Shield sites have methanes outside or partially outside these fields, which are thought to be abiogenic (high temperature, possibly even mantle) in origin (Sherwood Lollar et al., 1989, 2002). Based on where they plot in Figure 36, the Lupin methanes would be classified as a mixture of abiogenic and biogenic (Figure 36B), if only the bulk hydrocarbon $\delta^{13}C$ and $\delta^{2}H$ values were considered.

To attempt to further classify the Lupin hydrocarbon gases, the proportional volumes of $C_1/(C_2 + C_3)$ are plotted against the bulk $\delta^{13}C_{CH4}$ value of the gases (Figure 37). Methanes from Lupin fall in a field dominated by many of the other shield sites which are believed to be mixtures of abiogenic and biogenic gases. However, Lupin samples are at the low end (<10 %) of biogenic mixing, indicating that only a small bacterial component of gas with an unknown age may be present in some samples.

Additional carbon isotope analyses (both $\delta^{13}C$ and ^{14}C) on the dissolved inorganic carbon component show indications that some of the DIC may be derived from bacterial conversion of methane to CO_2 (Frape et al., 2004). The CO_2 produced, for example by acetate fermentation, can be incorporated into the dissolved carbon pool. Three boreholes 890-188, 1130-181 and 1130-192 gave ^{14}C (pmc) values of 8.72, 2.78 and 16.2, respectively in February 2003 (Table 9). However, the $\delta^{13}C$ values were -4.5‰, -1.9 ‰ and +7.7 ‰ respectively (Table 9). The enriched value for borehole 1130-192 (one of the most concentrated saline fluids), coupled with the hole's higher than normal HCO_3 concentration, may indicate bacterial reduction/oxidation of methane. Further work will be concentrated on determining if the DIC is related to methane oxidation/reduction, and if so, if it is due to current bacterial activity or if it is a palaeophenomenon.

In Figure 38, the $\delta^{13}C$ values are plotted versus their $\delta^{2}H$ values, and compared to abiogenic gases from Kidd Creek, and to thermogenic gases from southwest Ontario. Although $\delta^{13}C$ values for $C_1 – C_3$ components are available for gas samples from Lupin, $\delta^{2}H$ values are available only for C_1 and C_2 gas components, with the exception of 7 samples where it was possible to measure $\delta^{2}H$ values of C_3 (Table 8; Figure 38). This increases the uncertainty of any interpretation of the trends in the $\delta^{13}C$ values as a function of $\delta^{2}H$. However, although the absolute $\delta^{2}H$ values of the Lupin gases are different from the other Shield gases plotted in Figure 38, it appears that there is a positive correlation between $\delta^{13}C$ and $\delta^{2}H$. This is an established trend for thermogenic gas reservoirs worldwide (Sherwood Lollar et al. 2002), and is significantly different than the trend observed for hydrocarbon gases from Kidd Creek (abiogenic).

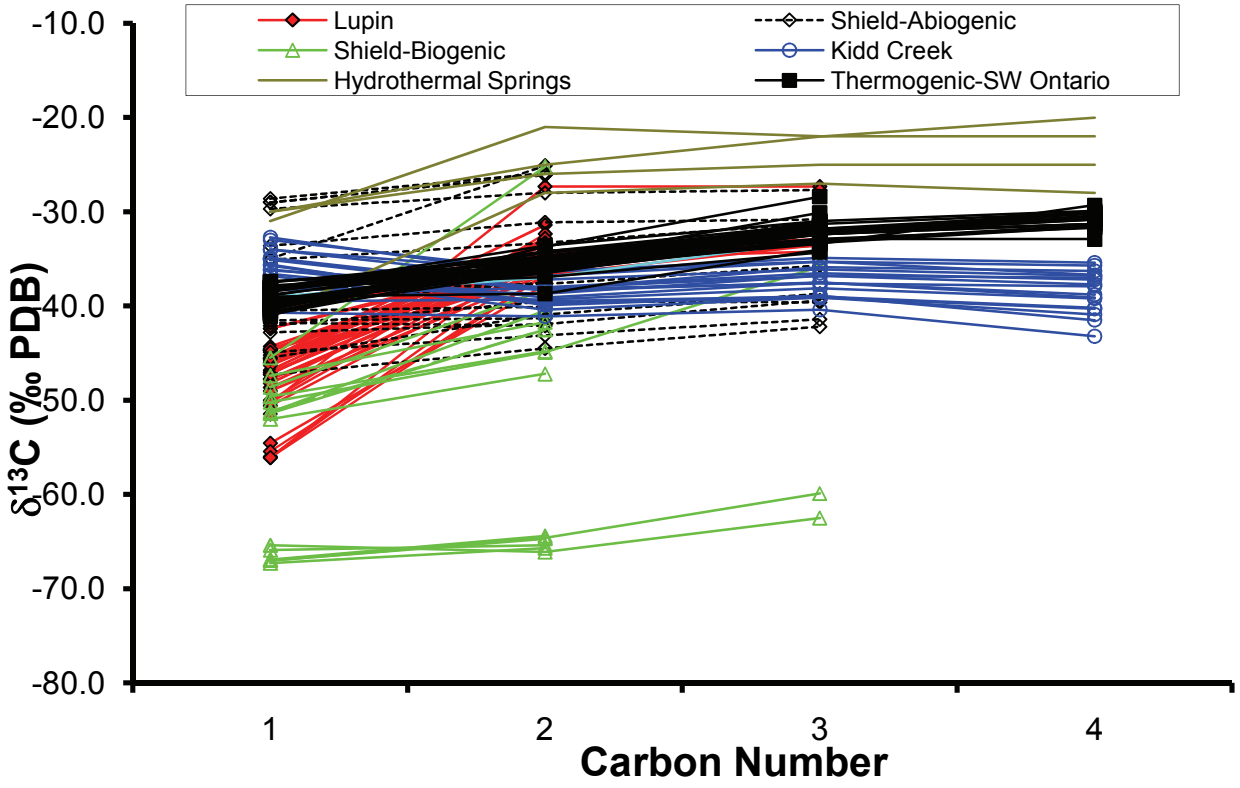

Figure 35: $\delta^{13}C$ values of individual hydrocarbons versus carbon number for gas samples from the Kidd Creek Mine (Sherwood Lollar et al. 2002), for other abiogenic Shield gases (Sherwood Lollar et al. 1993a), for biogenic Shield gases (Sherwood Lollar et al. 1993b), for thermogenic gases from southwest Ontario natural gas fields (Sherwood Lollar et al. 1994), for gases associated with hydrothermal springs (Des Marais 1981) and for gases associated with deep groundwaters from the Lupin Site. Modified from Sherwood Lollar et al. (2002).

A.

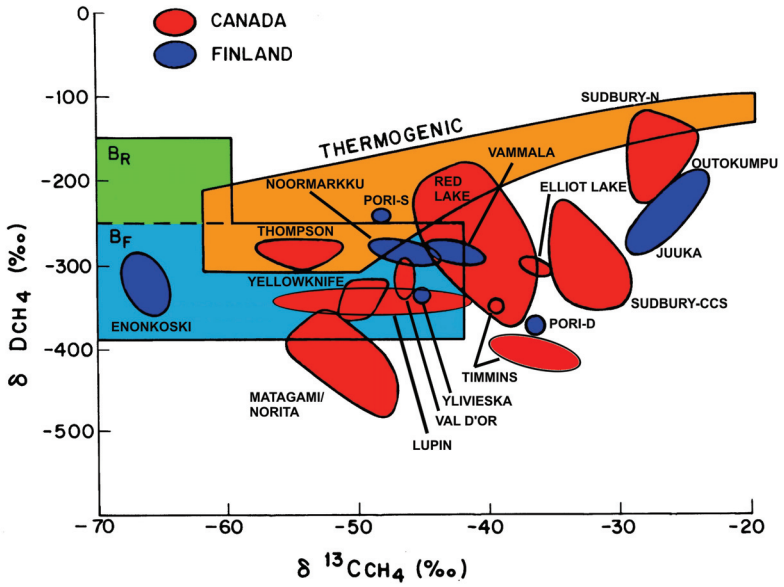

B.

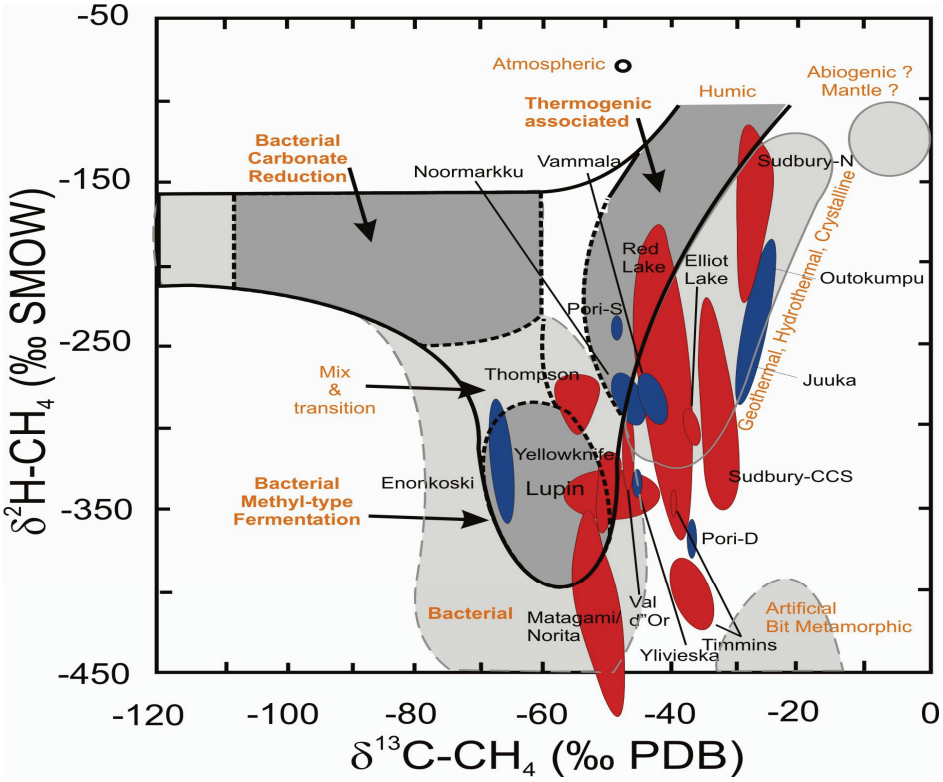

Figure 36: Isotopic compositions of methanes from Lupin compared to selected Canadian and Finnish sites. (A) Modified from Sherwood Lollar et al. (1989), (B) modified from Whiticar (1999). B_R is the potential field of bacterial methane attributed to CO_2 reduction and B_F is the field of potential methanes attributed to acetate fermentation.

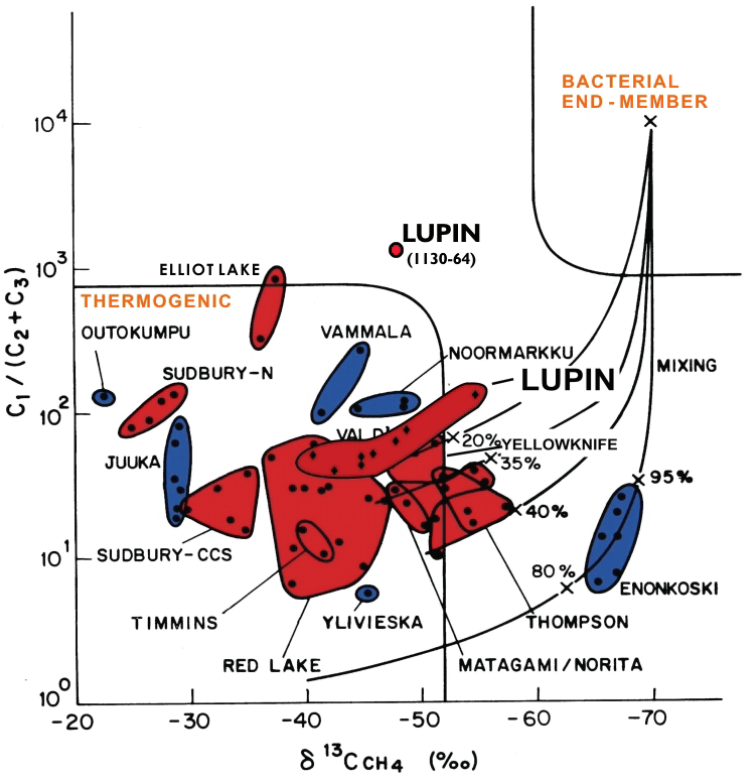

Figure 37: $\delta^{13}C_{CH4}$ versus C1/(C2+C3) ratios for Canadian and Fennoscandian Shield gases. Adapted from Sherwood Lollar et al. 1993b.

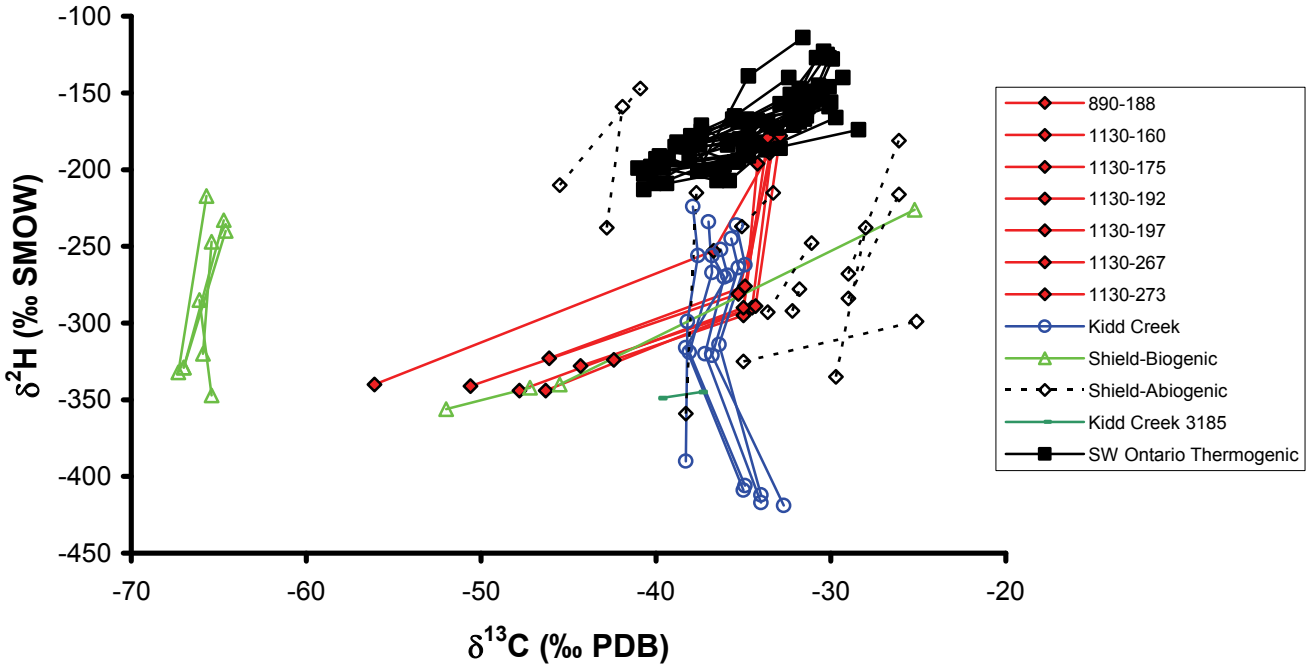

Figure 38: Plot of $\delta^{13}C$ vs. $\delta^{2}H$ Values for C_1-C_4 for samples from Kidd Creek (Sherwood Lollar et al. 2002), thermogenic gases from southwest Ontario (Sherwood Lollar et al. 1994), from Canadian and Fennoscandian Shield biogenic gases (Sherwood Lollar et al. 1993b) and abiogenic gases (Sherwood Lollar et al. 1993a) and from Lupin.

Knowledge of the maximum subsurface temperature reached by groundwaters is useful in determining groundwater evolution (Clark and Fritz, 1997). Plots of $\delta^{13}C$ of C1 versus C2, or C2 versus C3, can be used as geothermometers to estimate methane gas temperatures in groundwater (Figure 39; James 1983). The C1-C2 plot suggests CH_4 temperatures of 300-400 K for most Lupin samples, most similar to thermogenic and biogenic samples from other sites (Figure 39A). A higher methane temperature of 400 to 700 K is predicted by the C2-C3 geothermometer, more similar to other abiogenic Shield sites (Figure 39B). The reason for the differences in the C1-C2 and C2-C3 geothermometers is not known at this time.

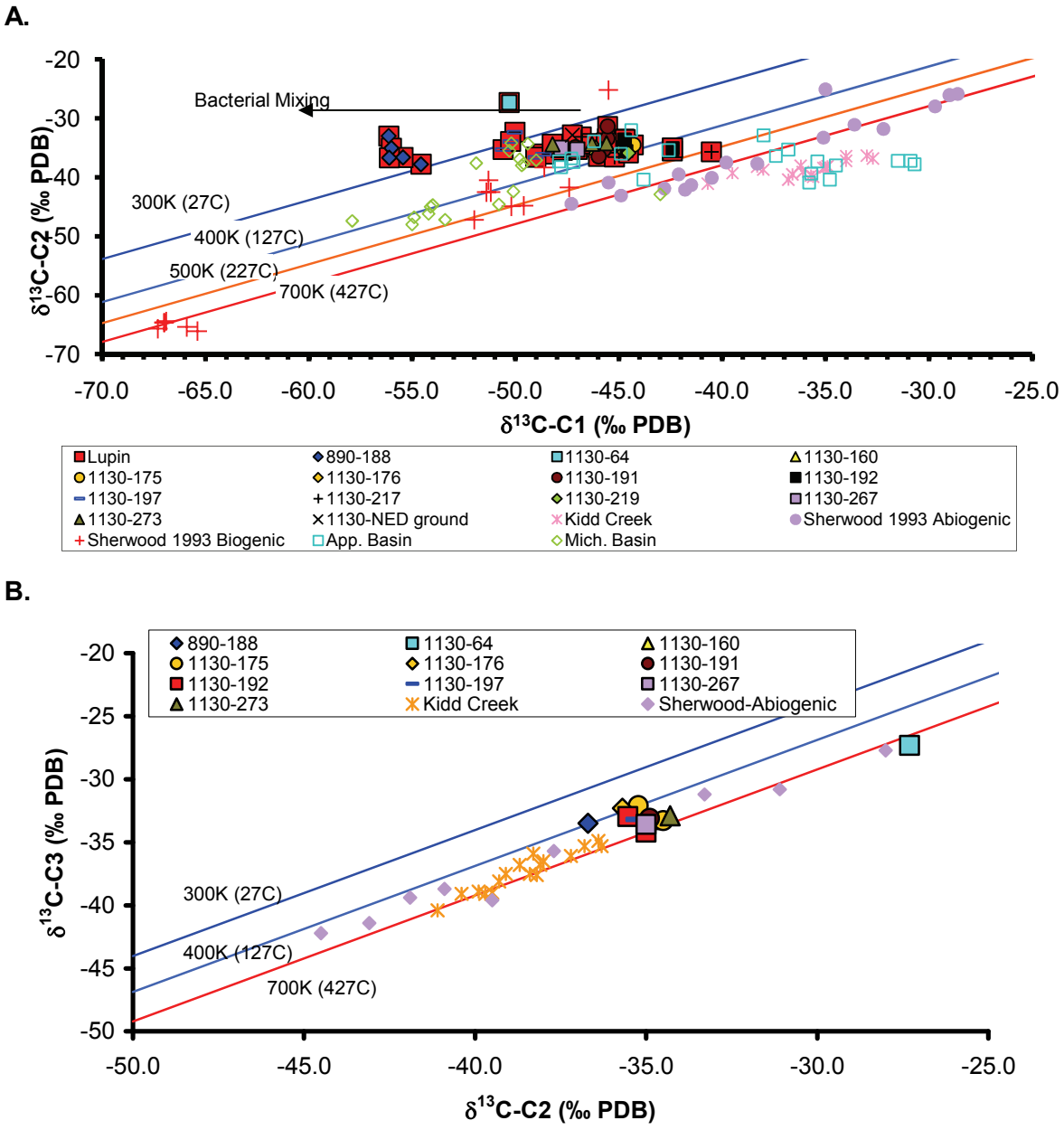

Figure 39: Gas data from Kidd Creek (Sherwood Lollar et al. 2002), Canadian and Fennoscandian Shields abiogenic (Sherwood Lollar et al. 1993a) and biogenic (Sherwood Lollar et al. 1993b), Michigan Basin (Martini et al. 2003), and from the Lupin site are presented. (A) C1-C2 carbon isotope geothermometers, from James (1983). While thermogenic sedimentary data is not presented, it generally plots in the same area as Lupin samples, and (B) C2-C3 Carbon isotope geothermometers, from James (1983).

Looking more closely at the various stable carbon and hydrogen plots (Figure 36A and B) suggests a potential for bacterial methyl type fermentation or early mature thermogenic gas formation. However, looking at a plot comparing δ^2H of CH_4 and H_2O at Lupin (Figure 40), the

Lupin data plots on the CO_2 reduction pathway, rather than the acetate fermentation pathway. If it is assumed that the gas was formed with the same water as is present at the site today, it is likely CO_2 reduction would have formed the methane. Possible reasons for these differing predictions regarding mechanisms of CH_4 formation at Lupin include the potential post-formational evolution of methane (freezing, diffusion, or depressurization) causing a shift in its isotopic signature. Alternatively, something other than present day water may have been the hydrogen source for the measured methane.

It is difficult to determine the age of the bacterial methane and the DIC at the site because the ^{14}C component is most likely derived from a carbon pool older than the dating method (i.e. >30 000 to 60 000 years). Two gas samples were analyzed (1130-267 and 1130-192), and as expected, measured ^{14}C values were close to 0 pmc (<0.3 pmc and 0.7 pmc, respectively) (Table 9). The thermogenic component of the hydrocarbon gases at Lupin is most likely derived from metamorphic heating of the original ocean bottom sediments (turbidites) into the metaturbidites and amphibolitic gneisses at the Lupin site. In this case, the majority of the gas component could be billions of years in age. Graphite observed at the site (Section 2.1) is the most likely solid remnant of this process.

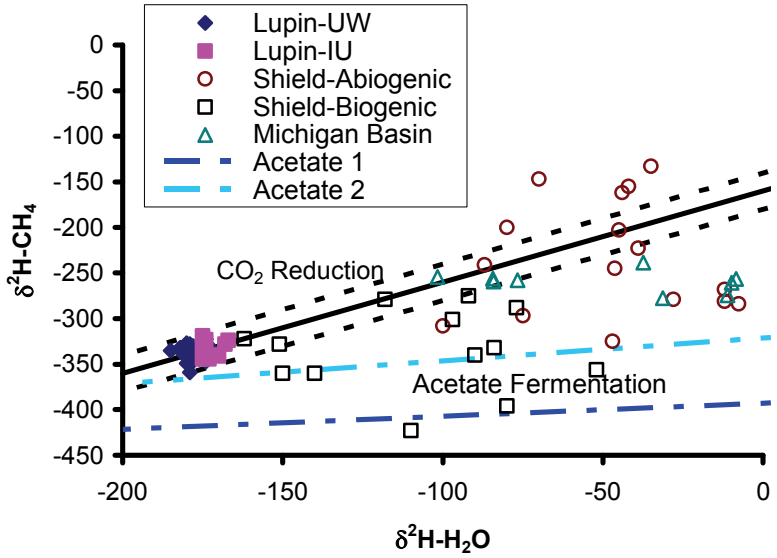

Figure 40: Deuterium of methanes versus deuterium values of the associated water for Lupin samples, from Shield abiogenic samples (Sherwood Lollar et al. 1993a), from Shield biogenic samples (Sherwood Lollar et al. 1993b), and from the Michigan Basin (Martini et al. 2003). CO_2 reduction line from Schoell (1980), acetate fermentation 1 line from Jenden and Kaplan (1986), and acetate fermentation 2 line from Whiticar et al. (1986).

An interesting comparison can be made between gas samples from a gas hydrate research well drilled in the Mackenzie Delta and samples from the Lupin site. The gas hydrate research well was drilled into approximately 640 m of permafrost to a depth of 1150 m. Using a standard interpretation of the gas composition and carbon isotopic composition, it was determined that gas in core cuttings in the shallow portions of the well were formed biogenically, then changed

to a microbial/thermogenic mix at 350 m depth, then purely thermogenic gas at 680 m (just below the permafrost) (Lorenson et al., 1999). Gas hydrate and gas of thermogenic origin were present from 890-1100 m, and below 1100 m only thermogenic gas was found. When compared with Lupin gas data from the 890 and 1130 levels, the carbon isotopes were of similar composition and exhibited similar fractionation between C1, C2, and C3 hydrocarbons as at the same levels in the hydrate research well (Figure 41). This suggests that hydrocarbons at the Lupin site may also be biogenically produced in shallow portions of the well, and that a transition to thermogenic methane may occur with depth. While it is probable this trend is due to a typical bacterial to thermogenic progression with depth, the potential for freezing effects on carbon isotopes in methane should be investigated further in order to determine whether this influences the $\delta^{13}C$ of CH_4 measured at the site.

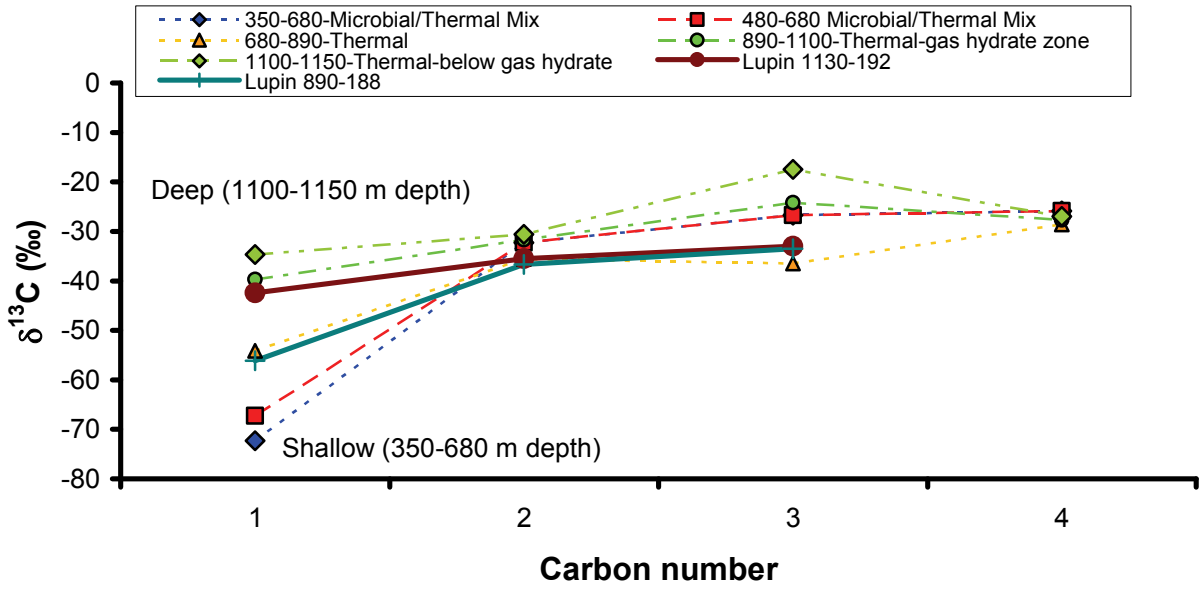

Figure 41: Comparison of Lupin gas $\delta^{13}C$ with the JAPEX/JNOC/GSC Mallik 2L-38 gas hydrate research well in the MacKenzie Delta (Lorenson et al. 1999). Note the similarities of the carbon isotopic composition of gas at the 1130 level of the Lupin mine (1130-192 was used as a representative sample) with the average values from the 890-1100 m depths in the research borehole, and the similarity of the 890-188 borehole with the average values from the 680-890 m depths in the research borehole.

4.3 AGE INTERPRETATION

To estimate the age of water recharge at Lupin, both the ^{14}C of dissolved inorganic carbon and ^{36}Cl in groundwater samples were analyzed. Additionally, ^{14}C of methane was analyzed to try to determine if methane generation is a recent phenomenon (i.e. <60 000 years), and ^{36}Cl of the salt used to create drilling brine at the mine was analyzed to compare with ^{36}Cl values in the deep groundwater samples (Table 9).

There are several potential problems with using ^{14}C to date waters and gases at the Lupin site. Firstly, at depth, there is very little dissolved HCO_3^- (Figure 17), thus large sample volumes are needed. Additionally, the deep waters tend to be undersaturated with respect to calcite, thus it is possible for atmospheric CO_2 to dissolve during sampling, resulting in a contaminated sample with a much younger apparent age. This was not initially identified as a potential problem at the site, and ^{14}C analyses from early in the project show a range of ^{14}C dates from 15,000 ybp to 28,000 ybp (Table 9). However, the last set of ^{14}C samples, taken in October 2005, were collected in 2L glass bottles with a special procedure to eliminate the possibility of diffusion of CO_2 through the bottle. The bottles were filled with the sampling tube at the bottom of the bottle with minimum turbulence, forcing the air inside the bottle out. This proceeded until three bottle volumes of water had been pushed through the bottle. This whole process took place inside a bag. When the level of the water in the bag was over the top of the bottle, the bottle cap (with Teflon septa) was placed under water, carefully checked for air bubbles, the tube removed from the bottle, and the bottle sealed under water to minimize the potential for atmospheric contamination. The results of this last sampling are very consistent, between 25,000 ybp and 26,800 ybp. The one exception to this is the short 1130-64 borehole, which, as discussed in the gas section (4.2.2), is likely exposed to the mine atmosphere through fractures.

Table 9: ^{14}C, ^{3}H and ^{36}Cl data from Lupin samples. The ^{14}C samples taken with special precautions are shown in bold.

Depth	Sample	Date	$\delta^{13}C$	^{14}C pMC*	^{14}C 'Age'**	^{3}H	^{36}Cl	TDS (g/L)
	Salt		--	--	--	--	<0.0014	-
Lake	Contwoyto	22-Jun-02	--	--	--	-	1.0738	-
390	Drips	26-Oct-00	--	--	--	-	<0.0004	-
390	WZA	27-Nov-04	-9.84	14.02	15729	9	0.0022	-
550	112	30-Nov-04	--	--	--	-	0.0043	-
570	105	27-Nov-04	--	--	--	-	0.0069	-
890	188	21-Feb-03	*-4.5*	8.72	19546	0.9	--	-
890	188	26-Nov-04	-5.21	5.58	23130	<0.8	0.0112	2.8
1130	64	26-Nov-04	-8.5	16.4	14468	<0.8	0.0116	2.6
1130	**64**	**8-Oct-05**	***-22.8***	**7.67**	**20570**	**-**	**--**	**-**
1130	181	27-Feb-03	*-1.9*	2.78	28740	<0.8	--	-
1130	192	22-Feb-03	*7.7*	16.2	14572	<0.8	--	-
1130	192	26-May-04	-	-	-	-	0.0116	-
1130	**192**	**10-Oct-05**	***10.5***	**3.5**	**26870**	**-**	**--**	**-**
1130	192-CH_4		-	0.7	-	--	--	-
1130	**197**	**10-Oct-05**	***-1.7***	**4.41**	**25030**	**-**	**--**	**-**
1130	267	25-Nov-04	-8.3	6.49	21922	0.9	0.0128	6.1
1130	267-CH_4			<0.3		--	--	-
1130	273	25-Nov-04	-1.83	11.02	23130	<0.8	0.0138	7.9
1130	273	30-Nov-04	--	--	--	-	0.0111	-
1130	**273**	**10-Oct-05**	***9.6***	**4.4**	**25040**	**-**	**--**	**-**

- = not analyzed

*pMC = percent modern carbon

**'Age' = years before present

Carbon associated with methane from two boreholes (1130-192 and 1130-197) was also dated, and both samples were very near or below the detection limit, so ^{14}C ages could not be determined.

Age dating was also carried out on ten groundwater samples, a sample of salt used by the mine for mixing brine, and Lake Contwoyto water, using ^{36}Cl analysis (Table 9). This technique was promising for age dating, and determining the potential for salt contamination from mine-mixed brine in the permafrost areas, as discussed in Section 4.1.1. The results of these analyses are presented in Table 9. Lake Contwoyto, with very low chloride content, shows a very high ^{36}Cl value of 1.0738 (Figures 42-44). While high ^{36}Cl values are expected due to the modern age of the lake water, the lake has very low chloride content, and so any amount of ^{36}Cl will have a strong influence on the ^{36}Cl value, and so the extremely high ^{36}Cl value is likely due to the desert-like conditions of the arctic, which results in the cycling and concentration of ^{36}Cl (Carlson et al. 1990, Stotler 2008). Concentrations of ^{36}Cl in the salt used for mixing drill brine were below the detection limit, typical for imported drilling salt (Stotler 2008).

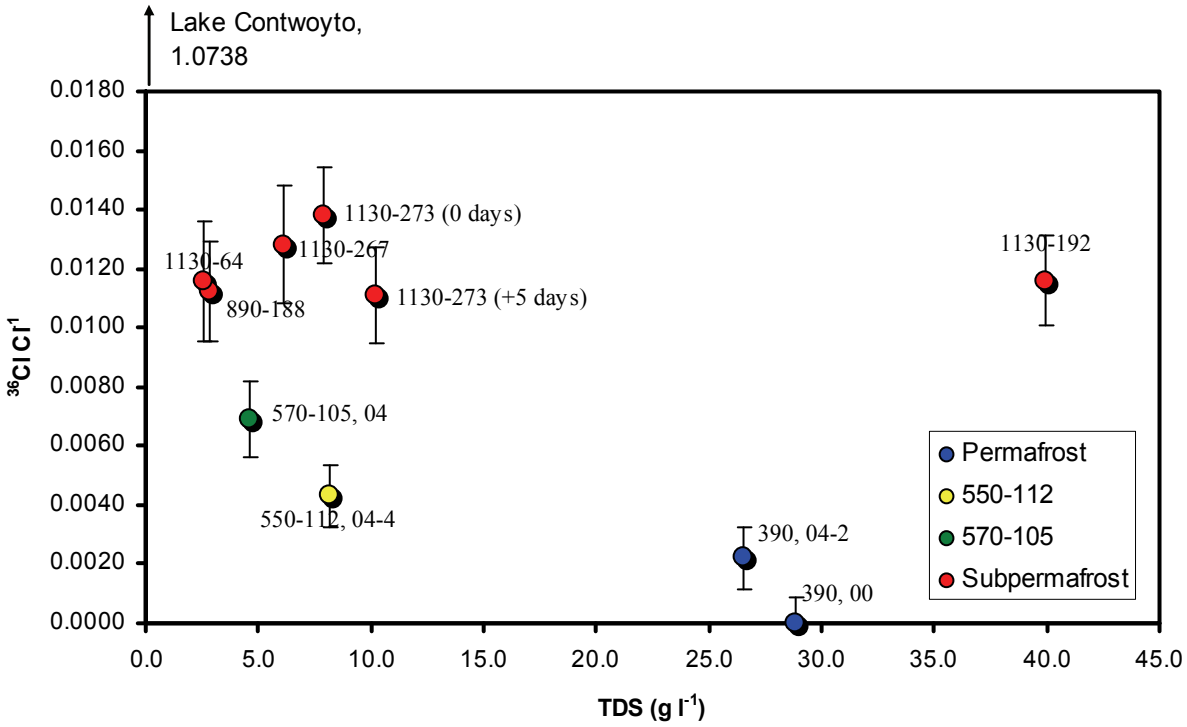

Figure 42: ^{36}Cl vs. TDS for Lupin water samples.

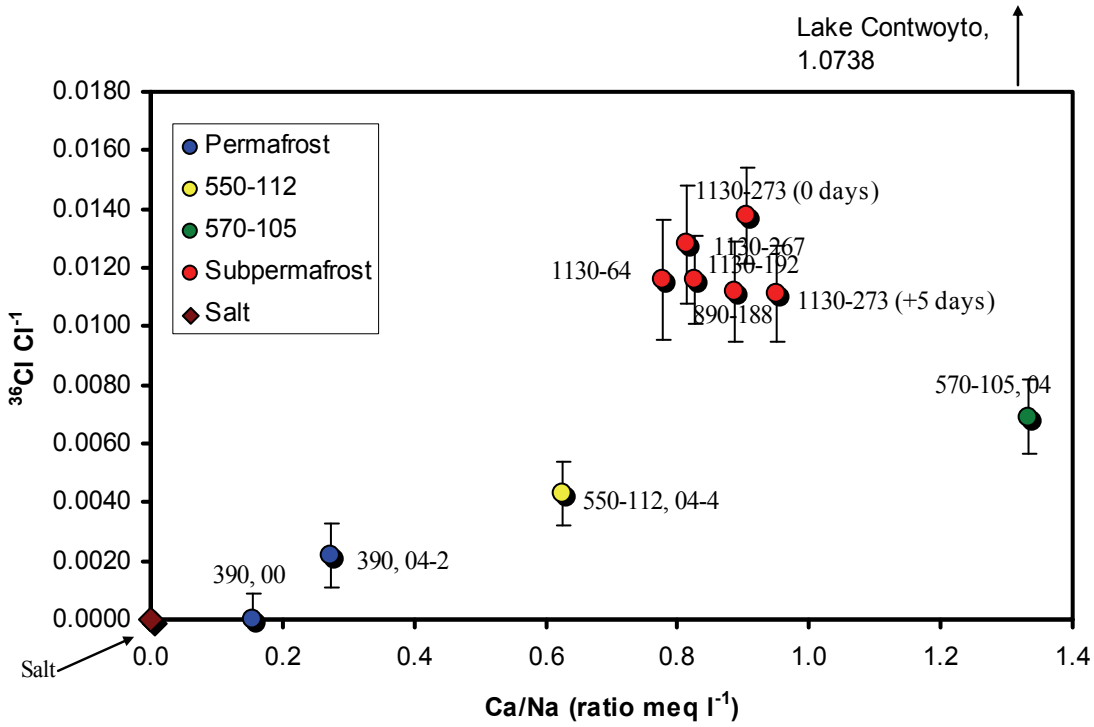

Figure 43: ^{36}Cl versus Ca/Na ratios. Data labels correspond to borehole number.

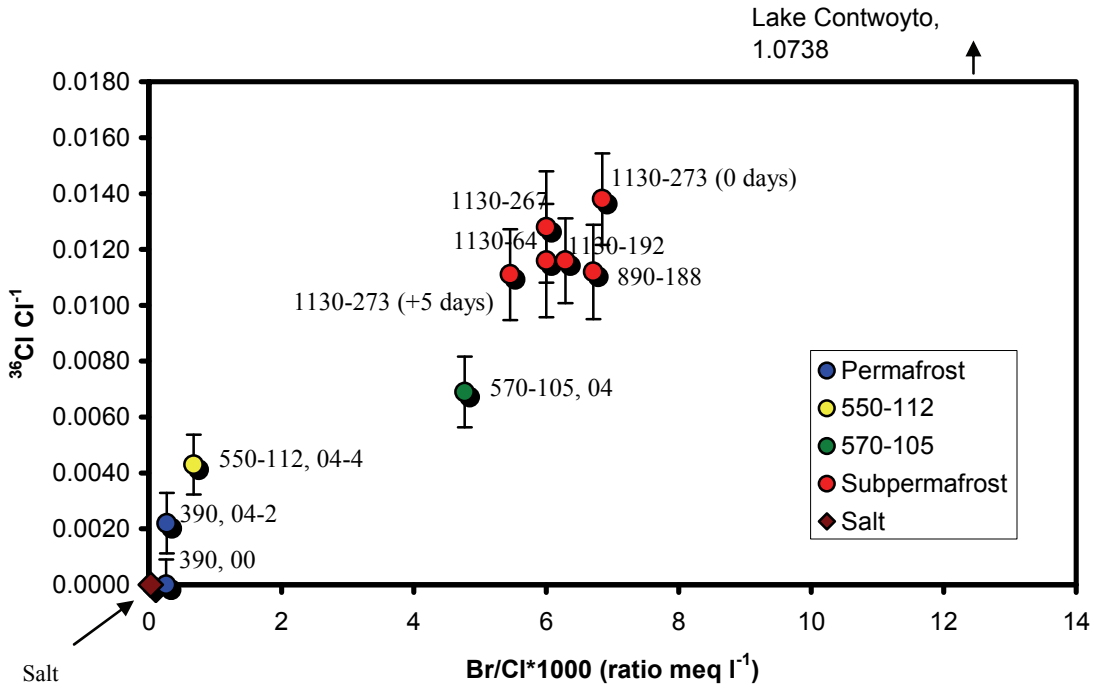

Figure 44: ^{36}Cl vs. Br/Cl ratio for Lupin waters and imported salt.

Values of ^{36}Cl from the permafrost samples are lower than the subpermafrost samples, and plot close to the salt values (Figures 43-44), which provides additional evidence that the chloride in the permafrost is from drill salt introduced by mining activities.

^{36}Cl values in the subpermafrost waters are within the range expected for equilibrium with subpermafrost nucleogenic production (Stotler, 2008), indicating the Cl in the subpermafrost system is likely older than the limit (0.5 to 1 million years) of the ^{36}Cl dating method (Phillips, 2000; Stotler, 2008).

5. FRACTURE MINERAL STUDIES

Isotopic composition ($\delta^{13}C$ and $\delta^{18}O$) and fluid inclusion microthermometry analyses were performed on a number of calcite samples collected from throughout the Lupin mine, both in grab samples and from core cuttings (Figure 49; Stotler 2008). The calcite isotopic compositions measured at Lupin show the largest range of any Canadian Shield site studied to date (Figure 45). One particularly large subhorizontal calcite vein, found at the 540 level along the access ramp had a particularly large range in values ($\delta^{13}C$ -2.08 ‰ to +30.09 ‰ and $\delta^{18}O$ -14.49 ‰ to -6.29 ‰) (Figure 46; Stotler 2008). The reason for this large range in stable isotope values is not known at this time.

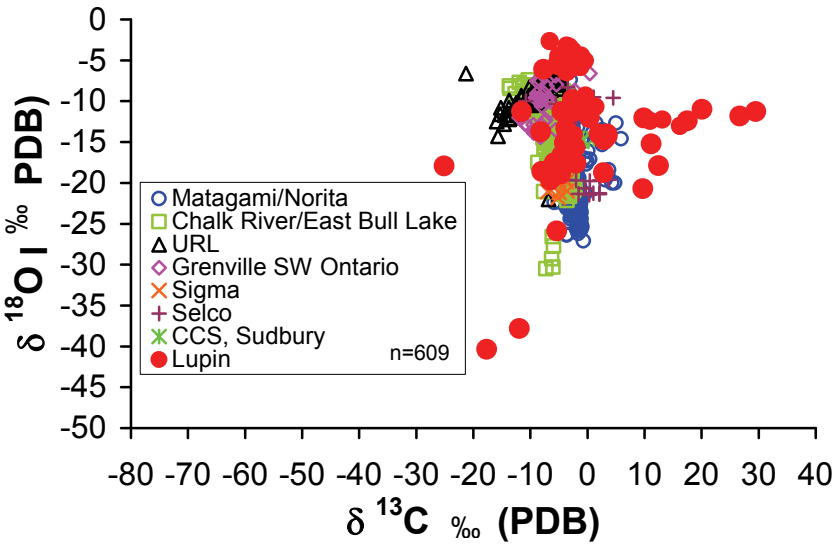

Figure 45: Comparison of the isotopic composition ($\delta^{13}C$, $\delta^{18}O$) of Lupin calcites with other reported Canadian Shield calcites. Adapted from Blyth (1993).

Figure 46: Sample from the large calcite vein found along the ramp at the 540 level in the Lupin Mine.

Several different fluid inclusion assemblages (FIA) were observed in the calcite samples studied at the Lupin site (Figure 50). One FIA consisted of only liquid phase inclusions. A second FIA had both liquid and gas phase inclusions, a high salinity (>26%), and the Ca/Mg fluid had homogenization temperatures between 73°C and 147°C. The next FIA observed had three-phase NaCl inclusions, salinity between 31 and 36%, and homogenization temperatures between 250°C and 271°C. Another FIA consisted of a low salinity (<3%) fluid, with homogenization temperatures between 132°C and 148°C. Finally, a FIA consisting of what appeared to be CH_4 inclusions was observed. Often, multiple sets of these FIA were found in the same fluid inclusion chips, in what appeared to be the same crystal, which is indicative of a boiling system at the time of crystallization. In addition, several chips that were prepared were found to be barren of useable fluid inclusions.

Following the methods of Blyth et al. (2000, 2004), homogenization temperatures and oxygen isotope compositions of the calcite emplacement waters were interpreted. The enriched $\delta^{18}O$ signatures of calcite in some of the most saline waters with the highest homogenization temperatures suggests they were likely emplaced by a heavy water, $\delta^{18}O$ > +10‰ SMOW (Figure 47). Another set appears to have been carried by a slightly lighter water, 0‰ SMOW > $\delta^{18}O$ > -10‰ SMOW, while a third group appeared to crystallize from an extremely light water, -20‰ SMOW > $\delta^{18}O$ > -30‰ SMOW (Figure 47). Further comparison of the microthermometric data with isotopic data (Figure 48) shows no apparent trends or patterns.

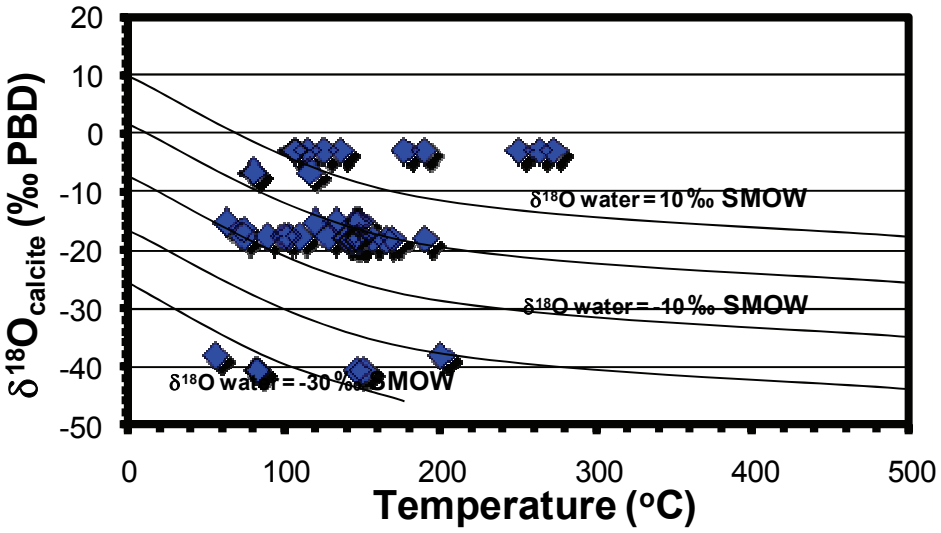

Figure 47: Data from 11 different fluid inclusion chips and the associated $\delta^{18}O$ composition.

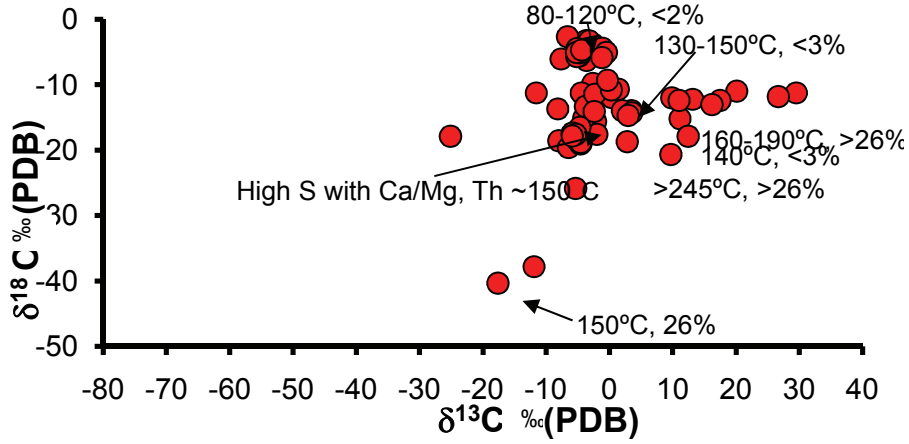

Figure 48: Fluid inclusion microthermometric data combined with calcite isotopic results. Temperatures are homogenization temperatures, salinities are in percent.

A.

B.

Figure 49: Examples of two calcites found at the Lupin Mine, along the access ramp. (A) Calcite with graphite interfingerings from the 270 m level. (B) Vuggy calcites with a light brown coating (oxy-iron-hydroxides) were found in the upper portions of the mine, like this one from the 440 m level.

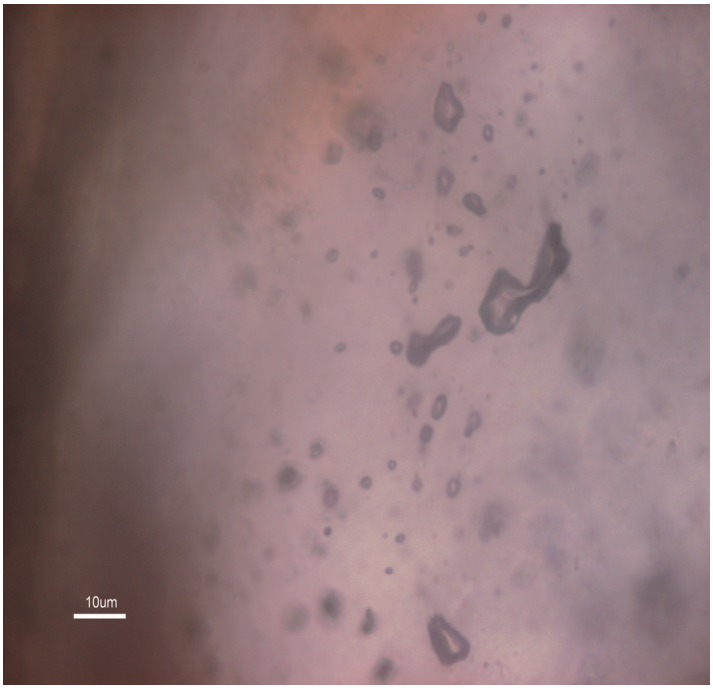

Figure 50: Examples of fluid inclusions from the Lupin site.

6. INTERPRETATION & CONCEPTUAL MODEL

Summary

Geophysical evidence (ground penetrating radar) shows the presence of taliks underneath Lake Contwoyto and several smaller lakes in the area (Section 3.1). Interpretation of ground penetrating radar and lake diameters in the Lupin area indicates that lakes smaller than 300 m in diameter will freeze throughout, while lakes 500 x 250 m or larger with a depth of at least 1.5 to 2.5 m may have open taliks beneath the lake. GPR interpretation suggests that lakes larger than 500 m diameter, such as Lake Contwoyto, have the potential to support through taliks. While the depths of the taliks at Lupin are unknown, based on the lake's size, it is probable that the talik under Lake Contwoyto is a through talik (Figure 51). The Lupin site was impacted by previous mining activities, so it is unclear from this study what impact taliks would have on waters at depth in an undisturbed system.

Variations in pressure (hydraulic head) and TDS measurements at the site suggest that the drilling of boreholes connected fracture networks which were previously independent. The existence of stable hydraulic head differences in boreholes 200 m apart provides evidence that any permeable pathways within the rock are poorly connected and that the system has a low bulk permeability (Section 3.2, Section 4.1.1.1). Hydraulic head measurements also confirmed the observation made in Phase II of the PERMAFROST Project that an unsaturated zone occurs below the base of the permafrost, which may be due to dewatering activities at the mine (Frape et al., 2004).

Permafrost Waters

Geochemical data from the Lupin site clearly show the permafrost water is distinct and unique from the subpermafrost water, and has been strongly impacted by mining activities at the site. Tritium concentrations in permafrost waters reflect the infiltration of tritiated surface waters due to drawdown from mining activities (Section 4.1.1.1). Ca, Na and Cl analysis (Section 4.1.1.1) illustrate the influence of salt (used in drilling, and a major salt spill) on permafrost waters. Cation and anion plots (Figure 25, 26) show the permafrost waters plotting closely to drill salt at the site. Concentrations of SO_4 and NO_3 are elevated within the permafrost zone, likely due to contamination from salt and blasting powder associated with mining at the site. Rare earth element (REE) analysis shows distinct patterns for permafrost waters and subpermafrost waters, suggesting they are of different origin/history, which further supports geochemical data indicating permafrost waters impacted by mining activities at the site. The impact of mining operations on permafrost waters is also seen in stable isotopic data from the permafrost waters ($\delta^{18}O$, $\delta^{2}H$), where the isotope values, and their slight deviation from the GMWL, likely reflects the mixing of surface waters for drilling with natural permafrost waters (Section 4.1.2.1). ^{36}Cl analysis of permafrost waters shows the permafrost waters plotting most closely to drill salt from the site (Figure 43), again supporting the interpretation of permafrost waters strongly impacted by mining operations at the site.

Subpermafrost Waters

Subpermafrost waters at the site are distinct from the contaminated permafrost waters, and may represent uncontaminated deep groundwater at the site. Deep groundwaters are Na-Ca-Cl or Ca-Na-Cl types with a range of TDS values, from 2 to 36 g/L. Small amounts of tritium were measured in the deeper subpermafrost fluids, possibly due to slight contamination from mining activity. In several boreholes, tritium levels decreased to below detection with time after the boreholes were packered and sealed (Stotler 2008), suggesting contamination with tritium occurred during drilling of the boreholes (Section 4.1.1.1). Low concentrations of HCO_3 were observed in the subpermafrost fluids, similar to values observed in fluids at similar depths at other Canadian Shield sites, and the isotopic composition of sulphate ($\delta^{18}O$, $\delta^{34}S$) in the subpermafrost waters is similar to other shield brines (Section 4.1.1.1). Major ion (Ca, Na, Cl, Br) data as well as REE analysis shows distinct subpermafrost water compositions from the permafrost waters which are strongly impacted by drill salt, indicating the deep subpermafrost samples have not been impacted by mining activities, and are representative of natural, in-situ waters. Stable isotopes of water ($\delta^{18}O$, $\delta^{2}H$) of the deep subpermafrost waters plot on the GMWL, and are again distinct from the contaminated permafrost waters, further supporting the interpretation that the deep waters have not been significantly impacted by drilling contamination. Methane is the dominant hydrocarbon gas associated with the deep subpermafrost groundwaters, and isotopic analysis of hydrocarbons from the deep groundwater indicates a thermogenic origin of the methane (Section 4.2.1). The thermogenic origin of the methane suggests the hydrocarbon gases, and by association the matrix fluids and most of the saline groundwaters, are hundreds of millions to billions of years old. This is supported by ^{36}Cl analysis which suggests that Cl^- in the subpermafrost system is older than the 0.5 to 1 my limit of the ^{36}Cl dating technique (Stotler 2008). ^{14}C dating indicates a recharge event of some kind occurred in the subpermafrost 22-26 ky before present.

Conceptual Model

A preliminary conceptual model for the Lupin site is presented here (Figure 51). Given that mining activities at the Lupin site have significantly impacted groundwaters, particularly in the permafrost, the conceptual model presented here reflects this anthropogenic influence, and is not necessarily representative of an undisturbed permafrost site. The conceptual model is based on information presented in this report, and in Stotler, 2008.

The Lupin mine is situated in an area of continuous permafrost that extends to ~500 m depths. Fractures in the crystalline rock may be associated with the foliation of the rocks (Figure 52) and at the apex of the folds. Structural heterogeneity exists at the site, as evidenced by spatial variation and differences in magnitudes of hydraulic heads in boreholes at the site. A lack of hydraulic connection between boreholes was observed in hydraulic testing during Phase II of the project (Frape et al., 2004). Differences in hydraulic head and salinity, and the lack of hydraulic connection between nearby boreholes indicate that the system is poorly connected, with a low bulk permeability. Smaller lakes (<300 m diameter) are frozen throughout, while lakes 300 – 500 m in diameter may support open taliks. Lakes larger than 500 m diameter (such as Lake Contwoyto) have the potential for through talik formation beneath the lake. Relatively dilute water may flow down from the permafrost and/or talik in fractures closer to the mine. The drawdown caused by pumping in the mine would encourage the downward flow in these fractures. Further from the mine, higher TDS water may be pushed up from depth. As boreholes are sealed, this higher TDS water would replace the less dense water in the boreholes, explaining the observation that TDS increased with time after sealing in some boreholes (Section 4.1.1.1). The Lupin site has been disturbed by mining activities making it unclear from this study what impact taliks would have on waters at depth in an undisturbed system.

The presence of an unsaturated zone beneath the base of the permafrost observed in Phase II was confirmed by hydraulic head measurements in this phase of the project, and is attributed to mine dewatering activities. Permafrost waters are significantly impacted by mining activities (drill salt), while the subpermafrost waters are more representative of uncontaminated in-situ waters. Methane is the dominant hydrocarbon gas associated with the deep subpermafrost groundwaters, and has a thermogenic origin (Section 4.2.1) suggesting the hydrocarbon gases, and by association the matrix fluids and most of the saline groundwaters, are hundreds of millions to billions of years old, which is supported by ^{36}Cl analysis of Cl in the subpermafrost system. However, radiocarbon dating of dissolved inorganic carbon suggests a recharge event of some kind in the subpermafrost waters 22,000 to 26,000 years before present.

.

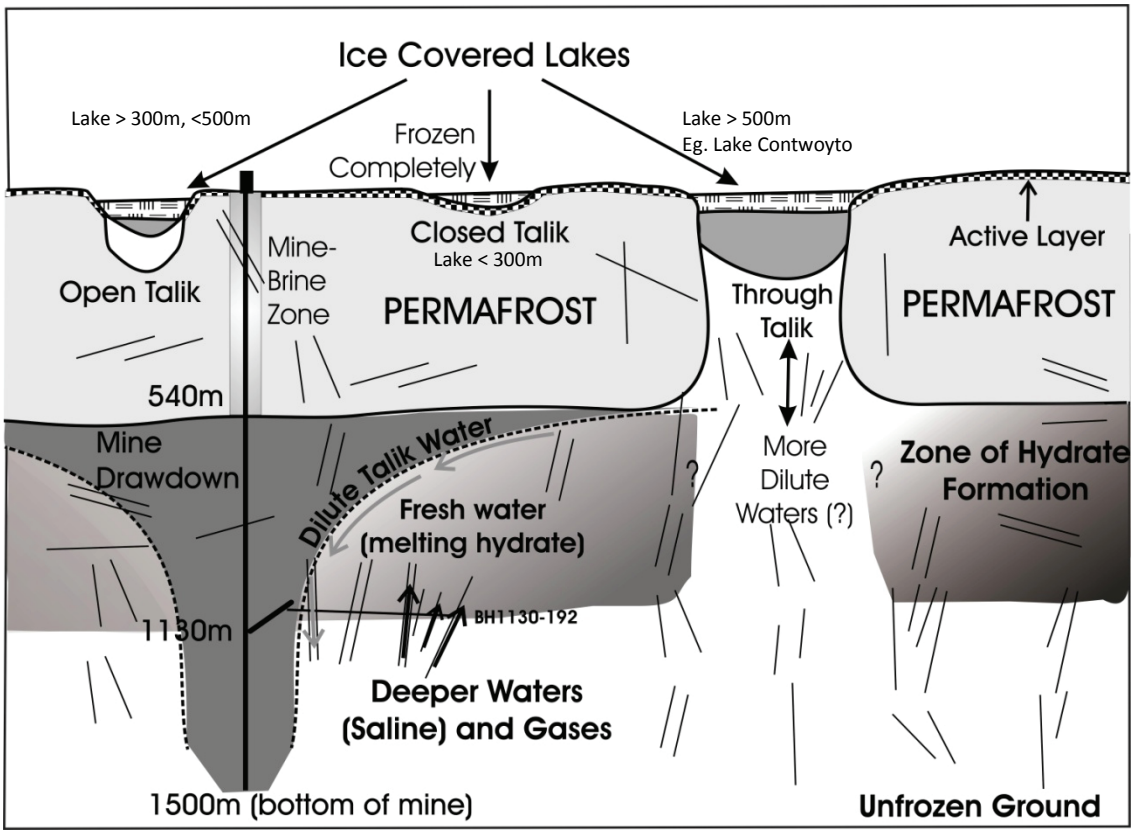

Figure 51: Conceptual diagram of the Lupin Mine area.

A.

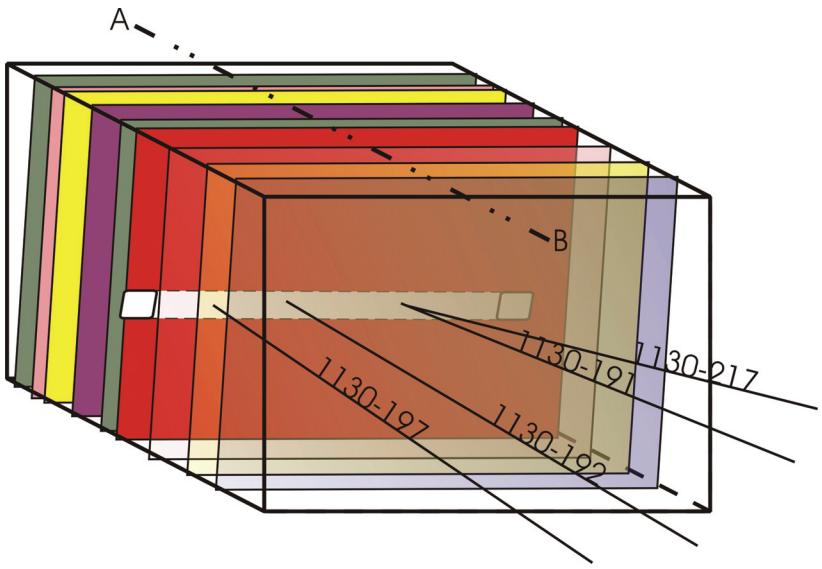

B.

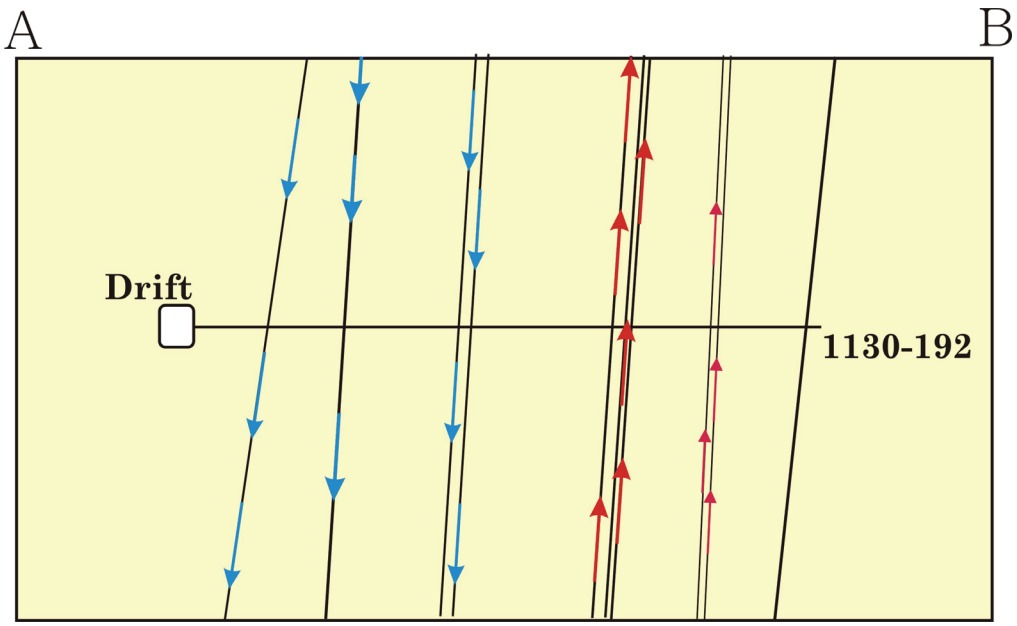

Figure 52: Conceptual model of groundwater flow in the Lupin mine. (A) Boreholes on the 1130 level crosscut foliation, some of which contains water and/or gas (B) a possible cross-sectional view of fracture flow directions in 1130-192. High salinity, gas containing water flows up in fractures further from the mine, while more dilute water flows down fractures closer to the mine. These fractures have been connected by the borehole.

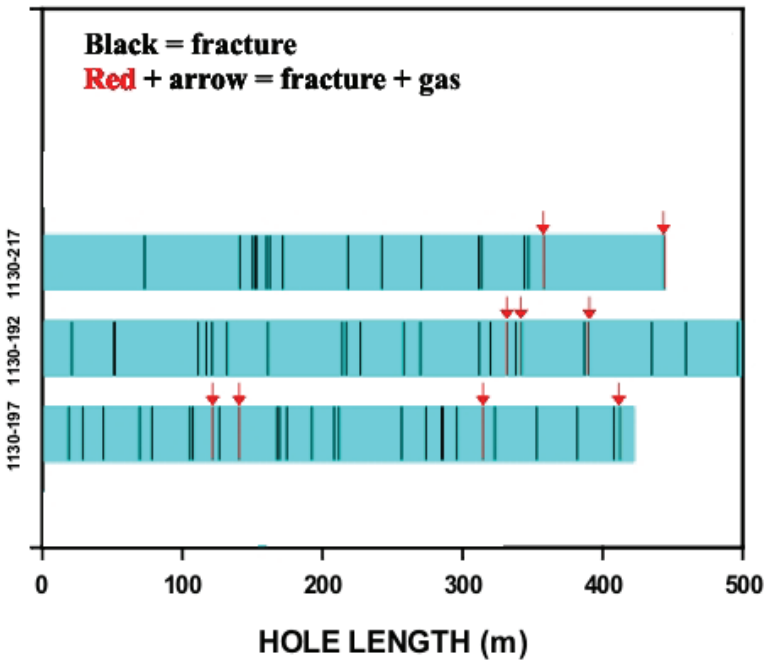

Figure 53: Open fracturing in boreholes 1130-197, 1130 192 and 1130-217 observed in video surveys (from Frape et al., 2004).

The results of the Phase III PERMAFROST project suggest that for hydrogeologic modeling studies in permafrost regions with numerous large lakes, the presence and influence of taliks should be considered. If through-taliks are developed, they may act as tube-like conduits through the frozen ground. At the Lupin site, the presence of through-taliks beneath Lake Contwoyto and several smaller lakes in the area is suggested by ground penetrating radar investigations. However, due to disturbances at the Lupin site from mining activities, it is not clear from this investigation what impact taliks might have on waters at depth in an undisturbed location. Further research to determine the role of taliks as pathways for groundwater flow is needed.

REFERENCES

Alexeev S. V. and Alexeeva L. P. 2003. Hydrogeochemistry of the permafrost zone in the central part of the Yakutian diamond-bearing province, Russia. *Hydrogeology Journal*, **11**, 574-581.

Bakermans, C., D.J. McGown, T. Ruskeeniemi, L. Ahonen, J. Telling, C. Boettiger, R. Ho, B. Soffientino, S.A. DiFurio, S.M. Pfiffner, B. Sherwood-Lollar, S. Frape, R. Stotler, L.M. Pratt, R.E. Sloup, T.A. Vishnivetskaya, T.C. Onstott. Microbial sulfur cycling in subpermafrost saline fracture water at the Lupin Gold Mine, Nunavut, Canada. Submitted to *Environmental Microbiology* Feb. 2008.

Bebout, G.E. and Fogel, M.L. 1992. Nitrogen-isotope compositions of metasedimentary rocks in the Catalina Schist, California: Implications for metamorphic devolatilization history. Geochimica et Cosmochimica Acta, **56** (7), 2839-2849

Bebout, G.E. 1997. Nitrogen isotope tracers of high-temperature fluid-rock interactions: Case study of the Catalina Schist, California. Earth and Planetary Science Letters. **151** (1-2), 77-90.

Blomqvist, R., Ruskeeniemi, T., Kaija, J., Ahonen, L., Paananen, M., Smellie, J., Grundfelt, B., Pedersen, K., Bruno, J., Perez del Villar, L., Cera, E., Rasilainen, K., Pitkanen, P., Suksi, J., Casanova, J., Read, D., and Frape, S. 2000. The Palmottu natural analogue project, Phase II: Transport of radionuclides in a natural flow system at Palmottu. European Commission nuclear science and technology report EUR 19611.

Blyth, A. 1993. The study of fracture filling calcite in the Fennoscandian and Canadian Shields as an indicator of past thermal and fluid history. M.Sc. Thesis, University of Waterloo, Waterloo, Ontario, Canada.

Blyth, A, S. Frape, R. Blomqvist, P. Nissinen. 2000. Assessing the past thermal and chemical history of fluids in crystalline rock by combining fluid inclusion and isotopic investigations of fracture calcite. *Appl. Geochem.* **15**, 1417-1437.

Blyth, A. 2004. Radioactive waste disposal in the crystalline rock of Scandinavia: case studies of the farfield environment. Ph.D. Dissertation, University of Waterloo, Waterloo, Ontario, Canada.

Brookins, D.G. 1989. Aqueous geochemistry of rare earth elements. *Reviews in Mineralogy and Geochemistry*, **21** (1), 201-225.

Burn, C.R. 2002. Tundra lakes and permafrost, Richards Island, western Arctic coast, Canada. *Can. J.Earth Sci*. **39**, 1281-1298.

Clark, I. and P. Fritz. 1997. *Environmental Isotopes in Hydrogeology*. Lewis Publishers: Boca Raton, 328p.

Des Marais, D.J., J.H. Donchin, N.L. Nehring, A.H. Truesdell. 1981. Molecular carbon isotopic evidence for the origin of geothermal hydrocarbons. *Nature* **292,** 826-828.

Frape, S.K. and P. Fritz. 1981. The Occurrence and Geochemistry of Groundwaters on the Canadian Shield. Report to AECL, project 002-08-18.

Frape, S.K., P. Fritz, R.H. McNutt. 1984. Water-rock interaction and chemistry of groundwater from the Canadian Shield. *Geochim. Cosmochim. Acta* **48**, 1617-1627.

Frape, S.K. and P. Fritz. 1987. Geochemical trends for groundwater from the Canadian shield. In *Saline Water and Gases in Crystalline Rocks*, Paper 33 (eds. P. Fritz and S.K. Frape). Geological Association of Canada, Memorial University, Newfoundland, pp. 19-38.

Frape, S.K., R.L. Stotler, T. Ruskeeniemi, L. Ahonen, M. Paannanen and M.Y. Hobbs. 2004. Hydrogeochemistry of groundwaters at and below the base of the permafrost at Lupin: Report of Phase II. Ontario Power Generation, Nuclear Waste Management Division. Supporting Technical Report, 06819-REP-01300-10047-R00.

Fritz, P. S.K. Frape, R.J. Drimmie, E.C. Appleyard, K. Hattori. 1994. Sulfate in brines in the crystalline rocks of the Canadian Shield. *Geochim. Cosmochim. Acta* **58,** 57-65.

Gascoyne, M. and DA Thomas. 1997. Impact of blasting on groundwater composition in a fracture in Canada's Underground Research Laboratory. *Journal of Geophysical Research*, **102** (B1): 573-584.

Haendel, D., Muhle, K., Nitzsche, H-M., Stiehl, G.,Wand, U. 1986. Isotopic variations of the fixed nitrogen in metamorphic rocks. Geochimica et Cosmochimica Acta, **50** (5), 749-758

Haskin, L.A. and Paster, T.P. 1979. Geochemistry and mineralogy of the rare earths. Handbook on the physics and chemistry of rare-earths. Vol. 3. Non-metallic compounds **1**, p. 1 - 80

Holden, B., Stotler, R.L., Frape, S.K., Ruskeeniemi, T., Talikka,M., Freifeld, B.M. 2009. High Lake Permafrost Comparison Site: Permafrost Phase IV. Nuclear Waste Management Organization. Toronto, Canada. NWMO-TR-2009-11.

Holloway J.M., Dahlgren R.A., Hansen B., Casey W.H. 1998. Contribution of bedrock nitrogen to high nitrate concentrations in stream water. *Nature*, **395** (6704), 785-788.

IAEA, Global Network of Isotopes in Precipitation (GNIP) and Isotope Hydrology Information System (ISOHIS). http://isohis.iaea.org.

James, A.T. 1983. Correlation of Natural Gas by Use of Carbon Isotopic Distribution Between Hydrocarbon Components. *AAPG Bulletin*, **67**, 1176-1191.

Jenden, P.D. and Kaplan, I.R. 1986. Comparison of microbial gases from the Middle America Trench and Scripps Submarine Canyon: implications for the origin of natural gas. *Appl. Geochem.* **1,** 631-646.

Jones, M.G. 1987. A study of the late-stage secondary fracture mineralization at sites across the Precambrian Canadian Shield. MSc. Thesis, Dept. of Earth Sciences, University of Waterloo, Waterloo, Ontario, Canada.

Kendall, C. and R. Aravena. 2000. Nitrate isotopes in groundwater systems. In P.G. Cook and A.L. Herczeg (Eds)*, Environmental Tracers in Subsurface Hydrology*, Kluwer Academic Publishers, p.261-297.

Kroopnick, P. and H. Craig. 1972. Atmospheric oxygen – isotopic composition and solubility fractionation. *Science* **175,** 54-55.

Krouse, H.R. and B. Mayer. 2000. Sulphur and oxygen isotopes in sulphate. In *Environmental Tracers in Subsurface Hydrology*, eds. P. Cook and A.L. Herczeg, Kluwer Academic Publishers, p. 195 -231.

Lorenson, T.D., M.J. Whiticar, A. Waseda, S.R. Dallimore, T.S. Collett. 1999. Gas Composition and isotopic geochemistry of cuttings, core, and gas hydrate from the JAPEX/JNOC/GSC Mallik 2L-38 gas hydrate research well; *in* Scientific Results from JAPEX/JNOC/GSC Mallik 2L-38 Gas Hydrate Research Well, Mackenzie Delta, Northwest Territories, Canada, (ed.) S.R. Dallimore, T. Uchida, and T.S. Collett; *Geological Survey of Canada, Bulletin* **544**, 143-163.

MacDonald, I.M. 1986. Water-rock interaction in felsic rocks of the Canadian Shield. MSc. Thesis, Dept.of Earth Sciences, University of Waterloo, Waterloo, Ontario, Canada.

Mackay, J.R. 1992. Lake stability in an ice-rich permafrost environment: examples from the western Arctic coast. *In* Aquatic ecosystems in semi-arid regions: implications for resource management (eds.R.D. Robarts and M.L. Bothwell). National Hydrology Research Institute, Environment Canada, Saskatoon. Symposium Series **7**, 1-26.

Martini, A.M., L.M. Walter, T.C.W. Ku, J.M. Budai, J.C. McIntosh, M. Schoell. 2003. Microbial production and modification of gases in sedimentary basins: a geochemical case study from a Devonian shale gas play, Michigan Basin. *AAPG Bull.* **87,** 1355-1375.

Mingram, B. and K. Bäuer. 2001. Ammonium concentration and nitrogen isotope composition in metasedimentary rocks from different tectonometamorphic units of the European Variscan Belt. *Geochim. Cosmochim. Acta* **65,** 273-287.

NWMO. 2005. Choosing a way forward. The future management of Canada's used nuclear fuel. Nuclear Waste Management Organization. (Available at www.nwmo.ca)

Ohmoto H. and Goldhaber MB. 1997. Sulfur and Carbon Isotopes *in Barnes, H.L. Geochemistry of Hydrothermal Ore Deposits. John Wiley & Sons.* pp. 517 – 611.

Paananen, M. and Ruskeeniemi, T., 2003. Permafrost at Lupin : interpretation of SAMPO electromagnetic soundings at Lupin. Geological Survey of Finland, Report YST-117. 22 p. + 4 app.

Peltier W. R. 2002. A design basis glacier scenario. Ontario power Generation, Report No: 06819-REP-01200-10069-R00, 63 p.

Rossi, A.P. 1999. Investigation of permafrost groundwater discharge at Screech Lake, NWT: a preliminary conceptual model for natural, flowing cryo-artesian conditions through a coupled talik in the continuous permafrost zone. MSc Thesis, Dept. of Earth Sciences, University of Waterloo, Waterloo, Ontario, Canada.

Ruskeeniemi, T., Paananen, M., Ahonen, L., Kaija, J., Kuivamäki, A., Frape, S., Moren, L. and Degnan P., 2002. Permafrost at Lupin : Report of Phase 1. Geological Survey of Finland, YST-112. 59 p. + 3 app.

Ruskeeniemi, T., L. Ahonen, M. Paananen, S. Frape, R. Stotler, M. Hobbs, J. Kaija, P. Degnan, R. Blomqvist, M. Jensen, K. Lehto, L. Moren, I. Puigdomenech, M. Snellman. 2004. Permafrost at Lupin: Report of Phase II. Geological Survey of Finland, Nuclear Waste Disposal Research. Report YST-119, 89 p.

Rye, D.M. and R.O. Rye. 1974. Homestake Gold Mine, South Dakota: 1, Stable Isotope Studies. *Econ.Geol.* **69**, 293-317.

Schoell, M. 1980. The hydrogen and carbon isotopic composition of methane from natural gases of various origins. *Geochim. Cosmochim. Atca* **44,** 649-661.

Sherwood Lollar, B., Frape, S. K., Fritz, P., Macko, S. A., Welhan, J. A. and Blomqvist, R., 1989. Gas geochemistry and its relationship to brines of the Canadian and Fennoscandian Shield. In: Geological Society of America 1989 Annual Meeting, St. Louis, Missouri, November 6-9, 1989. Geological Society of America. Abstracts with Programs **21** (6), A316

Sherwood Lollar, B., S.K. Frape, P. Fritz, S.A. Macko, J.A. Welhan, R. Blomqvist, P.W. Lahermo. 1993a. Evidence for bacterially generated hydrocarbon gas in Canadian Shield and Fennoscandian Shield rocks. *Geochim. Cosmochim. Acta* **57,** 5073-5086.

Sherwood Lollar, B., S.K. Frape, S.M. Weise, P. Fritz, S.A. Macko, J.A. Welhan. 1993b. Abiogenic methanogenesis in crystalline rocks. *Geochim. Cosmochim. Acta* **57,** 5087-5097.

Sherwood Lollar, B. Weise S. M., Frape S. K. and Barker J. F. 1994. Isotopic constraints on the migration of hydrocarbon and helium gases of southwestern Ontario. *Bull. Can. Petrol. Geol.*, **42**, 283-295.

Sherwood Lollar, B., Westgate, T. B., Ward, J. A., Slater G. F. And Lacrampe-Couloume G. L. 2002. Abiogenic formation of alkanes in the Earth's crust as a minor source for global hydrocarbon reserviors. *Nature*, **416**, 522-524.

Stotler, R.L. 2008. Evolution of Canadian Shield groundwaters and gases: Influence of deep permafrost. Ph.D. Thesis. University of Waterloo, Canada. 265p.

Whiticar, M.J., E. Faber, M. Schoell. 1986. Biogenic methane formation in marine and freshwater environments: CO2 reduction vs. acetate fermentation – isotope evidence. *Geochim. Cosmochim. Acta* **50**, 693-709.

Whiticar, M.J. 1999. Carbon and hydrogen isotope systematics of bacterial formation and oxidation of methane. *Chem. Geol.* **161,** 291-314.

Zhang, M. and Frape, S.K., 2002. Permafrost: Evolution of shield groundwater compositions during freezing. Ontario Power Generation, Report No: 06819-REP-01200-10098-R00, 49 p.